NASA CR-
ERIM 109600-71-F

NASA CR-
150998

N77-14557
Unclas
G3/43 00058

(E77-10058) FOREST CLASSIFICATION ACCURACY AS INFLUENCED BY MULTISPECTRAL SCANNER SPATIAL RESOLUTION Final Report, 15 May 1975 - 14 May 1976 (Environmental Research Inst. of Michigan) 130 p HC A07/MF A01

Final Report

# FOREST CLASSIFICATION ACCURACY AS INFLUENCED BY MULTISPECTRAL SCANNER SPATIAL RESOLUTION

F. SADOWSKI AND J. SARNO
Infrared and Optics Division

MAY 1976



Prepared for
NATIONAL AERONAUTICS AND SPACE ADMINISTRATION

Johnson Space Center
Earth Observations Division
Houston, Texas 77058
Contract No. NAS9-14123, Task 16
Technical Monitor: Dr. A. Potter/TF3

ENVIRONMENTAL
RESEARCH INSTITUTE OF MICHIGAN
FORMERLY WILLOW RUN LABORATORIES, THE UNIVERSITY OF MICHIGAN
BOX 618 • ANN ARBOR • MICHIGAN 48107

TECHNICAL REPORT STANDARD TITLE PAGE

| 1. Report No. NASA CR-ERIM 109600-71-F | 2. Government Accession No. | 3. Recipient's Catalog No. |
|---|---|---|
| 4. Title and Subtitle<br>Forest Classification Accuracy as Influenced by Multispectral Scanner Spatial Resolution | | 5. Report Date<br>May 1976<br>6. Performing Organization Code |
| 7. Author(s)<br>F. Sadowski and J. Sarno | | 8. Performing Organization Report No.<br>109600-71-F |
| 9. Performing Organization Name and Address<br>Environmental Research Institute of Michigan<br>Infrared & Optics Division<br>P.O. Box 618<br>Ann Arbor, Michigan 48107 | | 10. Work Unit No.<br>Task 16<br>11. Contract or Grant No.<br>NAS9-14123<br>13. Type of Report and Period Covered<br>Final Technical Report<br>May 15, 1975 through<br>May 14, 1976 |
| 12. Sponsoring Agency Name and Address<br>National Aeronautics & Space Administration<br>Johnson Space Center<br>Houston, Texas 77058 | | 14. Sponsoring Agency Code |

15. Supplementary Notes

The work was performed for the Earth Observations Division. Dr. Andrew Potter (TF3) was the technical monitor.

16. Abstract

The objective of this study was to determine the influence of multispectral scanner (MSS) spatial resolution on the classification of forest features at levels of detail appropriate to nationwide forest surveys and detailed in-place inventories. Such levels of detail or hierarchies might include vegetation units differentiated on the basis of physiognomy, forest cover types, and forest stand condition classes.

A supervised classification of U.S. Forest Service designated forest features within two separate ground areas of the Sam Houston National Forest was carried out for (2 meters)$^2$ spatial resolution MSS data. The data were then progressively coarsened to simulate 5 additional cases of spatial resolution ranging up to (64 meters)$^2$. Similar processing and analysis of all spatial resolutions enabled evaluations of the effect of spatial resolution on classification accuracy for various levels of detail and the effect on area proportion estimation for very general forest features. For very coarse resolutions a subset of spectral channels which simulated the proposed Thematic Mapper channels was used to study classification accuracy. The merits of multi-element techniques for improving classification accuracy were tested for one case of spatial resolution.

In general, classification accuracy improved as spatial resolution was degraded, when conventional single-element multispectral processing procedures were used. However, for this study, the large increase in the percent of unclassified elements confounded the results of the (64 meters)$^2$ case of resolution, causing the best results to be obtained with a spatial resolution of (32 meters)$^2$. Thus, we recommend that the

| 17. Key Words | 18. Distribution Statement |
|---|---|
| Spatial Resolution<br>Classification Accuracy<br>Forest Feature Hierarchies<br>Proportion Estimation<br>Nine-Point Rules | Initial distribution is listed at the end of this document. |

| 19. Security Classif. (of this report) | 20. Security Classif. (of this page) | 21. No. of Pages | 22. Price |
|---|---|---|---|
| Unclassified | Unclassified | xiv + 130 | |

approach used for setting decision rejection thresholds be re-examined. As would be expected, accuracies are highest for the most general of forest feature hierarchies.

The use of nine-point rules at the selected spatial resolution, $(32 \text{ meters})^2$, gave improved accuracy for both 5 and 11 channel classifications, especially for the most specific forest features. Use of these and other specialized techniques show promise for increasing classification accuracies at all spatial resolutions.

The subset of 5 channels chosen to simulate the spectral channels for the proposed Thematic Mapper classified the data with accuracy comparable to that of all 11 $M^2S$ channels for general forest features. This was not, however, the case for more specific forest features where the reduction in the number of spectral channels leads to reduced classification accuracies.

Area proportions of general forest features were well estimated. The optimum spatial resolution for proportion estimation is apparently dependent upon the forest features in the scene, and more data segments would be required to adequately determine the relationship.

# PREFACE

This report describes part of a comprehensive and continuing program of research concerned with advancing the state-of-the-art in remote sensing of the environment from aircraft and satellites. The research is being carried out for NASA's Lyndon B. Johnson Space Center, Houston, Texas, by the Environmental Research Institute of Michigan (ERIM). The basic objective of this multidisciplinary program is to develop remote sensing as a practical tool to provide the planner and decision-maker with extensive information quickly and economically.

Timely information obtained by remote sensing can be important to such people as the farmer, the city planner, the conservationist, and others concerned with problems such as crop yield and disease, urban land studies and development, water pollution, and forest management. The scope of our program includes:

1. extending the understanding of basic processes
2. discovering new applications, developing advanced remote-sensing systems, and improving automatic data processing to extract information in a useful form
3. assisting in data collection, processing, analysis, and ground-truth verification.

The research described herein was performed under NASA Contract No. NAS9-14123, Task 16, and covers the period from 15 May 1975 through 14 May 1976. Andrew Potter (TF3) was the NASA Contract Technical Monitor. The program was directed by Richard R. Legault, Vice President of ERIM and Head of the Infrared and Optics Division, Jon D. Erickson, Head of the Information and Analysis Department, and Richard F. Nalepka, Principal Investigator and Head of the Multispectral Analysis Section.

The authors wish to acknowledge the technical direction and assistance provided by R. F. Nalepka and W. A. Malila. Peter Lambeck was responsible for the calculations necessary for a realistic

simulation of spatially degraded data. Wyman Richardson provided computer programming support and technical consultation. Finally, Edwin P. F. Kan of Lockheed Electronics Company, Inc., Houston, Texas, was very helpful in providing the digital data and ground truth information required for this study. The ERIM number of this report is 109600-71-F.

CONTENTS

# FIGURES

FIGURES (CONT.)

FIGURES (CONT.) Page

FIGURES (CONT.)

FIGURES (CONT.)

TABLES

TABLES (CONT.) Page

# SUMMARY

The objective of this study was to determine the influence of multispectral scanner (MSS) spatial resolution on the classification of forest features at levels of detail appropriate to nationwide forest surveys and detailed in-place inventories. Such levels of detail or hierarchies might include vegetation units differentiated on the basis of physiognomy, forest cover types, and forest stand condition classes.

Our general approach was to acquire MSS data sets of varying spatail resolution such that the minimum area resolved ranged from individual components of forest stands to large areas approaching the resolution of the present Landsat systems. We desired the results of the study to be independent of complicating factors that might have been caused by temporal effects, differing signal-to-noise properties, differing number and placement of spectral bands, etc. Therefore, a single aircraft data set of inherent (2 meters)$^2$ resolution was degraded in successive steps to simulate 5 additional data sets having (4)$^2$, (8)$^2$, (16)$^2$, (32)$^2$, and (64 meters)$^2$ spatial resolutions. To degrade resolution as realistically as possible, we implemented an algorithm that utilized typical MSS optics and electronics properties in the form of two spatial weighting functions. System noise inherent to the (2 meters)$^2$ data was preserved in each simulated data set by inserting a quantity of randomly generated high-frequency noise sufficient to equal the amount of noise reduction caused by the weighting functions.

The MSS data set included 11 spectral channels collected from an altitude of 2000 feet. The data were collected as part of NASA Mission No. 290 on 20 November 1974 over the Conroe Unit of the Sam Houston National Forest in east Texas. Two segments of data providing ground coverage of 2 km x 1.25 km (approximately 1 million resolution elements) and 2.5 km x 1.25 km (approximately 1.2 million elements) were utilized

for the study. Forest features on one data segment were grouped into four hierarchies of generally decreasing detail that included condition class (cover types differentiated into stands on the basis of age and size class), cover type (areas having similar species composition), growth stage (areas having similar age and size class), and physiognomy (areas having similar vegetative and community structure as determined by the major characteristics of its plants). Features on the second data segment were grouped into the two hierarchies of condition class and physiognomy.

Prior to degrading spatial resolution, data quality was checked by determining dynamic range, high and low frequency noise, and variations in signal associated with scan angle. Variation in low frequency noise (observed as a shift in mean signal value along the flightline) necessitated a preprocessing correction to the data that incorporated a dynamic clamp algorithm. Assessment of signal variations associated with scan angle showed a lack of strong variation in most channels.

We processed all data sets of varying resolution with a supervised classification procedure that utilizes signatures extracted from training areas. Training areas for each forest feature covered equivalent ground areas for each case of spatial resolution.

For each case of spatial resolution, we classified forest features using a linear decision rule and all 11 spectral channels. For selected cases of spatial resolution, we performed additional classifications that included:

- the use of a single-element quadratic and four multi-element decision rules for classifying (32 meters)$^2$ data
- the use of a subset of 5 spectral channels most similar to the proposed Thematic Mapper channels for classifying (32)$^2$ and (64 meters)$^2$ data with all above mentioned decision rules.

Classification accuracies for each hierarchy of forest features were determined for each case of spatial resolution. Accuracies were

determined for training sets, total feature areas with boundary elements excluded (boundary exclusive test sets), and feature areas including boundary elements (boundary inclusive test sets). Area proportion estimates by feature were determined for the physiognomy hierarchy of each data segment. Accuracies were determined only for the region of data located within $30^{o}$ of the flightline nadir in order to avoid large MSS view angles.

Major conclusions reached by this study are:

1. Classification accuracy improved, in general, as spatial resolution was degraded, when conventional single-element multispectral processing procedures were used.
2. A standard processing approach which uses a constant decision rejection threshold level can result in large numbers of unclassified elements for coarser resolutions. For this study, possibly due to the great increase in unclassified elements at $(64 \text{ meters})^2$, best results were obtained with a spatial resolution of $(32 \text{ meters})^2$. Perhaps the standard approach for setting rejection levels should be re-examined.
3. More general (aggregated) forest features had substantially higher classification accuracies than the more specific features.
4. The impact of boundary elements on feature classification was shown to cause increasingly reduced accuracies for boundary inclusive test sets relative to boundary exclusive test sets, as spatial resolution was degraded.
5. Specialized classification techniques can improve classification for a given spatial resolution and show promise for increasing accuracies at all spatial resolutions. The increases with nine-point decision rules were most dramatic when classification accuracies were low, giving significant improvement for the more specific forest features.

6. Results with the subset of channels which simulated the proposed Thematic Mapper channels compared favorably to results obtained with all 11 $M^2S$ channels for physiognomies but not for the more specific forest features.
7. Area proportions were well estimated at the level of physiognomy for both data segments although the optimum spatial resolution was different for the two segments. To determine what resolution is optimum for various types of features, more data segments would have to be studied.
8. Differences in performance were noted for both classification accuracy and proportion estimation between equivalent hierarchies for the two data segments, indicating that performance depends on the characteristics of the features in the scene.

Specific recommendations regarding feature classification performance, training approaches, multi-element processing, and area proportion estimates are provided in Section 5.2.

# 2
# INTRODUCTION

Improper sensor specification may be a major cause for inadequate forest classification results frequently achieved from multispectral scanner (MSS) data. One major aspect of sensor specification concerns spatial resolution. The determination of optimal data spatial resolution for classifying forest features will enable forest managers to select the proper sensors and platforms to get the desired results. Without such guidelines, there is a possibility that data with too much or too little spatial resolution will be collected for particular forestry applications.

This report documents the methods and results of an empirical study to determine the influence of MSS spatial resolution on the classification of specific forest features. Because forest inventories can require vegetation classification for different levels of detail, the study considered hierarchies of forest features at levels that might be commensurate with nationwide forest surveys and detailed in-place inventories. A total of 6 cases of spatial resolution were processed that ranged from $(2 \text{ meters})^2$ to $(64 \text{ meters})^2$ in size. All degraded cases of resolution were simulated from the $(2 \text{ meters})^2$ data by incorporating an algorithm that utilized typical MSS optics and electronics properties and that preserved inherent system noise. Through extensive processing and analysis of the data, relationships were developed to illustrate classification accuracies as a function of spatial resolution for each of the hierarchies of forest features studied.

## 2.1 BACKGROUND

Recent studies have shown improvements in classification accuracy as a result of degrading spatial resolution of MSS data. Kan and Ball [1] reported higher classification accuracies for forest features as data resolution was degraded from $(8 \text{ meters})^2$ to simulated

resolutions of (16 meters)$^2$ and (24 meters)$^2$. The results, based only on statistical pairwise classification accuracies and divergence values computed for signatures extracted from training areas, were credited to a reduction in scene variation by virtue of averaging information over larger units. Thomson, et al., [ 2 ] reported similar results that were based on actual classification performance of agricultural features. However, decreased mensurational accuracies resulted from the larger areal impact of boundary element misclassification as spatial resolution was degraded. This report is intended to provide a more realistic and complete analysis of the effect of MSS spatial resolution on the classification of forest features.

# 3
# APPROACH

## 3.1 TEST SITE LOCATION AND DESCRIPTION OF FOREST FEATURES

The test site for this study is the Conroe Unit of the Sam Houston National Forest (SHNF), located in east Texas between Houston and Huntsville. Physiographically, the Unit lies on a narrow zone of indistinct depositional terraces that comprise a part of the Western Gulf Coastal Plain. Low elevation and relief are characteristic of the area. Soils vary greatly from deep loamy sands to heavy clays with a range in ability to support vegetation from southern timber types to open prairie types.

Extensive areas of pine and pine-hardwood forest vegetation identify the Conroe Unit as part of the east Texas "piney woods." The major forest type is Loblolly Pine. Shortleaf Pine and bottomland hardwood types are also present. Forest types are subdivided into condition class on the basis of age and size of the majority of trees in the stand.

Two separate ground areas within the Conroe Unit were addressed for this study. Forest features in these areas, classified as to cover type and condition class according to existing U.S. Forest Service (USFS) timber stand and compartment boundary maps, are listed in Table 1.

Locations of the forest features in the two ground areas are shown in Figures 1 and 2. The photographs illustrated in these two figures were taken some 19 months prior to the date for which the MSS data processed in this study were collected. The features in Figure 1 are displayed much as they existed for the MSS data, except for one small open area ("A") in feature 1.3 made as a result of a bark beetle salvage cutting. Several items in Figure 2 require update and/or explanation. The two features labeled 7.1 appear on the photo as cut-over but not site prepared; however, they were predominantly bare soil and

TABLE 1. FOREST FEATURES WITHIN THE CONROE UNIT THAT WERE ADDRESSED IN THE STUDY. COVER TYPE AND CONDITION CLASS DESIGNATIONS ARE FROM U.S. FOREST SERVICE TIMBER STAND AND COMPARTMENT BOUNDARY MAPS

| Physiognomic Formation* or Other General Description | Cover Type No. | Cover Type Description | Condition Class No. | Condition Class Description |
|---|---|---|---|---|
| Conifer Forest | 1 | Shortleaf Pine | 1.3 | Sawtimber-immature |
| | | | 1.4 | Sawtimber-mature |
| | 2 | Loblolly Pine | 2.5 | Sawtimber-immature |
| | | | 2.6 | Sawtimber-mature |
| Conifer Regeneration | 2 | Loblolly Pine | 2.3 | Seedling & Sapling-- adequately stocked |
| Hardwood Forest | 3 | Laurel Oak -- Willow Oak | 3.1 | Sawtimber-immature |
| | 4 | Sweetgum -- Nuttal Oak -- Willow Oak | 4.2 | Sawtimber-immature |
| Cut-over Land | 7 | None | 7.1 | Site Prepared and Windrowed |

* Physiognomic Formations -- vegetative community structure as determined by the major characteristics of its plants.


FIGURE 1. FOREST FEATURES IN GROUND AREA 1 (MSS DATA SEGMENT 1), CONROE UNIT, SHNF


FIGURE 2. FOREST FEATURES IN GROUND AREA 2 (MSS DATA SEGMENT 2), CONROE UNIT, SHNF. Lettered areas were excluded from the study: A, bark beetle salvage cut; B, pasture; C, water; and D, untyped private land.

herbaceous vegetation (site prepared and windrowed) for the MSS data. Areas labeled "A" at the left side of the photo indicate large bark beetle salvage cuttings that were made since the photo was taken. Area "B" in upper right corner represents a small pasture (private holding). Area "C" at bottom center represents an arm of a new impoundment that held water for the MSS data. And area "D" at the right side of the photo is untyped private land.

All lettered areas in Figure 2 were excluded from consideration in this study. Although salvage cut areas and pasture are legitimate forest features, they were not included in this study because of their limited areal extent and their position along the extreme edges of the MSS data (see Section 3.4). The water feature was considered not to be a forest feature for this study. Finally, the large parcel of non-homogeneous private land was excluded for lack of ground truth.

## 3.2 DATA DESCRIPTION AND QUALITY

To provide for a thorough investigation into the effect of MSS spatial resolution on the classification of forest features, we required data that provided several cases of varying spatial resolution. In addition, we required the range of resolution cases to vary from minimum areas small enough to resolve individual components of forest stands to areas large enough to nearly approximate the coarse resolution of the present Landsat systems. Although the use of several different data sets collected over a common test site might satisfy the spatial resolution requirements, results of such a study would be dependent on inconsistent sets of variables caused by temporal effects, differing number and placement of spectral bands, signal-to-noise characteristics, etc., that might exist between data sets. Therefore, we decided to degrade a single aircraft data set of inherent (2 meters)$^2$ resolution to simulate data sets having progressively larger resolution elements ranging up to (64 meters)$^2$ in size.

MSS data utilized for the study included 11 spectral channels collected by a Bendix-built Modular Multispectral Scanner ($M^2S$) from an altitude of 610 meters (2000 feet). The spectral coverages of the 11 channels are provided in Table 2. The data had been collected as part of NASA Mission 290 on 20 November 1974 and were supplied to us by personnel of the Forestry Applications Project located at Johnson Space Center, Houston, Texas.

Two segments of flightline 17, covering areas illustrated in Figures 1 and 2, were converted from Universal to ERIM format for processing. Segment 1 (Figure 1) of data provided ground coverage of about 2 km along the flightline and 1.25 km swath width and included approximately 1 million resolution elements. Segment 2 covered about 2.5 km of the flightline and included approximately 1.2 million elements.

A check of data quality was made to determine the signal-to-noise properties of the data and the need for preprocessing. We checked data quality by assessing dynamic range, high and low frequency noise, and variations in signal associated with scan angle. A substantial low frequency signal variation along the flightline (a contrast variation known as "banding") necessitated development of a preprocessing correction in the form of a dynamic clamp algorithm. By virtue of the differences in magnitude and pattern of occurrence for the "banding" artifact between the two data segments, the dynamic clamp correction was applied separately to each segment. Differences in the mean level adjustments made for each segment created some concern for the legitimacy of radiometric comparisons between the two segments. Thus, in the subsequent processing procedure, each data segment was classified separately with its own set of signatures.

Lack of strong signal variations associated with scan angle for most spectral channels were considered in detail relative to the atmosphere and the bidirectional reflectance properties of the scene components. Details of the data quality analysis are contained in Appendix I.

TABLE 2. SPECTRAL COVERAGE PROVIDED BY THE MSS DATA OF MISSION 290

| Sensor Channel | Spectral Band Limits (μm) at 50% Response Points |
|---|---|
| 1 | 0.41 - 0.44 |
| 2 | 0.45 - 0.49 |
| 3 | 0.49 - 0.54 |
| 4 | 0.53 - 0.57 |
| 5 | 0.57 - 0.61 |
| 6 | 0.61 - 0.65 |
| 7 | 0.65 - 0.69 |
| 8 | 0.69 - 0.73 |
| 9 | 0.76 - 0.86 |
| 10 | 0.95 - 1.03 |
| 11 | 8 - 12 |

## 3.3 DEGRADATION OF SPATIAL RESOLUTION

The degradation of spatial resolution was carefully designed to create each case of degraded resolution in as realistic a manner as possible with inherent system noise levels preserved. Properties of typical MSS optics and electronics were used in conjunction with the $(2 \text{ meters})^2$ data to calculate two spatial weighting functions. Each weighting function was low pass filtered and truncated to span 5 successive resolution elements in directions along the scanline and along the flightline respectively. When quantized into 5 intervals and combined into an X-Y matrix, the two weighting functions created an array that, when successively centered on every other element in every other scanline and when multiplied and summed over the surrounding 5 by 5 group of pixels to generate a replacing pixel value, yielded a new data set having one-fourth the number of resolution elements per unit ground area (Figure 3). The new data set, of simulated $(4 \text{ meters})^2$ resolution, was thus an approximation of the original analog data values as influenced by the assumed typical MSS scanning and recording characteristics. System noise inherent to the original data was preserved in the simulated data by inserting a quantity of randomly generated high-frequency noise sufficient to compensate for the calculated amount of noise reduction caused by the spatial weighting array. Further details regarding calculation and implementation of the spatial weighting functions are provided in Appendix II.

Application of the spatial weighting array to each successive data set in turn enabled creating additional data sets for which the linear spatial resolution was doubled in each successive case. Five cases of spatial resolution were simulated in all. Thus, for each segment of data, we processed 6 cases of spatial resolution that included the inherent $(2 \text{ meters})^2$ data and simulated cases of $(4)^2$, $(8)^2$, $(16)^2$, $(32)^2$, and $(64 \text{ meters})^2$ data.

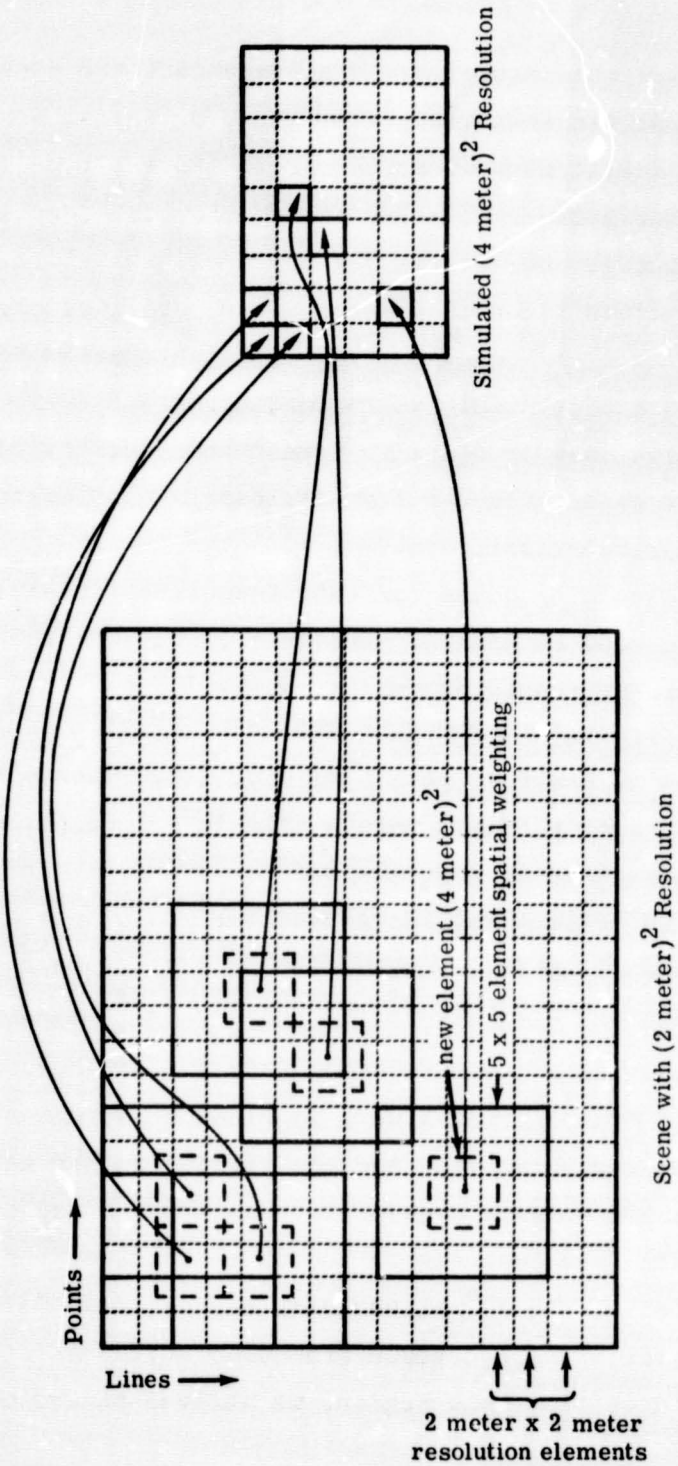


FIGURE 3. ILLUSTRATION OF TECHNIQUE FOR SIMULATED DOUBLING OF LINEAR SPATIAL RESOLUTION

## 3.4 SIGNATURE EXTRACTION

Our objectives for this study were concerned with the classification of forest features that are acknowledged by the U.S. Forest Service to be meaningful for forest management purposes. Forest type maps showing compartment and stand boundaries provide for the identity and location of such features. Our processing approach, therefore, incorporated a supervised classification procedure that utilized signatures extracted from training areas to classify forest features in each data segment. For each case of spatial resolution, signatures were extracted anew. Thus, signatures used to classify forest features for each case of spatial resolution were extracted from training areas located on that respective case of spatial resolution.

We required the training areas for each feature to cover equivalent ground areas for each case of spatial resolution. Because the number of resolution elements decreased by approximately 75% for each case of degraded spatial resolution, whenever possible the size of the training areas on the $(2 \text{ meters})^2$ data were made large enough that a statistically valid number of elements were available for computing signatures in the $(64 \text{ meters})^2$ data. For all but one signature, the number of elements in the in the $(64 \text{ meters})^2$ data used for computing each of the signatures ranged from 17 to 79. Feature 2.5 in data segment 1 (Figure 1) had only 6 within-boundary elements in the $(64 \text{ meters})^2$ data. Thus, no signature was computed for this feature for this case of resolution.

The locations of training areas were confined to a region of the data that avoided large scanner view angles. (This was not entirely possible for feature 4.2 in data segment 2.) Analysis of scan angle variations in the data (see Appendix I) led us to conclude that the region of data located within $30^{\circ}$ either side of the flightline nadir had a reasonable degree of independence from scan angle variations. By extracting signatures from this region, we strived to exclude

sources of variation among signatures that might stem from large changes in atmospheric path length or bidirectional reflectance phenomena.

### 3.5 DATA CLASSIFICATION AND PERFORMANCE EVALUATION

Forest features classified in each data segment are listed as condition classes in Table 3. Classification performance for this hierarchy of features represents the most detailed level of classification for this study. These results were aggregated to provide a measure of classification performance for features of more general hierarchies. In data segment 1, condition classes were combined into cover types on the basis of species (pine regeneration was retained as a separate feature), and alternately, into features based on maturity that we called growth stages. For the most general hierarchy, all pine sawtimber features were combined into a single physiognomic class to be compared with pine regeneration. In data segment 2, two condition classes of hardwood sawtimber were combined into a single physiognomic feature to be compared with pine sawtimber and cut-over land.

Each case of spatial resolution was classified using the ERIM linear decision rule (Appendix III) and all 11 spectral channels. For selected cases of spatial resolution, we performed additional classification that included:

- the use of the quadratic and four multi-element decision rules for classifying (32 meters)$^2$ data from data segment 1. (Appendix III provides a brief explanation of decision rules.)
- the use of a subset of 5 spectral channels most similar to the proposed Thematic Mapper channels for classifying (32)$^2$ and (64 meters)$^2$ data with all above mentioned decision rules.

All classification results were tallied to provide the number of resolution elements correctly classified as a percentage of the total number of resolution elements contained within individual and combined

TABLE 3. FOREST FEATURES AND HIERARCHIES IN EACH DATA SEGMENT FOR WHICH CLASSIFICATION PERFORMANCE IS REPORTED

DATA SEGMENT 1

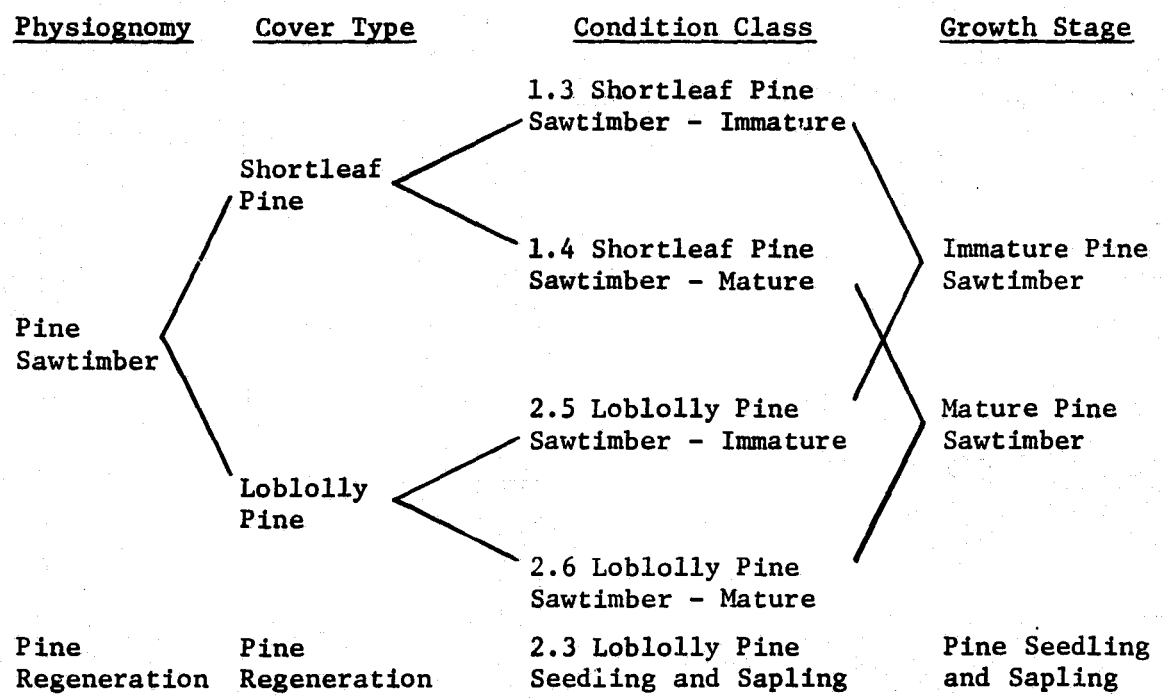


DATA SEGMENT 2

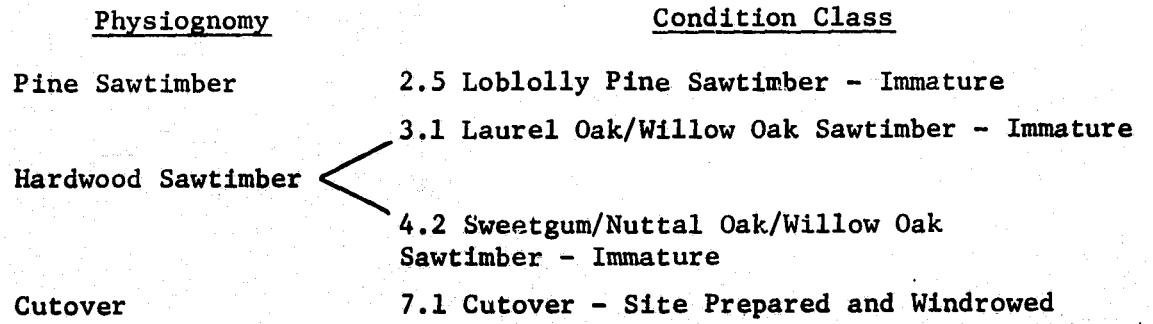

feature areas. The percent of all resolution elements correctly classified in the data set was calculated, giving an overall classification accuracy for hierarchies which was equivalent to combining feature percentages on a weighted area basis.

Classification performance was determined for three distinct regions within each data segment that included training sets, total feature sets with boundary elements excluded, and total feature sets including boundary elements. Results for each respected region illustrated:

- the ability of the signatures to uniquely characterize forest features defined by their training areas.
- the ability of the signatures to characterize the total population of resolution elements wholly within the boundaries of feature areas.
- the effect of the boundary pixels in reducing classification performance.

In addition, we compared the proportions of features, classified within the physiognomic hierarchy of each data segment with known ground area proportions.

To guard against undue influence to classification and proportional area estimation performances that might be caused by the large range of view angles inherent to aircraft MSS data, results are reported for the region of data located within $30^{o}$ either side of the flightline nadir.

# 4
# RESULTS AND DISCUSSION

## 4.1 CLASSIFICATION PERFORMANCE

### 4.1.1 Classification Accuracies Versus Spatial Resolution

All cases of spatial resolution were classified with the ERIM linear decision rule using a threshold corresponding to a 0.001 probability of rejection of signals from the assumed multivariate normal distributions of the signatures. Use of this threshold, which is common practice in the data processing community, provided an unclassified category for resolution elements too dissimilar from the signatures used for classification.

Data Segment 1

For the cases of spatial resolution ranging from (2 meters)$^2$ to (32 meters)$^2$, 6 signatures were used to classify the 5 condition classes (Table 3) in data segment 1. Because of the obvious difference in the density of the pine regeneration (Feature 2.3, Figure 1), we found it necessary to use two signatures -- one extracted from the more dense northern portion of the feature and the other from the less dense southern portion -- to best characterize the entire feature. A single signature was used for each of the other features.

For the (64 meters)$^2$ data, the very small number of resolution elements (6 within-boundary elements) for the immature Loblolly Pine sawtimber (Feature 2.5, Figure 1) prevented computing a valid signature. Thus, only 5 signatures defining four features were used to classify this data set.

Tables 4-6 summarize correct classification percentages for three distinct regions of the data segment over which performance was determined; namely, training sets, total feature areas with boundary elements excluded (boundary exclusive test sets), and total feature areas including boundary elements (boundary inclusive test sets). Each table provides the percent correct classification achieved for each of the forest

TABLE 4. PERCENT CORRECT CLASSIFICATION OF TRAINING SETS IN DATA SEGMENT 1 USING ALL 11 $M^2$S SPECTRAL CHANNELS

| | Spatial Resolution | | | | | | |
|---|---|---|---|---|---|---|---|
| | $(2M)^2$ | $(4M)^2$ | $(8M)^2$ | $(16M)^2$ | $(32M)^2$ | $(64M)^{2*}$ | % of Total Area |
| **Hierarchy: Condition Class** | | | | | | | |
| Conifer Regen. (2,3) | 51.1 | 55.9 | 61.3 | 67.7 | 70.5 | 87.3 | 36.4 |
| Loblolly-Imm. (2.5) | 29.1 | 37.0 | 44.5 | 58.7 | 65.2 | --- | 3.7 |
| Loblolly-Mature (2.6) | 16.9 | 15.5 | 16.8 | 21.9 | 19.6 | 44.4 | 14.8 |
| Shortleaf-Imm. (1,3) | 38.1 | 31.4 | 33.0 | 27.6 | 35.6 | 71.4 | 20.2 |
| Shortleaf-Mature (1,4) | 40.9 | 54.0 | 57.3 | 63.2 | 75.6 | 85.0 | 24.8 |
| Overall | 40.0 | 43.8 | 47.4 | 51.6 | 57.4 | 76.9 | |
| **Hierarchy: Growth Stage** | | | | | | | |
| Conifer Regen. (2.3) | 51.1 | 55.9 | 61.3 | 67.7 | 70.5 | 87.3 | 36.4 |
| Imm. Sawtimber | 54.2 | 52.7 | 57.7 | 61.1 | 60.6 | 65.1 | 23.9 |
| Mature Sawtimber | 42.0 | 48.8 | 50.0 | 55.0 | 62.2 | 71.6 | 39.7 |
| Overall | 48.2 | 52.3 | 55.9 | 61.1 | 65.1 | 76.2 | |
| **Hierarchy: Cover Type** | | | | | | | |
| Conifer Regen. (2,3) | 51.1 | 55.9 | 61.3 | 67.7 | 70.5 | 87.3 | 36.4 |
| Shortleaf Pine | 66.7 | 66.7 | 67.0 | 65.6 | 75.0 | 90.7 | 45.0 |
| Loblolly Pine | 37.5 | 40.9 | 45.4 | 53.5 | 44.8 | 45.7 | 18.6 |
| Overall | 55.6 | 58.0 | 60.9 | 64.1 | 67.8 | 80.7 | |
| **Hierarchy: Physiognomy** | | | | | | | |
| Conifer Regen. (2,3) | 51.1 | 55.9 | 61.3 | 67.7 | 70.5 | 87.3 | 36.4 |
| Pine Sawtimber | 84.2 | 83.5 | 84.9 | 87.1 | 88.0 | 90.9 | 63.6 |
| Overall | 72.1 | 73.4 | 76.3 | 80.0 | 81.2 | 89.5 | |

* The (64 meters)$^2$ data set did not contain a signature for Immature Loblolly Pine (2.5)

TABLE 5. PERCENT CORRECT CLASSIFICATION BOUNDARY EXCLUSIVE TEST SETS IN DATA SEGMENT 1 USING ALL 11 $M^2$S SPECTRAL CHANNELS

| | Spatial Resolution | | | | | | |
|---|---|---|---|---|---|---|---|
| | $(2M)^2$ | $(4M)^2$ | $(8M)^2$ | $(16M)^2$ | $(32M)^2$ | $(64M)^{2*}$ | % of Total Area |
| **Hierarchy: Condition Class** | | | | | | | |
| Conifer Regen. (2.3) | 49.9 | 54.8 | 59.3 | 64.6 | 71.4 | 78.6 | 37.3 |
| Loblolly-Imm. (2.5) | 26.3 | 32.3 | 39.1 | 49.6 | 56.8 | --- | 3.8 |
| Loblolly-Mature (2.6) | 19.7 | 19.2 | 20.9 | 26.6 | 19.4 | 31.0 | 13.8 |
| Shortleaf-Imm. (1.3) | 33.3 | 24.2 | 23.8 | 22.7 | 31.6 | 39.5 | 29.6 |
| Shortleaf-Mature (1.4) | 40.8 | 54.4 | 57.2 | 63.3 | 73.0 | 82.1 | 15.4 |
| Overall | 38.5 | 40.0 | 42.4 | 46.2 | 52.2 | 59.9 | |
| **Hierarchy: Growth Stage** | | | | | | | |
| Conifer Regen. (2.3) | 49.9 | 54.8 | 59.3 | 64.6 | 71.4 | 78.6 | 37.3 |
| Imm. Sawtimber | 50.7 | 45.0 | 48.6 | 50.2 | 53.5 | 40.2 | 33.5 |
| Mature Sawtimber | 40.9 | 46.5 | 47.5 | 52.6 | 54.2 | 59.3 | 29.2 |
| Overall | 47.5 | 49.1 | 52.3 | 56.3 | 60.7 | 61.9 | |
| **Hierarchy: Cover Type** | | | | | | | |
| Conifer Regen. (2.3) | 49.9 | 54.8 | 59.3 | 64.6 | 71.4 | 78.6 | 37.3 |
| Shortleaf Pine | 64.4 | 62.6 | 60.6 | 61.6 | 67.0 | 80.0 | 45.1 |
| Loblolly Pine | 38.0 | 41.1 | 46.0 | 53.4 | 42.4 | 33.3 | 17.6 |
| Overall | 53.9 | 55.8 | 57.6 | 61.1 | 64.6 | 71.8 | |
| **Hierarchy: Physiognomy** | | | | | | | |
| Conifer Regen. (2.3) | 49.9 | 54.8 | 59.3 | 64.6 | 71.4 | 78.6 | 37.3 |
| Pine Sawtimber | 82.7 | 81.5 | 82.3 | 84.7 | 82.8 | 80.4 | 62.7 |
| Overall | 70.5 | 71.4 | 73.6 | 76.8 | 78.3 | 79.6 | |

* The (64 meters)$^2$ data set did not contain a signature for Immature Loblolly Pine (2.5).

TABLE 6. PERCENT CORRECT CLASSIFICATION OF BOUNDARY INCLUSIVE TEST SETS IN DATA SEGMENT 1 USING ALL 11 $M^2S$ SPECTRAL CHANNELS

| | Spatial Resolution | | | | | | |
|---|---|---|---|---|---|---|---|
| | $(2M)^2$ | $(4M)^2$ | $(8M)^2$ | $(16M)^2$ | $(32M)^2$ | $(64M)^{2*}$ | % of Total Area |
| **Hierarchy: Condition Class** | | | | | | | |
| Conifer Regen. (2.3) | 50.0 | 54.8 | 58.9 | 63.0 | 70.1 | 76.3 | 37.3 |
| Loblolly -Imm. (2.5) | 26.5 | 32.1 | 38.5 | 48.1 | 47.1 | --- | 3.8 |
| Loblolly-Mature (2.6) | 19.7 | 19.1 | 20.9 | 26.5 | 17.4 | 34.6 | 13.8 |
| Shortleaf-Imm. (1.3) | 33.3 | 24.2 | 23.7 | 21.9 | 28.9 | 29.3 | 29.6 |
| Shortleaf-Mature (1.4) | 40.8 | 54.3 | 57.4 | 63.9 | 73.7 | 74.1 | 15.4 |
| Overall | 38.5 | 39.9 | 42.2 | 45.4 | 50.1 | 54.3 | 56.2 |
| **Hierarchy: Growth Stage** | | | | | | | |
| Conifer Regn. (2.3) | 52.0 | 54.8 | 58.9 | 63.0 | 70.1 | 76.3 | 37.3 |
| Imm. Sawtimber | 50.7 | 45.0 | 48.3 | 48.3 | 48.5 | 28.5 | 33.5 |
| Mature Sawtimber | 40.9 | 46.4 | 47.5 | 52.8 | 53.8 | 58.2 | 29.2 |
| Overall | 47.6 | 49.1 | 52.1 | 55.2 | 58.2 | 55.8 | 57.8 |
| **Hierarchy: Cover Type** | | | | | | | |
| Conifer Regn. (2.3) | 50.0 | 54.8 | 58.9 | 63.0 | 70.1 | 76.3 | 37.3 |
| Shortleaf Pine | 63.4 | 62.6 | 60.9 | 62.4 | 67.8 | 70.7 | 45.1 |
| Loblolly Pine | 38.1 | 41.0 | 45.9 | 53.5 | 40.3 | 37.9 | 17.6 |
| Overall | 53.9 | 55.8 | 57.5 | 61.0 | 63.7 | 67.5 | 69.9 |
| **Hierarchy: Physiognomy** | | | | | | | |
| Conifer Regen. (2.3) | 50.0 | 54.8 | 58.9 | 63.0 | 70.1 | 76.3 | 37.3 |
| Pine Sawtimber | 82.7 | 81.5 | 82.2 | 84.4 | 81.3 | 72.1 | 62.7 |
| Overall | 70.5 | 71.4 | 73.5 | 76.2 | 77.1 | 73.8 | |

* The (64 meters)$^2$ data set did not contain a signature for Immature Loblolly Pine (2.5).

features in the respective hierarchies and the overall percent correct classification accuracy is also provided for each hierarchy.

Results for individual features within the various hierarchies show that classification accuracies can vary widely from feature to feature for any one case of spatial resolution. For example, in Table 4 for (2 meters)$^2$ data, conifer regeneration exhibits 51.1% accuracy, whereas mature Loblolly Pine sawtimber is only 16.9% accurate. Furthermore, the trends in classification accuracy as a function of spatial resolution are not entirely uniform from feature to feature. To illustrate again in Table 4, mature Loblolly Pine sawtimber and immature Shortleaf Pine sawtimber are not consistently better classified in coarser resolution data as are the other condition class features in the hierarchy. Such results are more than likely caused by: (a) significant amounts of overlap among the distributions of the signatures, and (b) subtle changes in the size, shape, and hyperspace position of individual signature distributions relative to the data values as spatial resolution varies. Although an exhaustive signature analysis for each case of spatial resolution would in all likelihood enable explanation of results on a feature by feature basis, such an approach might not enable generalizations concerning the overall significance of spatial resolution which are cogent for this study. Thus, the discussion of results presented here will dwell primarily on the overall classification accuracies achieved for hierarchies, with the understanding that such accuracies are derived from the combined accuracies of individual features contained within the hierarchies.

Figures 4-7 illustrate the overall classification accuracies for each of the hierarchies of features considered in data segment 1. In each figure, accuracy is shown as a function of spatial resolution for the three regions of data for which performance was assessed. Note that for all such regions, accuracies improve for hierarchies of more general (aggregated) features. That is, improvement occurs as a

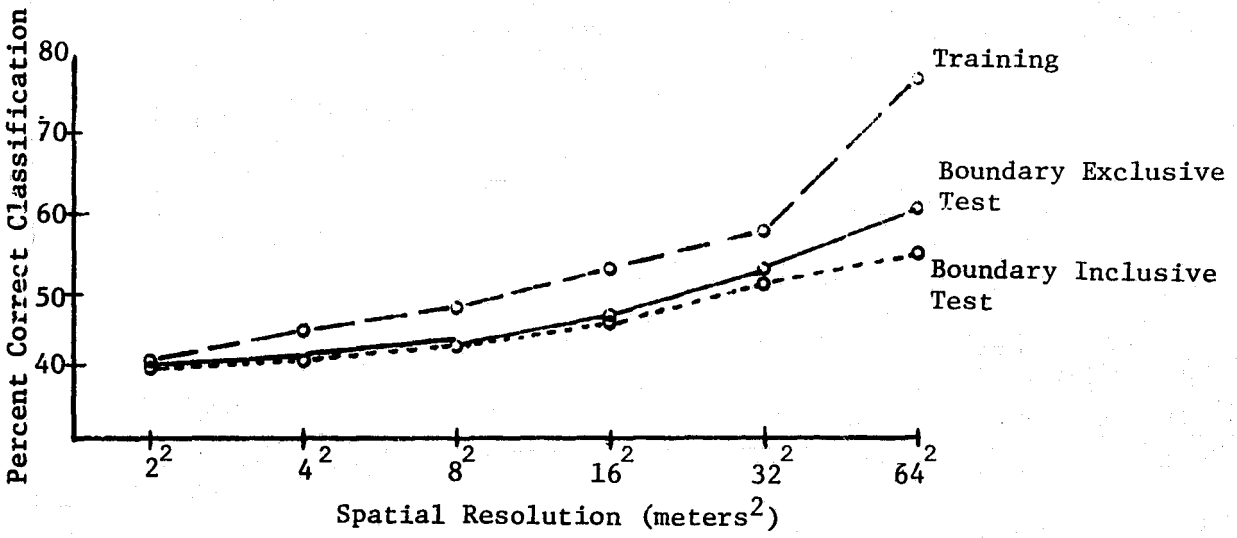


FIGURE 4. CLASSIFICATION ACCURACY PLOTTED AS A FUNCTION OF SPATIAL RESOLUTION FOR CONDITION CLASSES OF DATA SEGMENT 1

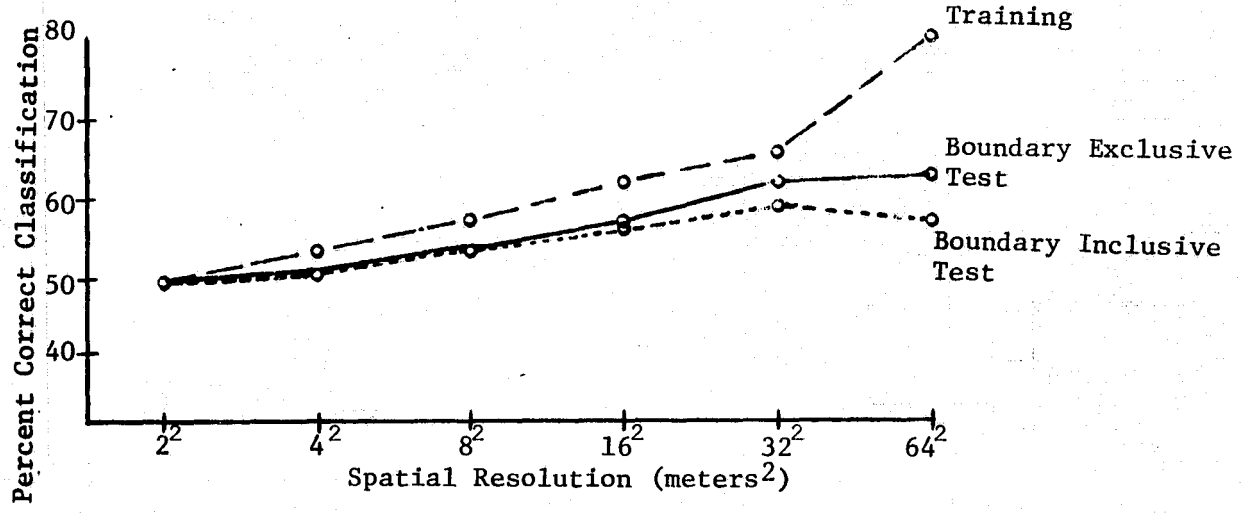


FIGURE 5. CLASSIFICATION ACCURACY PLOTTED AS A FUNCTION OF SPATIAL RESOLUTION FOR GROWTH STAGES OF DATA SEGMENT 1

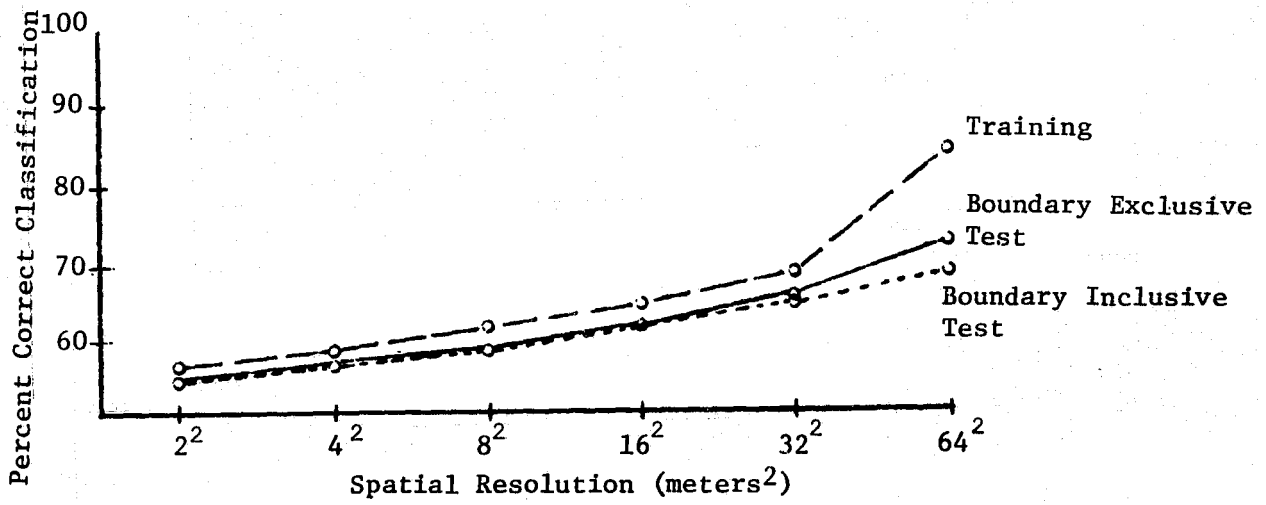


FIGURE 6. CLASSIFICATION ACCURACY PLOTTED AS A FUNCTION OF SPATIAL RESOLUTION FOR COVER TYPES OF DATA SEGMENT 1

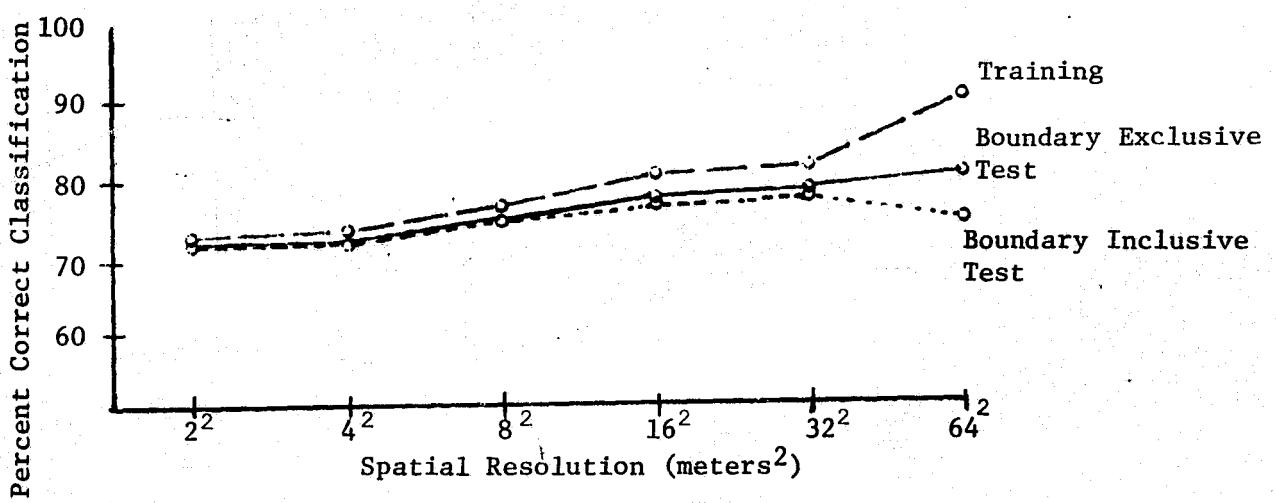


FIGURE 7. CLASSIFICATION ACCURACY PLOTTED AS A FUNCTION OF SPATIAL RESOLUTION FOR PHYSIOGNOMY OF DATA SEGMENT 1

result of aggregating the performance of specific condition class features into more general feature categories first on the basis of growth stage, second on cover type, and finally on physiognomy. For each general category of feature, previous misclassifications of resolution elements among its specific features were properly counted as correct classification, reducing the total amount of misclassified elements for the respective hierarchy. Thus, the overall accuracy for classifying the physiognomic hierarchy of forest features is higher than for hierarchies of more specific classes -- a not-surprising result. The greater overall accuracy for cover type hierarchy versus growth stage seems to be due to a greater occurrence of hardwood species in the Loblolly Pine stands.

In comparing classification performance for training sets, boundary exclusive test sets, and boundary inclusive test sets, overall accuracy for training sets improves with coarser spatial resolution for all hierarchies. Accuracies for total feature areas (both boundary exclusive test sets and boundary inclusive test sets) are somewhat lower for large cases of resolution, and do not necessarily continue to improve. These results can be attributed to changes in the number of resolution elements within each feature that are either wrongly classified (i.e., misclassified) or not classified (i.e., unclassified) as spatial resolution varies.

Classification accuracy for training sets can be regarded as an upper limit of performance for classifying this set of features with the specified procedures, since the resolution elements classified are the same ones used to create the signature distributions. In other words, by classifying training sets, we determine the expected-performance for classifying the entire data set assuming that the variance within each feature area is completely described by its training area. (Depending on the training procedure and the site information available, this latter assumption is not always true.) Figure 8 shows that, as resolution size

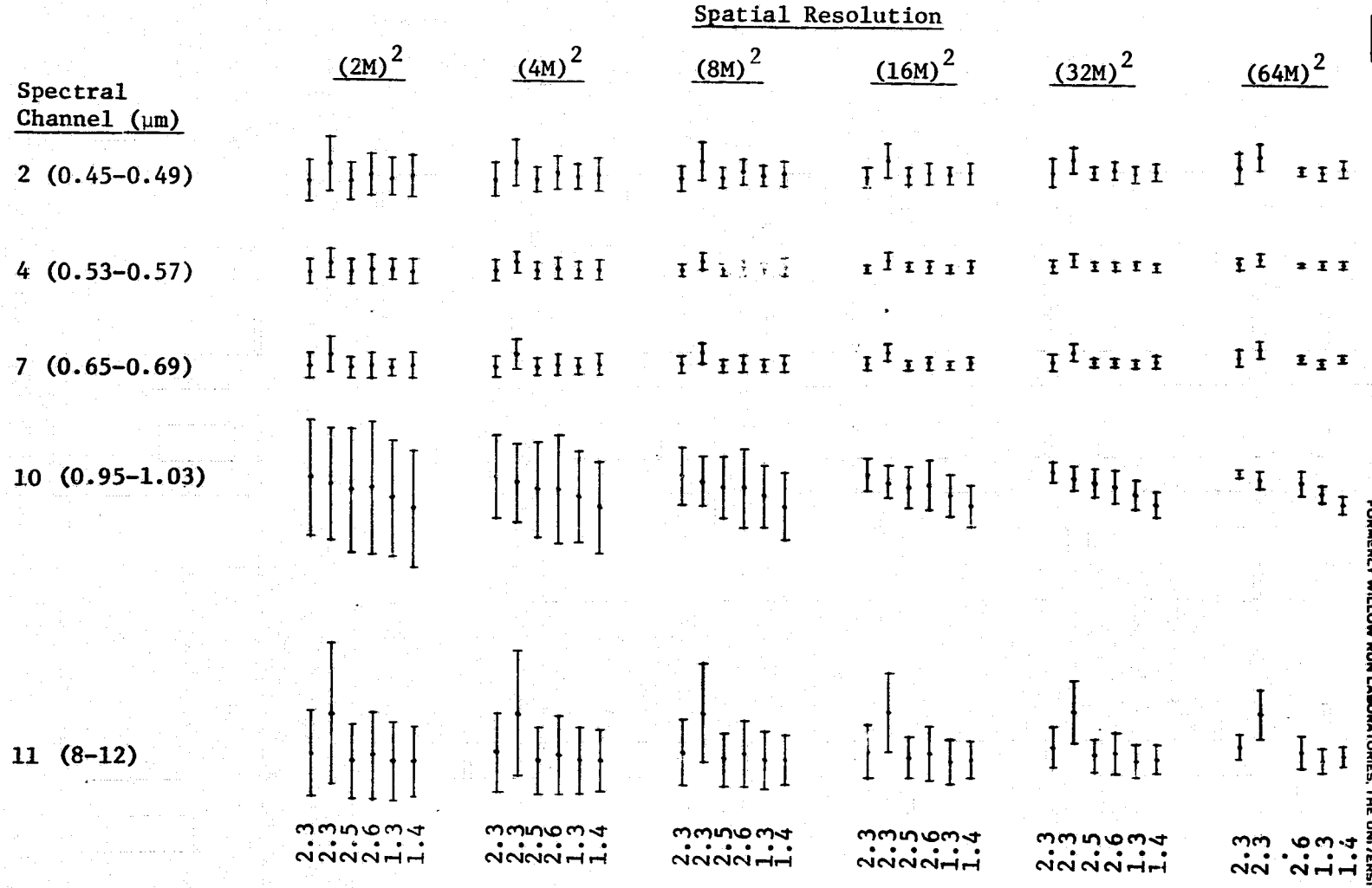


FIGURE 8. SIGNATURE MEANS AND STANDARD DEVIATIONS OF SELECTED SPECTRAL CHANNELS FOR SPATIAL RESOLUTIONS $(2)^2$ - $(64M)^2$

increases for each of the simulated data sets, the standard deviations of the signatures decrease. This indicates that the variance within each training set becomes smaller. Because the signature means for the most part remain unchanged as resolution varies, the amount of statistical overlap among the distributions of the signatures must decrease. As a result, resolution elements within training sets classified in the coarser resolution data sets have higher probabilities of being correctly classified. It is possible that an increased percentage of elements in coarser resolution data might also be unclassified if the rejection threshold remains constant since a relatively smaller total decision space is represented by the signature distributions. However, Figure 8 illustrates that, for this set of signatures, considerable statistical overlap exists in all spectral channels even for the coarse resolution data and Figure 9 verifies that for resolution elements within training sets, the total number of unclassified elements varied only slightly as a function of resolution.

The decreases in classification accuracy from training sets to total feature areas in Figures 4-7 are attributable to greater percentages of both misclassified and unclassified resolution elements within each feature area. Such decreases in accuracy are more than likely caused by the confounding effect on the decision process of the increased variability within feature areas not represented by training sets. For cases of fine spatial resolution, signature distributions are large enough to encompass much of the total variability manifested by data values from all feature areas. The low percentage of unclassified elements in Figure 9 for resolution cases of (2 meters)$^2$ through (16 meters)$^2$ indicates that much of the reduced classification accuracy over the entire feature areas for these resolution cases is due to increased misclassification of elements. The considerable overlap among the distributions would account for the great amount of misclassification. As resolution coarsens to (32 meters)$^2$ and (64 meters)$^2$

however, the reduced signature distributions may encompass less of the total data variability, and, thus, the percentage of unclassified data values increases greatly.

The inclusion of boundary elements into the decision process can be expected to introduce additional variance into the population of data values within each feature. Their impact on reducing classification accuracy for each feature will depend on the ratio of the number of boundary elements to total feature elements. Obviously, this ratio will increase as spatial resolution degrades. Thus, the classification results for boundary inclusive test sets in Figures 4-7 show a not-surprising reduced accuracy relative to boundary exclusive test sets as spatial resolution degrades. The effect of the boundary elements becomes substantial in $(64 \text{ meters})^2$ data; and for the hierarchies of growth stages and physiognomy, actually reduces performance below that achieved for $(32 \text{ meters})^2$ data.

Abrupt increases in classification accuracy that occur from $(32 \text{ meters})^2$ to $(64 \text{ meters})^2$ data for training sets (Figures 4-7) are most likely due to the fact that there is one less signature to classify the $(64 \text{ meters})^2$ data. Figure 8 illustrates (for 5 of the 11 channels) that the mean signal values for this set of signatures are very similar. As a result, the overlapping standard deviations make the unique classification of these features very difficult. Despite the decrease in statistical overlap that occurs in Figure 8 as spatial resolution degrades, a large amount of overlap still remains in the $(64 \text{ meters})^2$ data. In such circumstances, the less of one competing signature (immature Loblolly Pine sawtimber) from a tightly packed group of signatures might result in sufficient reduction of total statistical overlap among the signatures to reduce the number of misclassifications in the training set results of this study. The small 2% increase in unclassified elements of training sets from $(32 \text{ meters})^2$ to $(64 \text{ meters})^2$ data noted in Figure 9

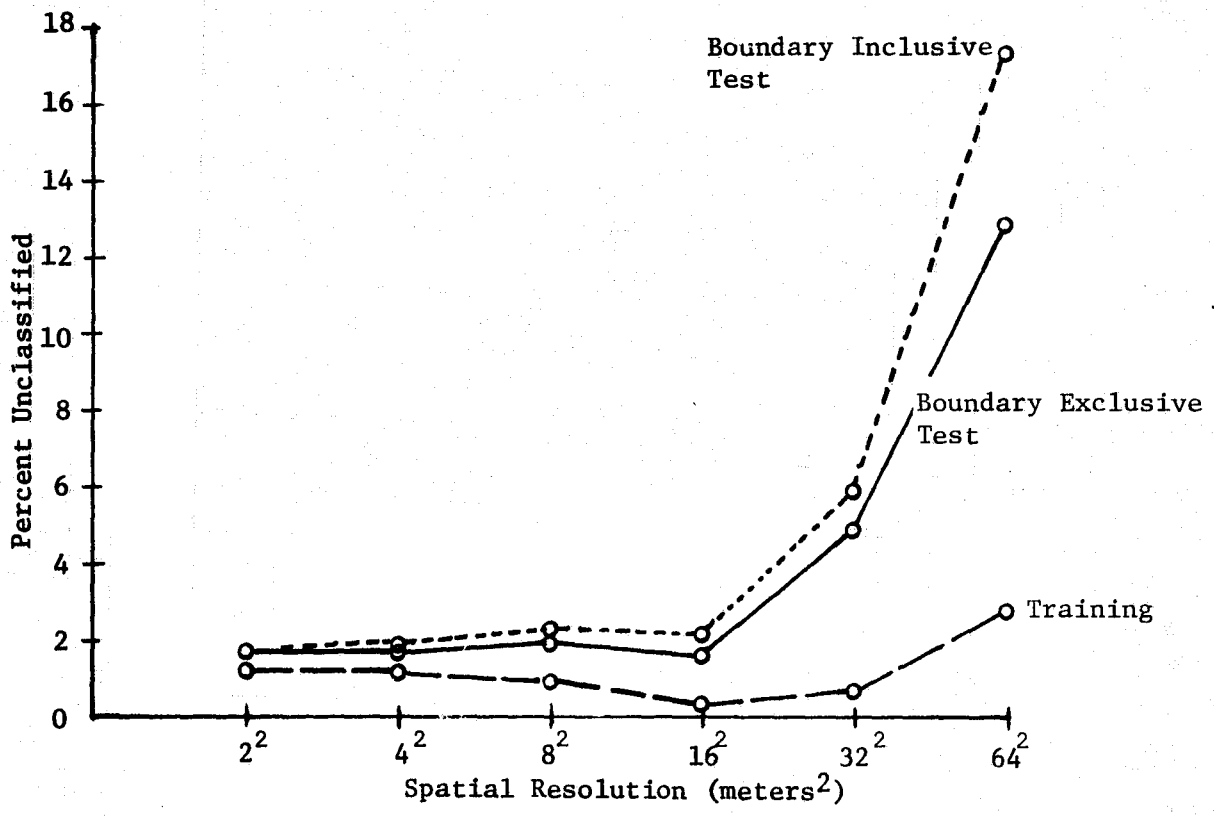


FIGURE 9. THE PROPORTION OF ELEMENTS FOR 11 CHANNEL $M^2S$ CLASSIFICATION WHICH WERE UNCLASSIFIED USING A REJECTION THRESHOLD OF 0.001 PLOTTED AS A FUNCTION OF SPATIAL RESOLUTION

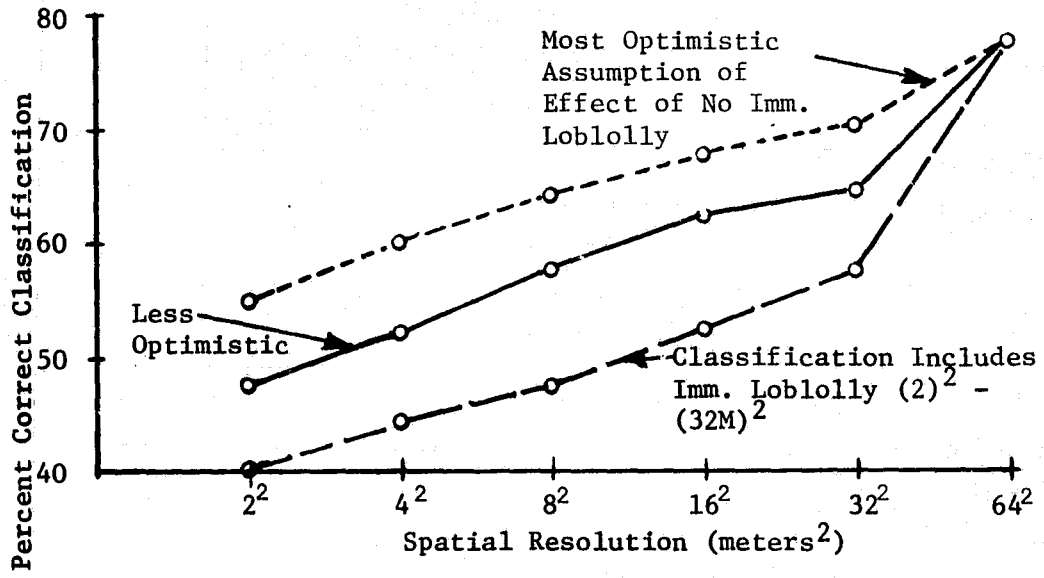


FIGURE 10. SIMULATION OF THE OVERALL PERCENT CORRECT CLASSIFICATION OVER CONDITION CLASSES FOR TRAINING SETS IN DATA SEGMENT 1 OMITTING THE IMMATURE LOBLOLLY PINE SIGNATURE

verifies that few resolution elements of training sets, classified as immature Loblolly Pine sawtimber in $(32 \text{ meters})^2$ data, were outside the decision boundaries of the remaining signatures in the $(64 \text{ meters})^2$ data. Thus, the dramatic improvement in classification accuracy for training sets in $(64 \text{ meters})^2$ data is due to the reduction in misclassification of resolution elements.

Figure 10 illustrates simulated results of having classified training sets on $(2 \text{ meters})^2$ through $(32 \text{ meters})^2$ data with the 5 signatures corresponding to those used to process $(64 \text{ meters})^2$ data. The topmost dashed curve assumes that all resolution elements previously misclassified as immature Loblolly Pine sawtimber would have been correctly classified. The lower dashed curve makes the less optimistic assumption that only the elements of features most frequently misclassified as immature Loblolly Pine sawtimber (namely, immature Shortleaf Pine sawtimber and mature Loblolly Pine sawtimber) would have been correctly classified. (Because of the very small percentage of unclassified elements shown for the $(64 \text{ meters})^2$ results in Figure 9, we did not allow for any increase in unclassified elements for these simulated results.) Note that both dashed curves show sizable improvements in training area classification performance as a result of corresponding decreases in misclassifications that were attributable to the deleted signature. We speculate that the less dramatic improvement in training area classification from $(32 \text{ meters})^2$ to $(64 \text{ meters})^2$ data is more representative of the results that would have been achieved if all cases of spatial resolution could have been processed uniformly.

To investigate the effects on whole feature areas, Figures 11 and 12 illustrate simulated results of having classified boundary exclusive test sets and boundary inclusive test sets in all cases of spatial resolution with the 5 signatures corresponding to those used to process the

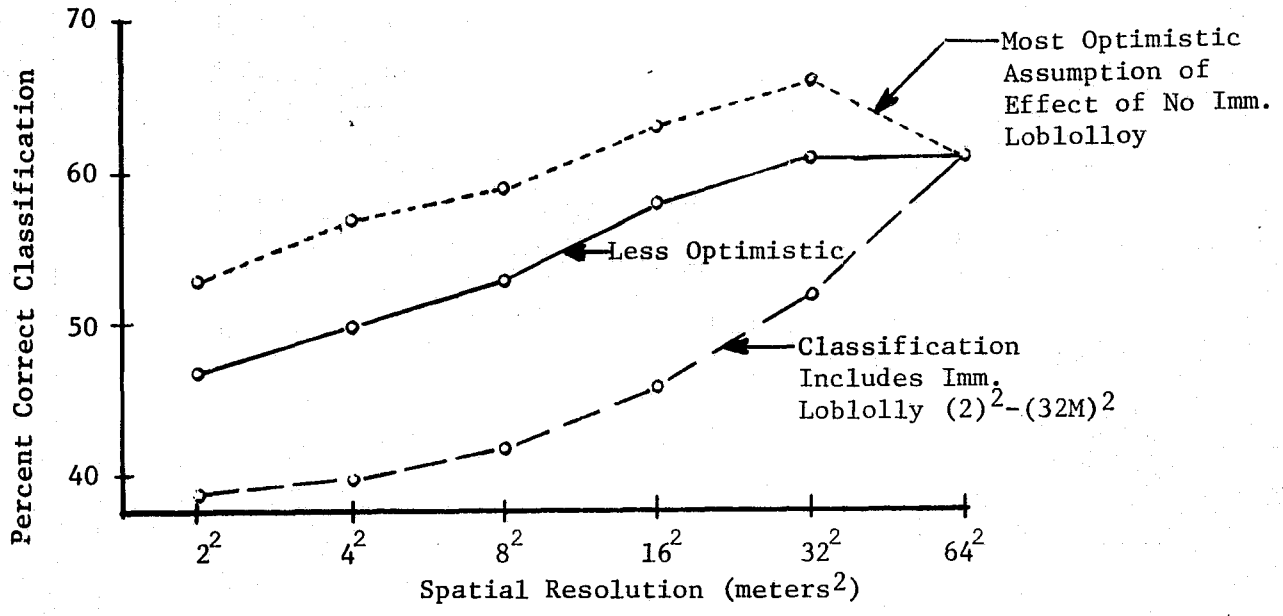


FIGURE 11. SIMULATION OF THE OVERALL PERCENT CORRECT CLASSIFICATION OVER CONDITION CLASSES FOR BOUNDARY EXCLUSIVE TEST SETS IN DATA SEGMENT 1 OMITTING THE IMMATURE LOBLOLLY PINE SIGNATURE

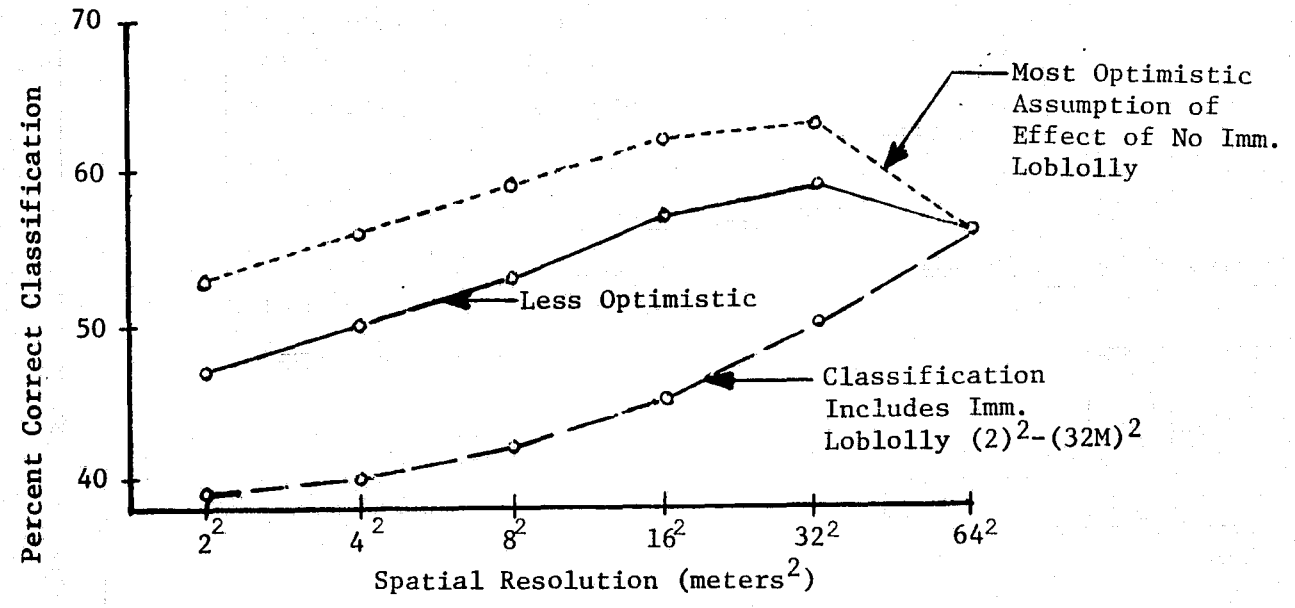


FIGURE 12. SIMULATION OF THE OVERALL PERCENT CORRECT CLASSIFICATION OVER CONDITION CLASSES FOR BOUNDARY INCLUSIVE TEST SETS IN DATA SEGMENT 1 OMITTING THE IMMATURE LOBLOLLY PINE SIGNATURE

(64 meters)$^2$ data. The assumptions for the two dashed curves in each figure are the same as for Figure 10. Again, no allowance was made for any increase in unclassified elements from (2 meters)$^2$ to (32 meters)$^2$. These figures illustrate that, for most cases of spatial resolution, sizable improvements in classification performance might again be achieved when misclassifications attributable to the deleted signature are reduced. However, for the (64 meters)$^2$ data, the large percentages of unclassified elements, noted in Figure 9, seem to overcompensate any improvement in performance due to reduced misclassifications. As a result, a net decrease in classification performance is indicated from (32 meters)$^2$ to (64 meters)$^2$ data. Although less abrupt, similar decreases in classification performance were noticeable for (64 meters)$^2$ data in Figures 5 and 7. Thus, it appears that for this data set, the effect of the increased variability in the data values of whole feature areas is to increase the percentages of unclassified resolution elements if the rejection threshold remains constant, and that the effect of unclassified elements begins to detract from overall classification accuracy as spatial resolution enlarges beyond (32 meters)$^2$. It is possible that a reduction in such an effect for the degraded resolution may be overcome by modifying the rejection threshold to reduce the number of unclassified elements while hopefully at the same time not unduly increasing the number of elements which are misclassified.

Data Segment 2

Six signatures were extracted from training sets and used to classify data segment 2 for all cases of spatial resolution. The large amount of scene variation within the immature Laurel Oak/Willow Oak feature (Feature 3.1, Figure 2) prompted us to extract three signatures to adequately characterize it. A single signature was used for each of the remaining features.

The correct classification results are summarized in Tables 7-9 for training sets, boundary exclusive test sets, and boundary inclusive

TABLE 7. PERCENT CORRECT CLASSIFICATION OF TRAINING SETS IN DATA SEGMENT 2 USING ALL 11 $M^2$S SPECTRAL CHANNELS

| | Spatial Resolution | | | | | | |
|---|---|---|---|---|---|---|---|
| Hierarchy: Condition Class | $(2M)^2$ | $(4M)^2$ | $(8M)^2$ | $(16M)^2$ | $(32M)^2$ | $(64M)^2$ | % of Total Area |
| Loblolly - Imm. (2.5) | 85.7 | 84.5 | 86.7 | 89.6 | 93.8 | 100.0 | 21.5 |
| Laurel Oak/Willow Oak (3.1) | 65.7 | 73.5 | 78.8 | 84.0 | 88.3 | 86.8 | 34.0 |
| Swtgm/N. Oak/W. Oak (4.2) | 12.8 | 18.8 | 24.7 | 30.1 | 40.9 | 48.1 | 33.4 |
| Cut Over (7.1) | 90.2 | 91.9 | 95.6 | 98.5 | 100.0 | 95.8 | 11.1 |
| Overall 1* | 55.0 | 59.6 | 64.2 | 68.7 | 74.5 | 76.3 | |
| Overall 2** | 76.2 | 80.1 | 84.2 | 88.2 | 92.1 | 92.6 | |
| Hierarchy: Physiognomy | | | | | | | |
| Conifer Sawtimber (2.5) | 85.7 | 84.5 | 86.7 | 89.6 | 93.8 | 100.0 | 21.5 |
| Hardwood Sawtimber | 72.1 | 80.6 | 86.2 | 91.5 | 96.6 | 89.8 | 67.4 |
| Cut Over (7.1) | 90.2 | 91.9 | 95.6 | 98.5 | 100.0 | 95.8 | 11.1 |
| Overall | 77.0 | 82.7 | 87.4 | 91.9 | 96.4 | 92.6 | |

*1 Overall calculated for all training sets.

**2 Overall calculated omitting 4.2

test sets, respectively. For training sets (Table 7), note that two sets of numbers are provided for the overall accuracies of the hierarchy containing condition class features. The lower accuracies were obtained by the usual combining of all training set accuracies weighted according to their respective proportions of total training area classified. The higher accuracies portray the results of combining all training set accuracies except the immature Sweetgum/Nuttal Oak feature (Feature 4.2, Figure 2).

Because of the great similarity between the two hardwood condition classes, competition for the data values within the training set of Feature 4.2 was probably biased in favor of the three signatures representing Feature 3.1 versus the single signature of Feature 4.2. Therefore, the classification accuracy for the Feature 4.2 training area is understandably quite low. However, as a result of the large proportion (33.4%) of total training set area it occupies, the effect of including it in the overall condition class hierarchy results is to create training set accuracies that are lower than those achieved for the same hierarchy over whole feature areas (Tables 8 and 9). Such results are inconsistent with expected trends in classification accuracy from training sets to whole feature areas. In addition, much of the training set for Feature 4.2 lies outside the previously defined nadir region of the data ($30^{o}$ either side of the flightline nadir). (Because only a small portion of this feature existed inside the nadir region, much of the training area required for a valid signature falls outside the region.) Since classification results for whole feature areas were computed only inside the nadir region, a comparison of results between training sets and whole feature areas involves different regions of the data if the training area for Feature 4.2 is included. By excluding the Feature 4.2 training set results from the overall classification accuracies of the condition class hierarchy in Table 7, we enable a more straightforward comparison of results from training sets to whole feature areas.

TABLE 8. PERCENT CORRECT CLASSIFICATION OF BOUNDARY EXCLUSIVE TEST SETS IN DATA SEGMENT 2 USING ALL 11 $M^2S$ SPECTRAL CHANNELS

| | Spatial Resolution | | | | | | |
|---|---|---|---|---|---|---|---|
| Hierarchy: Condition Class | $(2M)^2$ | $(4M)^2$ | $(8M)^2$ | $(16M)^2$ | $(32M)^2$ | $(64M)^2$ | % of Total Area |
| Loblolly - Imm. (2.5) | 73.8 | 71.2 | 71.8 | 73.2 | 79.7 | 86.0 | 19.1 |
| Laurel Oak/Willow Oak (3.1) | 61.8 | 67.4 | 70.0 | 74.6 | 76.9 | 62.1 | 49.6 |
| Swtgm/N. Oak/W. Oak (4.2) | 11.4 | 16.5 | 21.2 | 30.3 | 49.4 | 50.0 | 7.5 |
| Cut Over (7.1) | 78.4 | 80.6 | 81.6 | 85.3 | 91.1 | 75.4 | 23.9 |
| Overall | 64.2 | 67.5 | 69.5 | 74.1 | 79.0 | 69.3 | |
| Hierarchy: Physiognomy | | | | | | | |
| Conifer Sawtimber (2.5) | 73.8 | 71.2 | 71.8 | 73.2 | 79.7 | 86.0 | 19.1 |
| Hardwood Sawtimber | 69.9 | 78.3 | 83.7 | 89.2 | 94.2 | 84.3 | 57.1 |
| Cut Over (7.1) | 78.4 | 80.6 | 81.6 | 85.3 | 91.1 | 75.4 | 23.9 |
| Overall | 72.7 | 77.5 | 81.0 | 85.2 | 90.7 | 82.6 | |

TABLE 9. PERCENT CORRECT CLASSIFCATION OF BOUNDARY INCLUSIVE TEST SETS IN DATA SEGMENT 2 USING ALL 11 $M^2S$ SPECTRAL CHANNELS

| | Spatial Resolution | | | | | | |
|---|---|---|---|---|---|---|---|
| Hierarchy: Condition Class | $(2M)^2$ | $(4M)^2$ | $(8M)^2$ | $(16M)^2$ | $(32M)^2$ | $(64M)^2$ | % of Total Area |
| Loblolly - Imm. (2.5) | 74.0 | 71.1 | 70.6 | 70.5 | 71.0 | 72.9 | 19.1 |
| Laurel Oak/Willow Oak (3.1) | 61.8 | 67.3 | 69.8 | 74.0 | 74.8 | 59.7 | 49.6 |
| Swtgm/N. Oak/W. Oak (4.2) | 11.4 | 16.4 | 21.4 | 30.5 | 47.6 | 50.0 | 7.4 |
| Cut Over (7.1) | 78.6 | 80.6 | 81.2 | 84.0 | 89.3 | 74.2 | 23.9 |
| Overall | 64.4 | 67.5 | 69.0 | 72.6 | 75.3 | 64.9 | |
| Hierarchy: Physiognomy | | | | | | | |
| Conifer Sawtimber (2.5) | 74.0 | 71.1 | 70.6 | 70.5 | 71.0 | 72.9 | 19.1 |
| Hardwood Sawtimber | 70.0 | 78.3 | 83.6 | 88.8 | 94.1 | 85.5 | 57.1 |
| Cut Over (7.1) | 78.6 | 80.6 | 81.2 | 84.0 | 89.3 | 74.2 | 23.9 |
| Overall | 72.8 | 77.5 | 80.6 | 84.2 | 88.6 | 80.5 | |

Overall classification accuracies for the two hierarchies of features considered are illustrated in Figures 13 and 14. Many of the trends noted for data segment 1 are again in evidence here. These include: a continued improvement in classification accuracies for resolution cases increasing from (2 meters)$^2$ to (32 meters)$^2$; generally higher classification accuracies for the hierarchy of more general (aggregated) features; and a reduction in classification accuracies from training sets to total feature areas, with the inclusion of boundary elements further depressing accuracies as spatial resolution degrades.

Two major differences are noted for the results of Figures 13 and 14 versus those for the corresponding hierarchies of data segment 1. The first is that, for equivalent hierarchies between the two data segments, overall classification accuracies are higher in data segment 2. The second difference concerns a more obvious decrease in performance for the (64 meters)$^2$ case of spatial resolution in data segment 2 that occurs for whole feature areas and even training sets for the physiognomy hierarchy. These differences are most likely explained by the more unique characteristics of the features in data segment 2. Signatures of pines, hardwoods, and cutover land likely had less statistical overlap than signatures of the more similar types of features in data segment 1. Thus, misclassifications of resolution elements in data segment 2 may well have been lower, accounting for the generally higher classification performances for the hierarchies. For (64 meters)$^2$ data, the reduced size of these signature distributions may have resulted in a larger amount of unclassified decision space among the distributions, such that dramatic increases in the percentage of unclassified elements caused an abrupt decrease in classification performance.

### 4.1.2 Multi-element Processing Techniques for Improving Classification Performance

For conventional linear and quadratic decision rules, classification is based on each individual resolution element. Multi-element decision

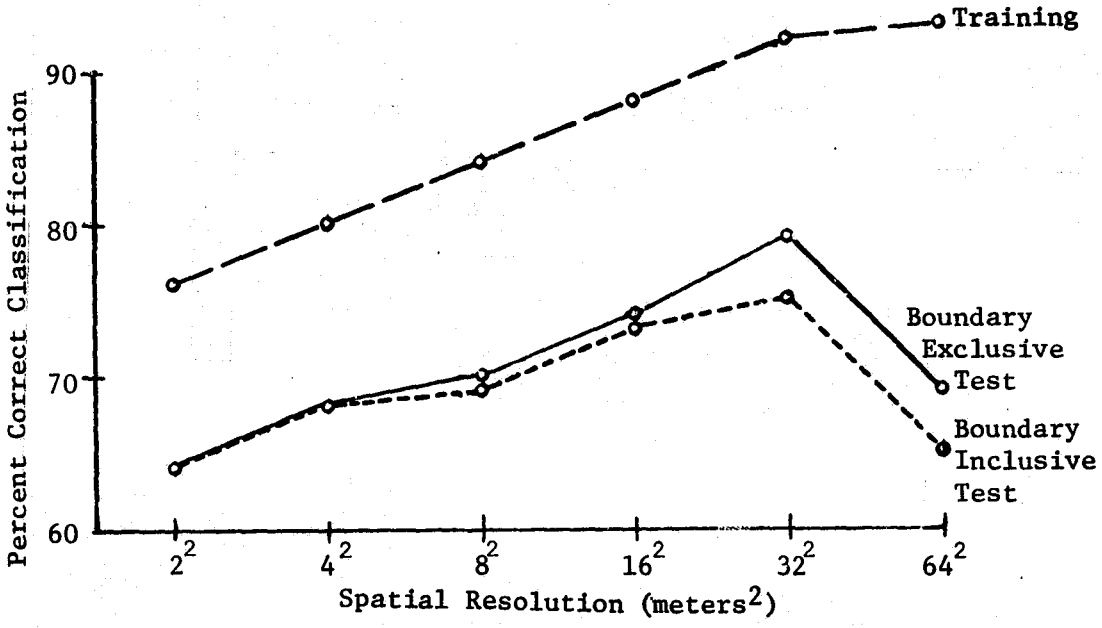


FIGURE 13. CLASSIFICATION ACCURACY PLOTTED AS A FUNCTION OF SPATIAL RESOLUTION FOR CONDITION CLASSES OF DATA SEGMENT 2

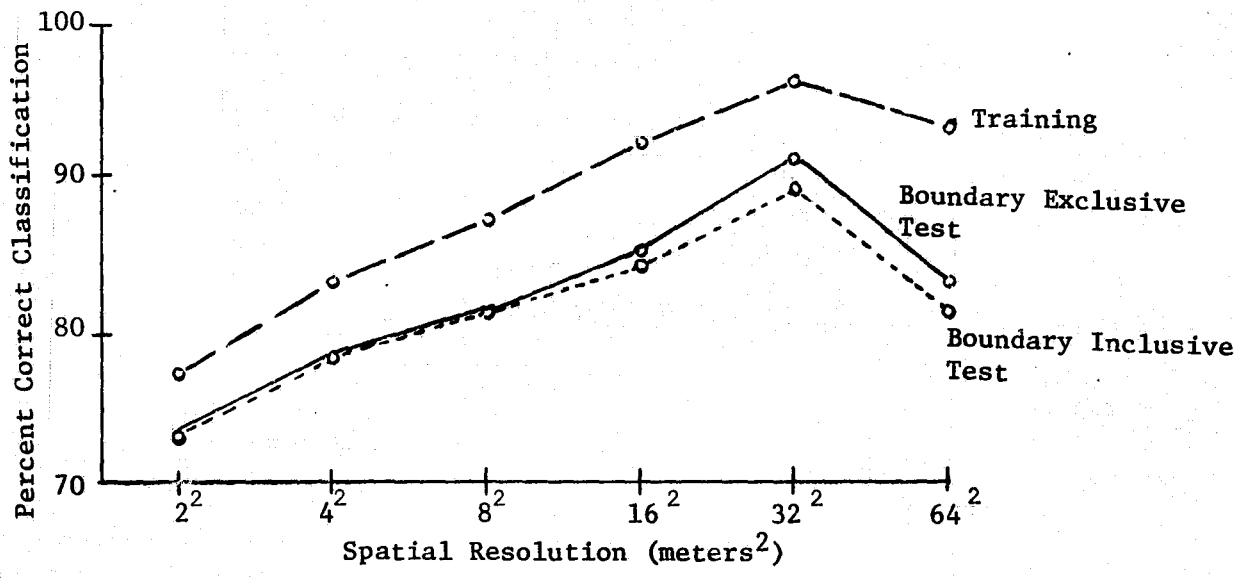


FIGURE 14. CLASSIFICATION ACCURACY PLOTTED AS A FUNCTION OF SPATIAL RESOLUTION FOR PHYSIOGNOMY OF DATA SEGMENT 2

rules, by contrast, use information from the surrounding elements when classifying the center element. Improvements in classification accuracy due to degraded spatial resolution (Section 4.1.1) are apparently due to the reduced variation within the scene that occurs by averaging information over larger ground areas. By using information from surrounding elements, multi-element decision rules attempt to provide the improved classification advantages of coarser spatial resolutions without the loss of scene information, i.e., locational accuracy or area measurement capabilities, inherent in coarser resolutions.

To evaluate the performance of multi-element processing on forestry data, four of the nine-point decision rules developed at ERIM [3] were used to classify the $(32 \text{ meters})^2$ resolution case for data segment 1. A brief description of the nine-point rules, BAYES9, PRIOR9, PREF9, and VOTE9, is given in Appendix III. Classification results were compared with the performance of the linear rule classification of the $(32)^2$ and $(64 \text{ meters})^2$ resolution cases, and in addition, with the quadratic rule performance for the $(32 \text{ meters})^2$ case. Because the nine-point rules classify all resolution elements, (e.g., allow for no unclassified elements), the $(32 \text{ meters})^2$ and $(64 \text{ meters})^2$ linear rule results, and $(32 \text{ meters})^2$ quadratic rule results used as a basis of comparison were generated with no decision boundary threshold stated for the signatures. Thus, the accuracies for these standard classification procedures may be different than previously reported in Section 4.1.1 since all resolution elements are classified.

The overall percent correct classification, averaged over elements, was calculated for each hierarchy. Classification accuracy for whole feature areas excluding boundary elements (boundary exclusive sets) is displayed in Table 10 for individual features as well as overall hierarchy results. Table 11 gives percent correct classification for boundary inclusive test sets.

TABLE 10. PERCENT CORRECT CLASSIFICATION OF VARIOUS DECISION RULES ON BOUNDARY EXCLUSIVE TEST SETS USING ALL 11 $M^2$S SPECTRAL CHANNELS

| | (32 Meter)$^2$ | | | | | | (64 Meter)$^2$ |
|---|---|---|---|---|---|---|---|
| Hierarchy: Condition Class | Linear Rule | Q Rule | Bayes 9 | Prior 9 | Pref 9 | Vote 9 | Linear Rule |
| Conifer Regen. (2.3) | 73.3 | 74.2 | 90.0 | 79.8 | 94.1 | 90.2 | 91.3 |
| Loblolly-Imm. (2.5) | 56.8 | 73.6 | 75.0 | 69.4 | 77.8 | 83.3 | 0.0 |
| Loblolly-Mature (2.6) | 19.9 | 41.3 | 69.9 | 51.5 | 65.8 | 60.2 | 39.5 |
| Shortleaf-Imm. (1.3) | 32.7 | 38.1 | 56.7 | 46.1 | 55.7 | 49.0 | 43.8 |
| Shortleaf-Mature (1.4) | 76.8 | 74.5 | 96.0 | 88.1 | 97.0 | 96.0 | 84.2 |
| Overall | 53.7 | 58.7 | 77.9 | 66.9 | 78.9 | 74.5 | 69.1 |
| Hierarchy: Growth Stage | | | | | | | |
| Conifer Regen. (2.3) | 73.3 | 74.2 | 90.0 | 79.8 | 94.1 | 90.2 | 91.3 |
| Imm. Sawtimber | 57.4 | 51.5 | 60.5 | 55.7 | 61.3 | 56.6 | 43.4 |
| Mature Sawtimber | 55.6 | 64.0 | 83.7 | 73.9 | 81.7 | 79.4 | 67.1 |
| Overall | 63.3 | 64.0 | 78.8 | 70.4 | 80.2 | 76.4 | 70.9 |
| Hierarchy: Cover Type | | | | | | | |
| Conifer Regen. (2.3) | 73.3 | 74.2 | 90.0 | 79.8 | 94.1 | 90.2 | 91.3 |
| Shortleaf Pine | 69.7 | 73.3 | 88.2 | 81.2 | 88.6 | 85.9 | 84.7 |
| Loblolly Pine | 44.4 | 56.8 | 72.8 | 61.6 | 70.3 | 67.7 | 41.5 |
| Overall | 66.8 | 70.8 | 86.5 | 77.5 | 87.9 | 84.3 | 81.4 |
| Hierarchy: Physiognomy | | | | | | | |
| Conifer Regen. (2.3) | 73.3 | 74.2 | 90.0 | 79.8 | 94.1 | 90.2 | 91.3 |
| Pine Sawtimber | 87.3 | 88.4 | 93.1 | 91.8 | 92.9 | 91.3 | 88.7 |
| Overall | 81.7 | 82.8 | 91.9 | 87.0 | 93.4 | 90.8 | 89.8 |

TABLE 11. PERCENT CORRECT CLASSIFICATION OF VARIOUS DECISION RULES ON BOUNDARY INCLUSIVE TEST SETS USING ALL 11 $M^2$S SPECTRAL CHANNELS

| | (32 Meter)$^2$ | | | | | | (64 Meter)$^2$ |
|---|---|---|---|---|---|---|---|
| | Linear Rule | Q Rule | Bayes 9 | Prior 9 | Pref 9 | Vote 9 | Linear Rule |
| Hierarchy: Condition Class | | | | | | | |
| Conifer Regen. (2.3) | 72.4 | 73.4 | 88.8 | 79.4 | 92.2 | 89.4 | 91.9 |
| Loblolly-Imm. (2.5) | 56.9 | 56.9 | 75.0 | 68.8 | 79.2 | 81.3 | 0.0 |
| Loblolly-Mature (2.6) | 18.1 | 38.4 | 64.4 | 47.8 | 60.4 | 55.4 | 40.4 |
| Shortleaf-Imm. (1.3) | 30.2 | 36.8 | 52.2 | 43.1 | 52.4 | 44.7 | 36.4 |
| Shortleaf-Mature (1.4) | 78.2 | 74.0 | 92.8 | 84.0 | 95.4 | 93.3 | 82.7 |
| Overall | 52.6 | 57.2 | 74.8 | 64.6 | 76.1 | 71.8 | 65.9 |
| Hierarchy: Growth Stage | | | | | | | |
| Conifer Regen. (2.3) | 72.4 | 73.4 | 88.8 | 79.4 | 92.2 | 89.4 | 91.9 |
| Imm. Sawtimber | 52.6 | 48.5 | 56.5 | 52.4 | 58.3 | 52.2 | 34.5 |
| Mature Sawtimber | 55.8 | 62.8 | 79.5 | 70.2 | 78.4 | 76.0 | 66.7 |
| Overall | 61.3 | 62.2 | 75.6 | 68.0 | 77.3 | 73.5 | 67.2 |
| Hierarchy: Cover Type | | | | | | | |
| Conifer Regen. (2.3) | 72.4 | 73.4 | 88.8 | 79.4 | 92.2 | 89.4 | 91.9 |
| Shortleaf Pine | 72.1 | 74.1 | 85.9 | 79.8 | 86.4 | 82.4 | 83.3 |
| Loblolly Pine | 44.8 | 54.8 | 70.0 | 59.6 | 68.1 | 65.9 | 42.9 |
| Overall | 67.4 | 70.5 | 84.4 | 76.3 | 85.7 | 82.5 | 81.0 |
| Hierarchy: Physiognomy | | | | | | | |
| Conifer Regen. (2.3) | 72.4 | 73.4 | 88.8 | 79.4 | 92.2 | 89.4 | 91.9 |
| Pine Sawtimber | 87.2 | 87.1 | 90.7 | 89.6 | 91.1 | 88.1 | 85.3 |
| Overall | 81.3 | 81.8 | 89.9 | 85.6 | 91.5 | 88.6 | 88.1 |

General trends observed in Section 4.1.1 are also seen for multi-element results. For example, a comparison of overall correct classification results in Table 10 with those in Table 11 indicate that the inclusion of boundary elements decreases classification accuracy since a higher proportion of these elements are misclassified. These tables also show that the hierarchies consisting of more general (aggregated) features give higher classification accuracies than those containing more specific features. Thus, the condition class hierarchy shows the lowest classification performance while physiognomy shows the highest. The fact that cover types (species designation) are shown to have higher performance than growth stages is again predominantly due to the greater percentage of hardwoods present in both Loblolly Pine features.

Figures 15-18 are bar graphs showing overall hierarchy classification results for each of the decision rules used to classify both boundary exclusive tests sets and boundary inclusive test sets. For every case, the performance of the quadratic rule is better than that of the linear rule when compared for the $(32 \text{ meters})^2$ data, and $(64 \text{ meters})^2$ linear rule results show still higher performance than either of the $(32 \text{ meters})^2$ results using standard classification procedures. Of the four nine-point rules examined in this study, three always show performances for $(32 \text{ meters})^2$ data that are higher than the linear rule classification results of the $(64 \text{ meters})^2$ data. PRIOR9 results are variable, sometimes giving higher accuracy than $(64 \text{ meters})^2$ linear rule results but frequently giving poorer performances. Thus, it appears that judicious selection of a nine-point rule can offer improved classification performance that is greater than an improvement that might be realized with standard classification procedures used on coarser resolution data.

The relationships that exist among the four nine-point rules in terms of ranked classification performance is the same for both boundary

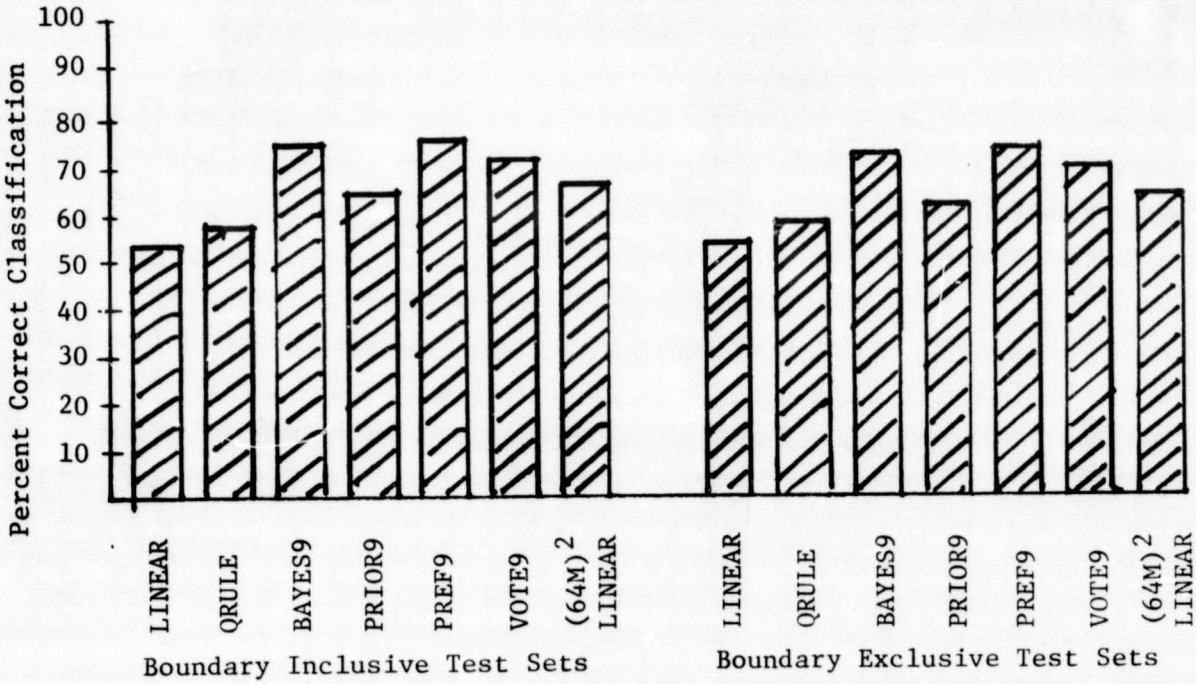


FIGURE 15. COMPARISON OF PERFORMANCE OF LINEAR RULE, QUADRATIC RULE, AND FOUR 9-POINT RULE CLASSIFICATIONS FOR CONDITION CLASSES

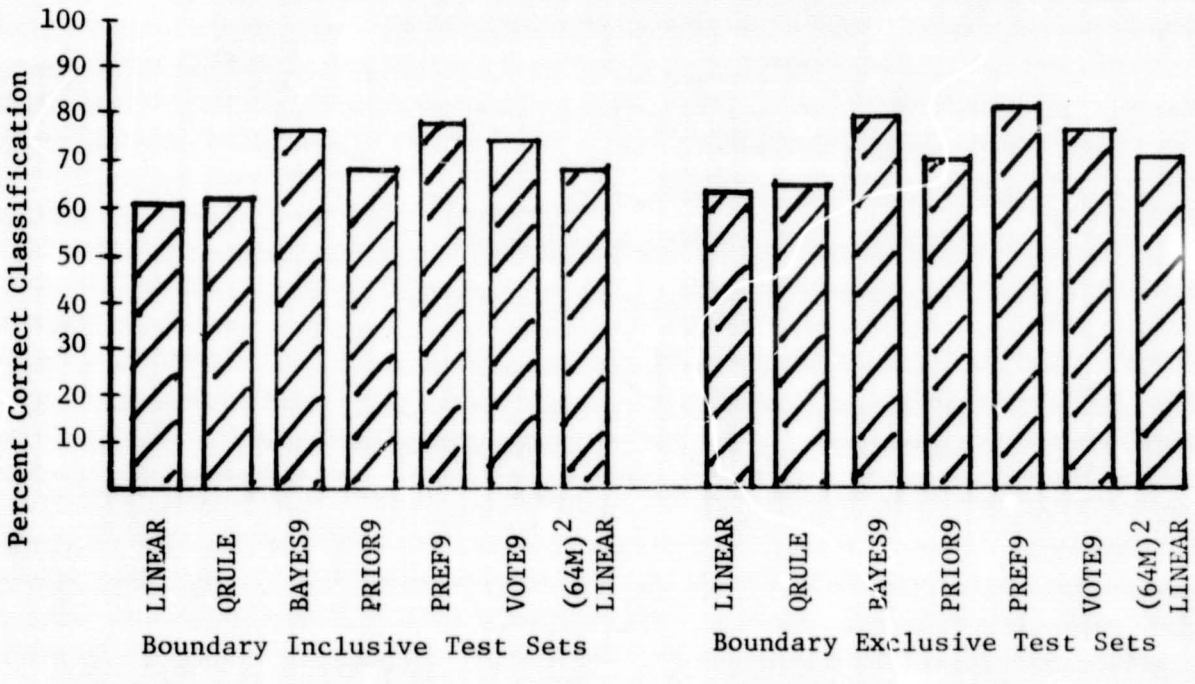


FIGURE 16. COMPARISON OF PERFORMANCE OF LINEAR RULE, QUADRATIC RULE, AND FOUR 9-POINT RULE CLASSIFICATION FOR GROWTH STAGES

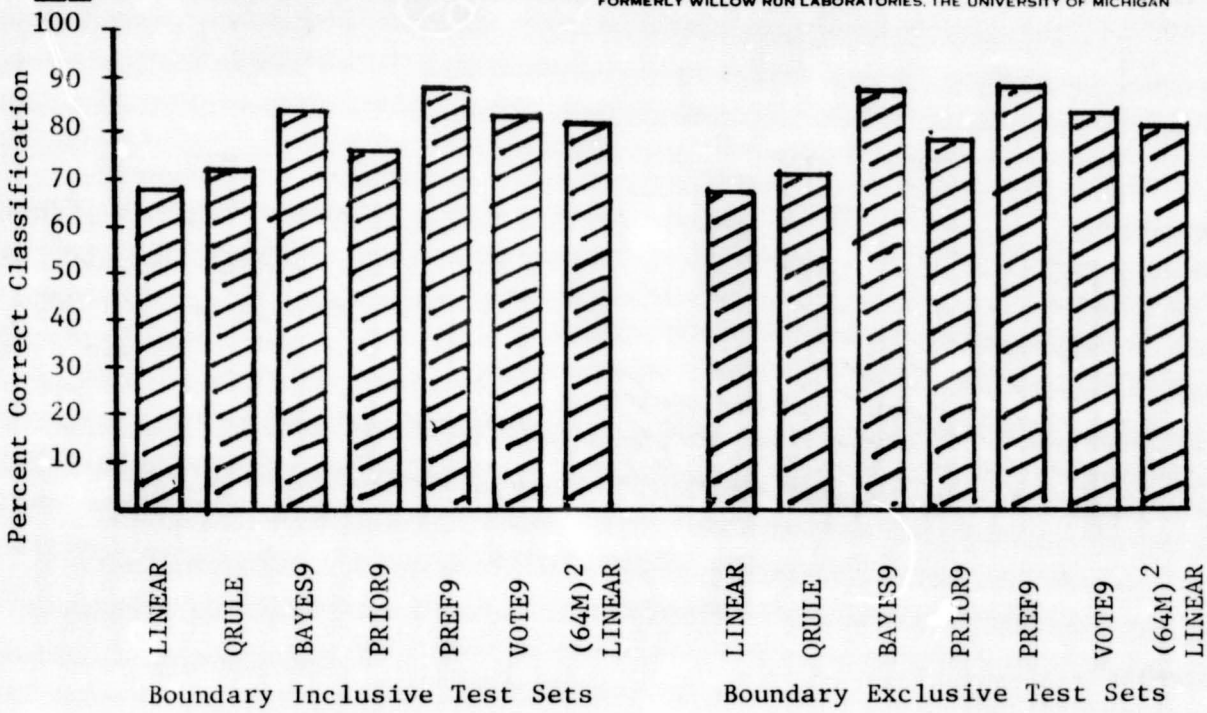


FIGURE 17. COMPARISON OF PERFORMANCE OF LINEAR RULE, QUADRATIC RULE, AND FOUR 9-POINT RULE CLASSIFICATION FOR COVER TYPES

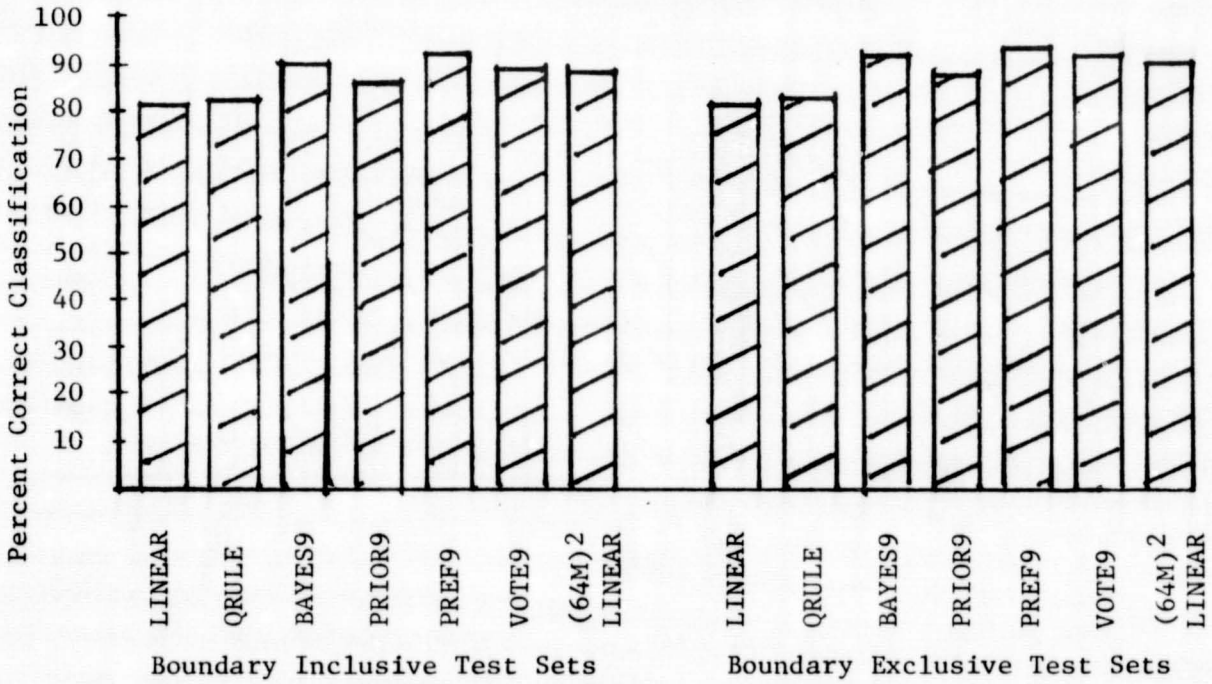


FIGURE 18. COMPARISON OF PERFORMANCE OF LINEAR RULE, QUADRATIC RULE, AND FOUR 9-POINT RULE CLASSIFICATION FOR PHYSIOGNOMY

inclusive test sets and boundary exclusive test sets. PREF9 always gives the best performance with BAYES9 giving only slightly reduced accuracies by comparison. VOTE9, although still better than the $(64 \text{ meters})^2$ linear rule results, does not do as well as either PREF9 or BAYES9. PRIOR9 gives the lowest classification accuracies of all four nine-point rules. The ranked performance of these results are consistent with results for agricultural applications. Preliminary tests on nine-point rules using aircraft data collected over the Imperial Valley, California [3] show the same relative performances for the four decision rules.

Comparison of the best nine-point decision rule results (i.e., PREF9) with the results of the single element rules indicates that there is always a substantial increase in accuracy for PREF9. The performance increase is largest for the hierarchy of condition classes with lesser increases in performance noted for hierarchies of more general features. This trend indicates that when classification accuracy is low using standard techniques, then specialized recognition techniques give more improved accuracy than when accuracy was high with standard techniques. Thus, nine-point rules appear to offer a greater advantage for use in improving the classification of detailed features that may be required in some forest surveys.

4.1.3 Thematic Mapper Simulation Study

To evaluate how well the proposed Landsat D Thematic Mapper (TM) might classify forest features, a spectral simulation of the Thematic Mapper was undertaken by selecting the most appropriate $M^2S$ spectral channels. Although there is not a direct correspondence in the spectral range for the two systems, Table 12 gives the 7 proposed Thematic Mapper spectral channels and the 5 $M^2S$ channels which most closely coincide. This subset of 5 $M^2S$ spectral channels was used to classify the $(32)^2$ and $(64 \text{ meters})^2$ data.

TABLE 12. THEMATIC MAPPER AND SELECTED SUBSET OF $M^2S$ SPECTRAL CHANNELS

| TM | $M^2S$ |
|---|---|
| 0.45-0.52 | 0.45-0.49 |
| 0.52-0.60 | 0.53-0.57 |
| 0.63-0.69 | 0.65-0.69 |
| 0.74-0.80 } | 0.76-0.86 |
| 0.80-0.91 } | |
| 1.55-1.75 | |
| 10.4-12.5 | 8.0-12.0 |

Table 13 summarizes the overall percent correct classification results considered for all cases, while Tables 14-19 give more detailed comparisons of $M^2S$ classification results using all 11 channels and the TM 5 channel subset to classify training sets, boundary exclusive test sets, and boundary inclusive test sets of both data segments. We see that the 5 channel classification results show the same general trends as the 11 channel classifications. Overall classification accuracy increases as the hierarchies considered consist of more general (aggregated) features. Training sets were more accurately classified than test sets, and the boundary inclusive test sets were the least accurately classified.

Tables 14 and 17 display the classification accuracy over training sets for 11 channel versus 5 channel classifications. Examination of the most specific hierarchy, condition class, shows that when the subset of 5 channels is used, overall accuracy is reduced by 13.7 percentage points for $(32)^2$ and 22.2 percentage points for $(64 \text{ meters})^2$ in data segment 1 and 7.3 percentage points for $(32)^2$ and 7.9 percentage points for $(64 \text{ meters})^2$ in data segment 2. This reduction in accuracy is expected, since the smaller number of spectral channels should give

TABLE 13. OVERALL PERCENT CORRECT CLASSIFICATION RESULTS FOR ALL 11 $M^2S$ CHANNELS COMPARED WITH THE RESULTS OBTAINED FOR THE TM 5 CHANNEL SUBSET OVER $(32)^2$ AND $(64\ METERS)^2$ CASES OF SPATIAL RESOLUTION FOR BOTH DATA SEGMENTS

| | ALL 11 $M^2S$ CHANNELS | | | | | | TM 5 CHANNEL SUBSET | | | | | |
|---|---|---|---|---|---|---|---|---|---|---|---|---|
| | $(32\ Meters)^2$ | | | $(64\ Meters)^2$ | | | $(32\ Meters)^2$ | | | $(64\ Meters)^2$ | | |
| | TRAINING SETS | BOUNDARY EXCLUSIVE TEST SETS | BOUNDARY INCLUSIVE TEST SETS | TRAINING SETS | BOUNDARY EXCLUSIVE TEST SETS | BOUNDARY INCLUSIVE TEST SETS | TRAINING SETS | BOUNDARY EXCLUSIVE TEST SETS | BOUNDARY INCLUSIVE TEST SETS | TRAINING SETS | BOUNDARY EXCLUSIVE TEST SETS | BOUNDARY INCLUSIVE TEST SETS |
| DATA SEGMENT 1 | | | | | | | | | | | | |
| (Unclassified Elements) | (0.7) | (4.9) | (5.9) | (2.8) | (12.9) | (17.3) | (0.3) | (2.5) | (3.6) | (0.6) | (1.8) | (5.1) |
| Condition Class | 57.4 | 52.2 | 50.1 | 76.9 | 59.9 | 54.3 | 43.7 | 42.7 | 41.9 | 54.7 | 59.2 | 54.3 |
| Growth Stage | 65.1 | 60.7 | 58.2 | 79.8 | 61.9 | 55.8 | 57.4 | 57.6 | 55.7 | 61.3 | 64.8 | 55.8 |
| Cover Type | 67.8 | 64.6 | 63.7 | 84.4 | 71.8 | 67.5 | 55.4 | 56.3 | 56.6 | 65.4 | 70.8 | 67.5 |
| Physiognomy | 81.2 | 78.3 | 77.1 | 89.5 | 79.6 | 73.8 | 77.2 | 76.8 | 75.9 | 77.9 | 82.0 | 73.8 |
| DATA SEGMENT 2 | | | | | | | | | | | | |
| (Unclassified Elements) | (1.3) | (3.8) | (4.4) | (7.0) | (14.4) | (16.4) | (1.2) | (2.4) | (3.1) | (3.3) | (4.2) | (6.3) |
| Condition Class | 74.5 | 79.0 | 75.3 | 76.3 | 69.3 | 64.9 | 67.2 | 77.7 | 74.5 | 68.4 | 81.4 | 74.7 |
| Physiognomy | 96.4 | 90.7 | 88.6 | 92.6 | 82.6 | 80.5 | 92.7 | 89.3 | 87.4 | 94.9 | 92.4 | 89.9 |

TABLE 14. COMPARISON OF PERCENT CORRECT CLASSIFICATION FOR TRAINING SETS IN DATA SEGMENT 1 USING ALL 11 $M^2$S SPECTRAL CHANNELS VERSUS USING THE 5 CHANNELS WHICH SIMULATE THE THEMATIC MAPPER

| | 11 Channels | | 5 Channels | |
|---|---|---|---|---|
| | $(32\ M)^2$ | $(64\ M)^2$ | $(32\ M)^2$ | $(64\ M)^2$ |
| (unclassified elements) | (0.7) | (2.8) | (0.3) | (0.6) |
| Hierarchy: Condition Class | | | | |
| Conifer Regen. (2.3) | 70.5 | 87.3 | 63.1 | 83.8 |
| Loblolly-Imm. (2.5) | 65.2 | - | 52.2 | 0.0 |
| Loblolly-Mature (2.6) | 19.6 | 44.4 | 4.9 | 7.4 |
| Shortleaf-Imm. (1.3) | 35.6 | 71.4 | 21.2 | 62.9 |
| Shortleaf-Mature (1.4) | 75.6 | 85.0 | 53.0 | 45.0 |
| Overall | 57.4 | 76.9 | 43.7 | 54.7 |
| Hierarchy: Growth Stage | | | | |
| Conifer Regen. (2.3) | 70.5 | 87.3 | 63.1 | 83.8 |
| Imm. Sawtimber | 60.6 | 65.1 | 65.8 | 62.8 |
| Mature Sawtimber | 62.2 | 71.6 | 47.0 | 40.3 |
| Overall | 65.1 | 76.2 | 57.4 | 61.3 |
| Hierarchy: Cover Type | | | | |
| Conifer Regen. (2.3) | 70.5 | 87.3 | 63.1 | 83.8 |
| Shortleaf Pine | 75.0 | 90.7 | 54.3 | 78.7 |
| Loblolly Pine | 44.8 | 45.7 | 41.6 | 5.7 |
| Overall | 67.8 | 80.7 | 55.4 | 65.2 |
| Hierarchy: Physiognomy | | | | |
| Conifer Regen. (2.3) | 70.5 | 87.3 | 63.1 | 83.8 |
| Pine Sawtimber | 88.0 | 90.9 | 86.1 | 76.4 |
| Overall | 81.2 | 89.5 | 77.2 | 77.9 |

TABLE 15. COMPARISON OF PERCENT CORRECT CLASSIFICATION FOR BOUNDARY EXCLUSIVE TEST SETS IN DATA SEGMENT 1 USING ALL 11 $M^2$S SPECTRAL CHANNELS VERSUS USING THE 5 CHANNELS WHICH SIMULATE THE THEMATIC MAPPER

| | 11 Channels | | 5 Channels | |
|---|---|---|---|---|
| | $(32\ M)^2$ | $(64\ M)^2$ | $(32\ M)^2$ | $(64\ M)^2$ |
| (unclassified elements) | (4.9) | (12.9) | (2.5) | (1.8) |
| Hierarchy: Condition Class | | | | |
| Conifer Regen. (2.3) | 71.4 | 78.6 | 64.9 | 81.5 |
| Loblolly-Imm. (2.5) | 56.8 | - | 61.4 | 0.0 |
| Loblolly-Mature (2.6) | 19.4 | 31.0 | 6.3 | 7.1 |
| Shortleaf-Imm. (1.3) | 31.6 | 39.5 | 22.7 | 60.3 |
| Shortleaf-Mature (1.4) | 73.0 | 82.1 | 55.0 | 53.9 |
| Overall | 52.2 | 59.9 | 42.7 | 59.2 |
| Hierarchy: Growth Stage | | | | |
| Conifer Regen. (2.3) | 71.4 | 78.6 | 64.9 | 81.5 |
| Imm. Sawtimber | 53.5 | 40.2 | 59.7 | 61.9 |
| Mature Sawtimber | 54.2 | 59.3 | 45.1 | 43.2 |
| Overall | 60.7 | 61.9 | 57.6 | 64.8 |
| Hierarchy: Cover Type | | | | |
| Conifer Regen. (2.3) | 71.4 | 78.6 | 64.9 | 81.5 |
| Shortleaf Pine | 67.0 | 80.0 | 55.6 | 86.3 |
| Loblolly Pine | 42.4 | 33.3 | 38.4 | 6.3 |
| Overall | 64.6 | 71.8 | 56.3 | 70.8 |
| Hierarchy: Physiognomy | | | | |
| Conifer Regen. (2.3) | 71.4 | 78.6 | 64.9 | 81.5 |
| Pine Sawtimber | 82.8 | 80.4 | 84.5 | 82.4 |
| Overall | 78.3 | 79.6 | 76.8 | 82.0 |

TABLE 16. COMPARISON OF PERCENT CORRECT CLASSIFICATION FOR BOUNDARY INCLUSIVE TEST SETS IN DATA SEGMENT 1 USING ALL 11 $M^2$S SPECTRAL CHANNELS VERSUS USING THE 5 CHANNELS WHICH SIMULATE THE THEMATIC MAPPER

| | 11 Channels | | 5 Channels | |
|---|---|---|---|---|
| | $(32\ M)^2$ | $(64\ M)^2$ | $(32\ M)^2$ | $(64\ M)^2$ |
| (unclassified elements) | (5.9) | (17.3) | (3.6) | (5.1) |
| Hierarchy: Condition Class | | | | |
| Conifer Regen. (2.3) | 70.1 | 76.3 | 64.6 | 81.6 |
| Loblolly-Imm. (2.5) | 47.1 | - | 57.4 | 0.0 |
| Loblolly-Mature (2.6) | 17.4 | 34.6 | 6.6 | 5.8 |
| Shortleaf-Imm. (1.3) | 28.9 | 29.3 | 21.2 | 44.3 |
| Shortleaf-Mature (1.4) | 73.7 | 74.1 | 55.0 | 48.3 |
| Overall | 50.1 | 54.3 | 41.9 | 54.3 |
| Hierarchy: Growth Stage | | | | |
| Conifer Regen. (2.3) | 70.1 | 76.3 | 64.6 | 81.6 |
| Imm. Sawtimber | 48.5 | 28.5 | 54.8 | 44.9 |
| Mature Sawtimber | 53.8 | 58.2 | 42.2 | 40.9 |
| Overall | 58.2 | 55.8 | 55.7 | 55.8 |
| Hierarchy: Cover Type | | | | |
| Conifer Regen. (2.3) | 70.1 | 76.3 | 64.6 | 81.6 |
| Shortleaf Pine | 67.8 | 70.7 | 56.4 | 74.3 |
| Loblolly Pine | 40.3 | 37.9 | 40.0 | 6.1 |
| Overall | 63.7 | 67.5 | 56.6 | 67.5 |
| Hierarchy: Physiognomy | | | | |
| Conifer Regen. (2.3) | 70.1 | 76.3 | 64.6 | 81.6 |
| Pine Sawtimber | 81.3 | 72.1 | 82.8 | 71.7 |
| Overall | 77.1 | 73.8 | 75.9 | 73.8 |

TABLE 17. COMPARISON OF PERCENT CORRECT CLASSIFICATION FOR TRAINING SETS IN DATA SEGMENT 2 USING ALL 11 $M^2$S SPECTRAL CHANNELS VERSUS USING THE 5 CHANNELS WHICH SIMULATE THE THEMATIC MAPPER

| | 11 Channels | | 5 Channels | |
|---|---|---|---|---|
| | $(32\ M)^2$ | $(64\ M)^2$ | $(32\ M)^2$ | $(64\ M)^2$ |
| (unclassified elements) | (1.3) | (7.0) | (1.2) | (3.3) |
| Hierarchy: Condition Class | | | | |
| Loblolly-Imm. (2.5) | 93.8 | 100.0 | 89.8 | 100.0 |
| Laurel Oak/Willow Oak (3.1) | 88.3 | 86.8 | 82.5 | 79.4 |
| Swtgm/N. Oak/W. Oak (4.2) | 40.9 | 48.1 | 27.4 | 31.7 |
| Cut Over (7.1) | 100.0 | 95.8 | 100.0 | 100.0 |
| Overall | 74.5 | 76.3 | 67.2 | 68.4 |
| Hierarchy: Physiognomy | | | | |
| Conifer Sawtimber (2.5) | 93.8 | 100.0 | 89.8 | 100.0 |
| Hardwood Sawtimber | 96.6 | 89.8 | 92.3 | 92.5 |
| Cut Over (7.1) | 100.0 | 95.8 | 100.0 | 100.0 |
| Overall | 96.4 | 92.6 | 92.7 | 94.9 |

TABLE 18. COMPARISON OF PERCENT CORRECT CLASSIFICATION FOR BOUNDARY EXCLUSIVE TEST SETS IN DATA SEGMENT 2 USING ALL 11 $M^2$S SPECTRAL CHANNELS VERSUS USING THE 5 CHANNELS WHICH SIMULATE THE THEMATIC MAPPER

| | 11 Channels | | 5 Channels | |
|---|---|---|---|---|
| | $(32\ M)^2$ | $(64\ M)^2$ | $(32\ M)^2$ | $(64\ M)^2$ |
| (unclassified elements) | (3.8) | (14.4) | (2.4) | (4.2) |
| Hierarchy: Condition Class | | | | |
| Loblolly-Imm. (2.5) | 79.7 | 86.0 | 79.3 | 86.0 |
| Laurel Oak/Willow Oak (3.1) | 76.9 | 62.1 | 77.0 | 76.6 |
| Swtgm/N. Oak/W. Oak (4.2) | 49.4 | 50.0 | 25.3 | 25.0 |
| Cut Over (7.1) | 91.1 | 75.4 | 92.0 | 96.7 |
| Overall | 79.0 | 69.3 | 77.7 | 81.4 |
| Hierarchy: Physiognomy | | | | |
| Conifer Sawtimber (2.5) | 79.7 | 86.0 | 79.3 | 86.0 |
| Hardwood Sawtimber | 94.2 | 84.3 | 91.5 | 92.8 |
| Cut Over (7.1) | 91.1 | 75.4 | 92.0 | 96.7 |
| Overall | 90.7 | 82.6 | 89.3 | 92.4 |

TABLE 19. COMPARISON OF PERCENT CORRECT CLASSIFICATION FOR BOUNDARY INCLUSIVE TEST SETS IN DATA SEGMENT 2 USING ALL 11 $M^2$S SPECTRAL CHANNELS VERSUS USING THE 5 CHANNELS WHICH SIMULATE THE THEMATIC MAPPER

| | 11 Channels | | 5 Channels | |
|---|---|---|---|---|
| | $(32\ M)^2$ | $(64\ M)^2$ | $(32\ M)^2$ | $(64\ M)^2$ |
| (unclassified elements) | (4.4) | (16.4) | (3.1) | (6.3) |
| Hierarchy: Condition Class | | | | |
| Loblolly-Imm. (2.5) | 71.0 | 72.9 | 71.7 | 71.4 |
| Laurel Oak/Willow Oak (3.1) | 74.8 | 59.7 | 75.2 | 71.4 |
| Swtgm/N. Oak/W. Oak (4.2) | 47.6 | 50.0 | 30.2 | 33.3 |
| Cut Over (7.1) | 89.3 | 74.2 | 90.4 | 95.5 |
| Overall | 75.3 | 64.9 | 74.5 | 74.7 |
| Hierarchy: Physiognomy | | | | |
| Conifer Sawtimber (2.5) | 71.0 | 72.9 | 71.7 | 71.4 |
| Hardwood Sawtimber | 94.1 | 85.5 | 91.5 | 92.3 |
| Cut Over (7.1) | 89.3 | 74.2 | 90.4 | 95.5 |
| Overall | 88.6 | 80.5 | 87.4 | 89.9 |

a less well defined signature set. All other hierarchies of data segment 1 show similar, but lesser reductions in accuracy for training set classification. In data segment 2, only the $(64 \text{ meters})^2$ case for the physiognomy hierarchy does not follow the rule; but instead shows a slight increase in accuracy.

Tables 15, 16, 18, and 19 give classification accuracy over test sets. Again, the $(32 \text{ meters})^2$ case shows the decrease in accuracy expected when fewer channels are used to classify the data. But for the $(64 \text{ meters})^2$ case several of the test set results show an increase in classification accuracy. Figure 19 represents the percent of unclassified elements for the $(32)^2$ and $(64 \text{ meters})^2$ cases of both data segments using 5 and 11 channel classification. This figure shows that the 5 channel classifications do not display the large jump in unclassified elements for $(64 \text{ meters})^2$ test sets that is characteristic of the 11 channel classifications. Thus, 5 channel classification accuracy is greater than 11 channel accuracy, apparently due to a smaller percentage of unclassified elements (which were considered to be incorrectly classified). The number of elements which are misclassified is smaller for the corresponding 11 channel classification in all cases.

Tables 20 and 21 show classification results of data segment 1 for the 5 TM channels using the nine-point rules previously reported for all 11 channels in Section 4.1.2. Comparison of Tables 20 and 21 with Tables 10 and 11 shows that the results using the 5 TM channels display the same trends as the 11 channel classifications though the accuracies are lower. In general, the nine-point rules do not produce as great an improvement in classification accuracy with 5 channels as with all 11 channels. The one exception is the physiognomy hierarchy which did not improve very much in the 11 channel case due to the already high accuracy.

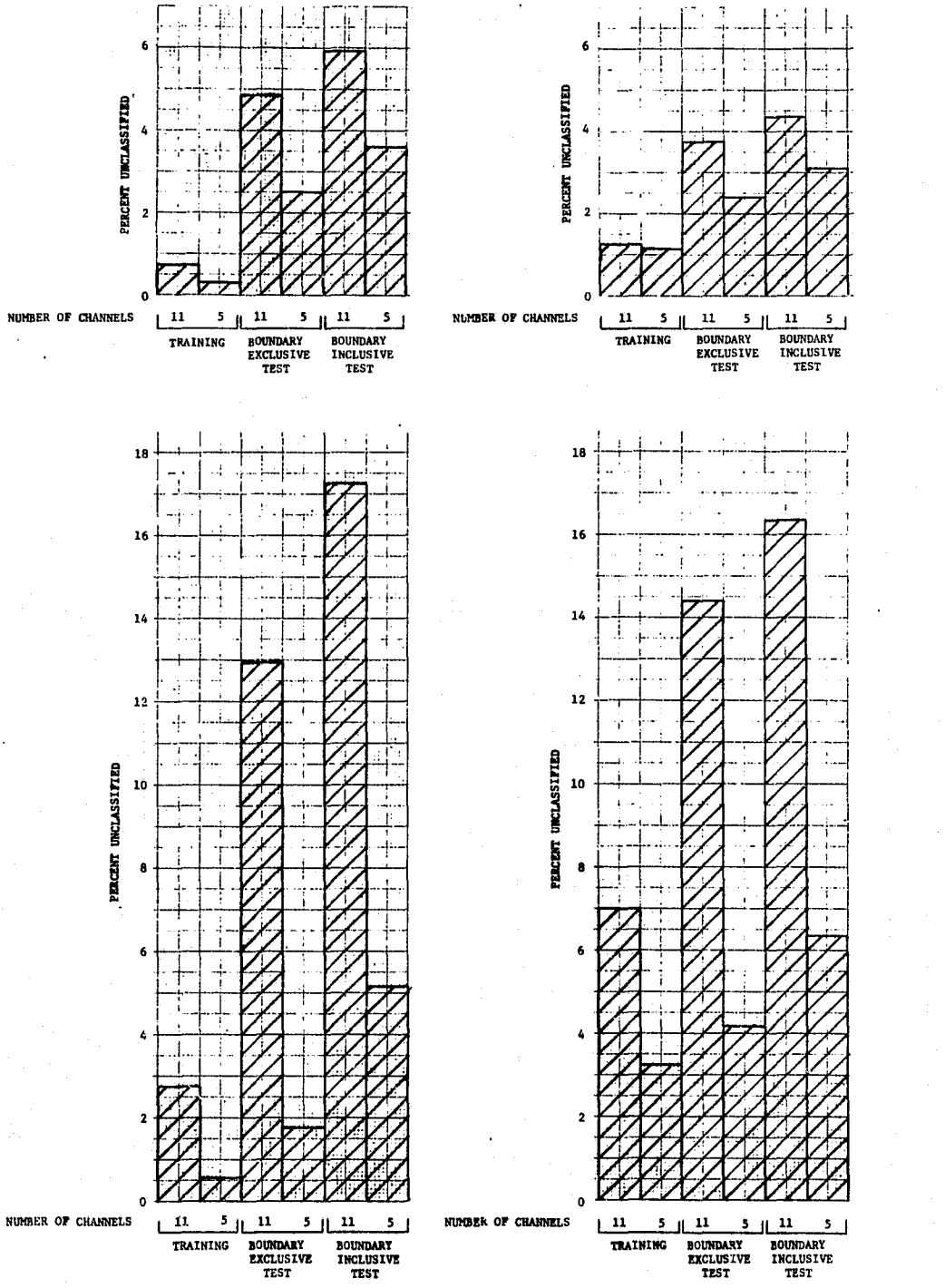


FIGURE 19. COMPARISON OF THE PERCENT OF ELEMENTS UNCLASSIFIED USING ALL 11 $M^2$S CHANNELS VERSUS THE TM 5 CHANNEL SUBSET TO CLASSIFY THE $(32)^2$ AND $(64\ \text{METERS})^2$ CASES FOR BOTH DATA SEGMENTS

TABLE 20. PERCENT CORRECT CLASSIFICATION OF VARIOUS DECISION RULES ON BOUNDARY EXCLUSIVE TEST SETS USING THE 5 CHANNELS WHICH SIMULATE THE THEMATIC MAPPER

| | (32 Meter)$^2$ | | | | | | (64 Meter)$^2$ |
|---|---|---|---|---|---|---|---|
| | Linear Rule | Q Rule | Bayes 9 | Prior 9 | Pref 9 | Vote 9 | Linear Rule |
| **Hierarchy: Condition Class** | | | | | | | |
| Conifer Regen. (2.3) | 65.9 | 63.5 | 82.4 | 71.9 | 88.8 | 77.6 | 84.1 |
| Loblolly-Imm. (2.5) | 61.4 | 56.8 | 66.7 | 61.1 | 66.7 | 72.2 | 0.0 |
| Loblolly-Mature (2.6) | 6.3 | 13.6 | 28.1 | 18.9 | 20.9 | 4.1 | 7.9 |
| Shortleaf-Imm. (1.3) | 23.1 | 31.6 | 41.5 | 35.1 | 36.3 | 33.7 | 60.0 |
| ShortleafMature (1.4) | 57.4 | 54.0 | 87.1 | 72.8 | 89.6 | 81.7 | 55.3 |
| Overall | 43.5 | 45.6 | 63.2 | 53.6 | 63.6 | 55.0 | 62.5 |
| **Hierarchy: Growth Stage** | | | | | | | |
| Conifer Regen. (2.3) | 65.9 | 63.5 | 82.4 | 71.9 | 88.8 | 77.6 | 84.1 |
| Imm. Sawtimber | 61.0 | 53.0 | 56.2 | 55.1 | 51.2 | 51.6 | 61.4 |
| Mature Sawtimber | 45.5 | 44.8 | 64.6 | 56.3 | 62.6 | 53.8 | 44.7 |
| Overall | 58.7 | 54.9 | 69.0 | 62.2 | 69.5 | 62.7 | 67.0 |
| **Hierarchy: Cover Type** | | | | | | | |
| Conifer Regen. (2.3) | 65.9 | 63.5 | 82.4 | 71.9 | 88.8 | 77.6 | 84.1 |
| Shortleaf Pine | 57.1 | 64.4 | 81.9 | 74.6 | 82.5 | 78.7 | 86.4 |
| Loblolly Pine | 38.4 | 43.2 | 49.6 | 46.6 | 44.0 | 47.4 | 7.3 |
| Overall | 57.4 | 60.4 | 76.9 | 69.0 | 78.8 | 73.2 | 74.0 |
| **Hierarchy: Physiognomy** | | | | | | | |
| Conifer Regen. (2.3) | 65.9 | 63.5 | 82.4 | 71.9 | 88.8 | 77.6 | 84.1 |
| Pine Sawtimber | 86.5 | 85.3 | 92.2 | 90.1 | 90.1 | 90.4 | 83.0 |
| Overall | 78.3 | 76.7 | 88.3 | 82.8 | 89.6 | 85.2 | 83.5 |

TABLE 21. PERCENT CORRECT CLASSIFICATION OF VARIOUS DECISION RULES ON BOUNDARY INCLUSIVE TEST SETS USING THE 5 CHANNELS WHICH SIMULATE THE THEMATIC MAPPER

| | (32 Meter)$^2$ | | | | | | (64 Meter)$^2$ |
|---|---|---|---|---|---|---|---|
| | Linear Rule | Q Rule | Bayes 9 | Prior 9 | Pref 9 | Vote 9 | Linear Rule |
| Hierarchy: Condition Class | | | | | | | |
| Conifer Regen. (2.3) | 66.1 | 63.8 | 81.9 | 72.0 | 87.9 | 77.2 | 84.4 |
| Loblolly-Imm. (2.5) | 58.6 | 51.7 | 66.7 | 62.5 | 66.7 | 72.9 | 0.0 |
| Loblolly-Mature (2.6) | 6.5 | 12.5 | 25.2 | 17.1 | 18.9 | 3.6 | 6.4 |
| Shortleaf-Imm. (1.3) | 20.9 | 29.1 | 38.4 | 32.9 | 33.5 | 31.5 | 46.4 |
| Shortleaf-Mature (1.4) | 57.8 | 51.3 | 79.3 | 66.2 | 82.3 | 72.6 | 53.9 |
| Overall | 43.0 | 44.2 | 60.5 | 51.8 | 61.0 | 52.9 | 57.4 |
| Hierarchy: Growth Stage | | | | | | | |
| Conifer Regen. (2.3) | 66.1 | 63.8 | 81.9 | 72.0 | 87.9 | 77.2 | 84.4 |
| Imm. Sawtimber | 55.9 | 49.5 | 52.6 | 52.4 | 48.0 | 49.4 | 46.2 |
| Mature Sawtimber | 46.4 | 44.3 | 60.6 | 52.3 | 59.0 | 49.9 | 44.4 |
| Overall | 57.3 | 53.6 | 66.3 | 60.1 | 66.8 | 60.5 | 61.9 |
| Hierarchy: Cover Type | | | | | | | |
| Conifer Regen. (2.3) | 66.1 | 63.8 | 81.9 | 72.0 | 87.9 | 77.2 | 84.4 |
| Shortleaf Pine | 59.1 | 62.9 | 77.5 | 70.4 | 77.4 | 72.4 | 80.2 |
| Loblolly Pine | 40.0 | 43.4 | 48.1 | 45.9 | 43.0 | 47.0 | 7.1 |
| Overall | 51.9 | 59.9 | 74.4 | 67.0 | 75.9 | 70.2 | 71.2 |
| Hierarchy: Physiognomy | | | | | | | |
| Conifer Regen. (2.3) | 66.1 | 63.8 | 81.9 | 72.0 | 87.9 | 77.2 | 84.4 |
| Pine Sawtimber | 86.4 | 84.4 | 89.4 | 87.5 | 86.8 | 86.7 | 76.1 |
| Overall | 78.4 | 76.3 | 86.4 | 81.4 | 87.2 | 83.0 | 79.6 |

The 5 channel classification to simulate the Thematic Mapper indicates accuracy is higher for (64 meters)$^2$ than (32 meters)$^2$ data. For the most general (aggregated) hierarchy of forest features (physiognomy), the TM channels give satisfactory results compared to the 11 channel results; but, for the most specific cases, i.e., condition class, accuracy is seriously reduced compared to the 11 channel M$^2$S data.

4.2 AREA PROPORTION ESTIMATION AS A FUNCTION OF SPATIAL RESOLUTION

The previous sections have been concerned with evaluating the ability of computers to accurately classify desired features by making a decision for each resolution element and then determining whether or not the decision was correct, relative to the true identity of that element. This section is concerned with how well the proportion of total scene area of each feature class present in the classified scene can be estimated, without regard to location. Such proportion estimation may be useful for surveys of extensive areas where information is to to be specified in statistical summaries by geographic or political subdivisions.

A recent study has noted little or no correlation between in-place classification accuracy of terrain features and good performance on estimating the proportions of terrain features [4]. Compensating errors in the classification results can cause the classified proportions of features to match the true proportions. However, the extent of such errors is dependent on the types of features to be classified. For example, the situation in data segment 2, where one condition class of hardwoods (Feature 4.2) is consistently classified as another hardwood condition class (Feature 3.1), will lead to Feature 3.1 being overestimated, while Feature 4.2 is underestimated. Thus, in order to avoid the difficulties in separating hardwood condition classes in data segment 2 and the various pine sawtimber condition classes of data segment 1, proportion estimates were calculated only for the physiognomic features of each data segment. We believe that proportions based on

physiognomy represent a level of information most appropriate for surveys of extensive areas.

Within each data segment, proportions of each physiognomic feature were estimated from the total number of resolution elements that fell within the previously defined boundary inclusive test sets (i.e., all total feature areas). Since previous sections have shown that unclassified elements constituted a large percentage of the total for cases of coarse spatial resolution, estimated proportions were calculated two ways: (1) using all the elements in the test area, and (2) using only those elements which were classified as belonging to one of the established features. This allows partial examination of the effects of unclassified elements on proportion estimation results.

Two measures of proportion estimation accuracy were computed. One was the percent difference between estimated and actual proportions for each feature. The other was the RMS error for each data segment, computed from these differences as follows:

$$E_{RMS} = \left( \frac{1}{N} \sum_{i=1}^{N} (p_i - \hat{p}_i)^2 \right)^{\frac{1}{2}}$$

where: $p_i$ = ground truth proportion for one feature in the test area,

$\hat{p}_i$ = estimated proportion for the same feature in the test area,

$N$ = number of features considered.

RMS error is plotted in Figure 20(a) as a function of spatial resolution for all elements in the test area of each data segment while Figure 20(b) gives the RMS error calculated using only classified elements. Comparison of these figures illustrates a much larger RMS error for the $(64 \text{ meters})^2$ case when unclassified elements are included.

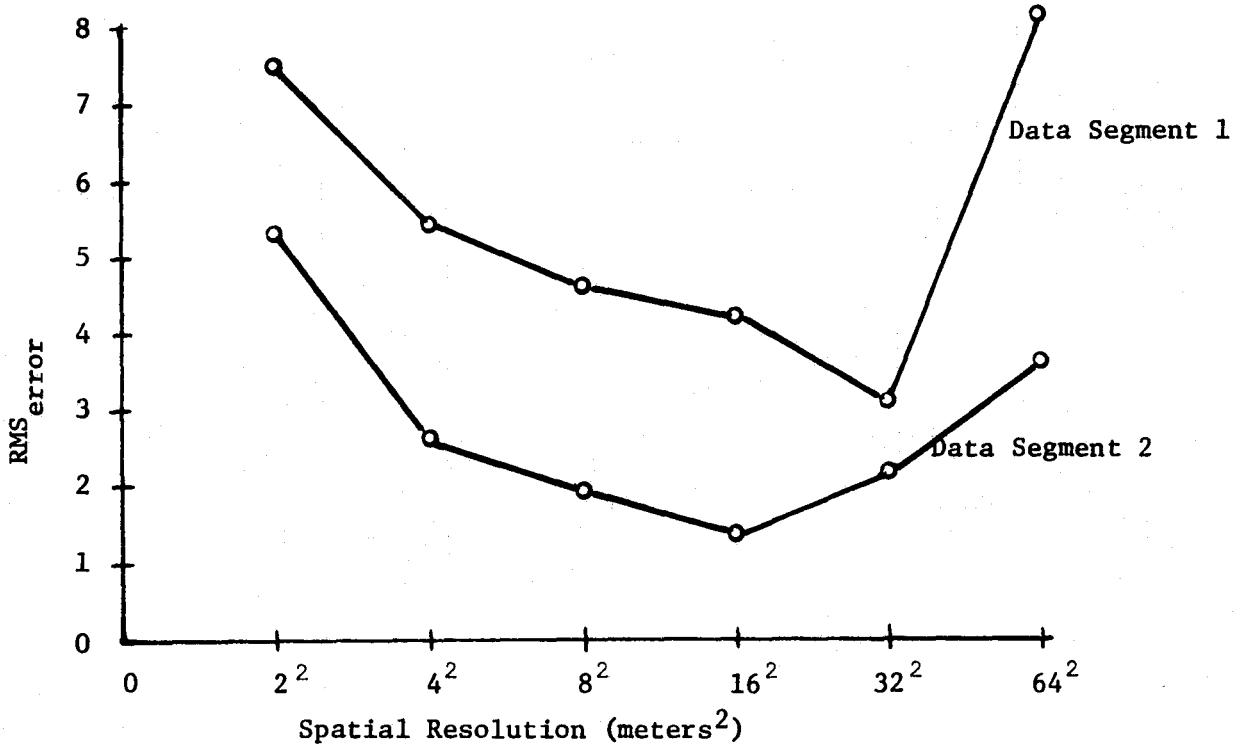


(a) RMS Error Calculated For All Elements In Each Data Segment

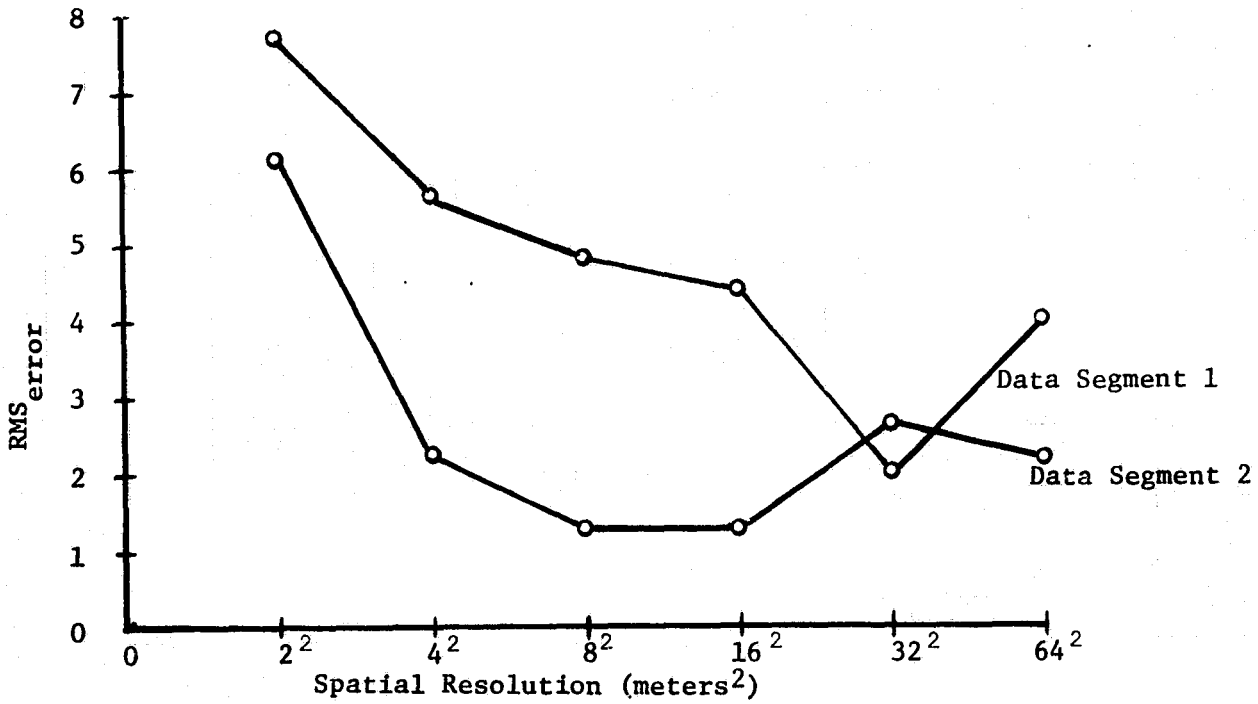


(b) RMS Error Calculated For Only Classified Elements In Each Data Segment

FIGURE 20. RMS ERROR PLOTTED AS A FUNCTION OF SPATIAL RESOLUTION

The best spatial resolution for proportion estimation as seen in these figures is $(32 \text{ meters})^2$ for data segment 1 and $(16 \text{ meters})^2$ for data segment 2. Figures 21-24 are plots showing the percent difference of the estimated proportion of each physiognomic feature compared to the ground truth proportion. For Figures 21 and 22, the estimated percentages are shown for all elements in the test area. These figures show the effect of large numbers of unclassified elements as all features in both $(64 \text{ meters})^2$ data segments are underestimated.

Figures 23 and 24 give results calculated for only the classified elements. These figures give more insight into how the features of each data segment interrelate. At low spatial resolutions in data segment 1, pine sawtimber is overestimated while regeneration is underestimated. The estimates of both features improve through the $(32 \text{ meters})^2$ data set, and then at $(64 \text{ meters})^2$ regeneration is overestimated while pines are underestimated. These results are due to the fact that, as spatial resolution coarsens, less of the regeneration area is misclassified as pine sawtimber, increasing the proportion of elements classified as regeneration while decreasing the estimated proportion of pine sawtimber. In data segment 2 (Figure 24) the situation might appear to be more complicated since there are three features. However, the cut over feature is sufficiently unique that little interaction occurs with the other two features and its estimated proportion varies little from its true ground proportion for all cases of resolution. Thus, the only interaction is between hardwoods and pine. While pines are overestimated at low spatial resolutions, hardwoods are underestimated; but for resolutions of $(16 \text{ meters})^2$ and greater, pines are underestimated and hardwoods overestimated. These results reflect the improvement in hardwood classification accuracy as a funtion of increasing spatial resolution which increases the proportion of elements classified as hardwoods, but decreases the estimated proportion of pines since fewer hardwoods are misclassified as pines.

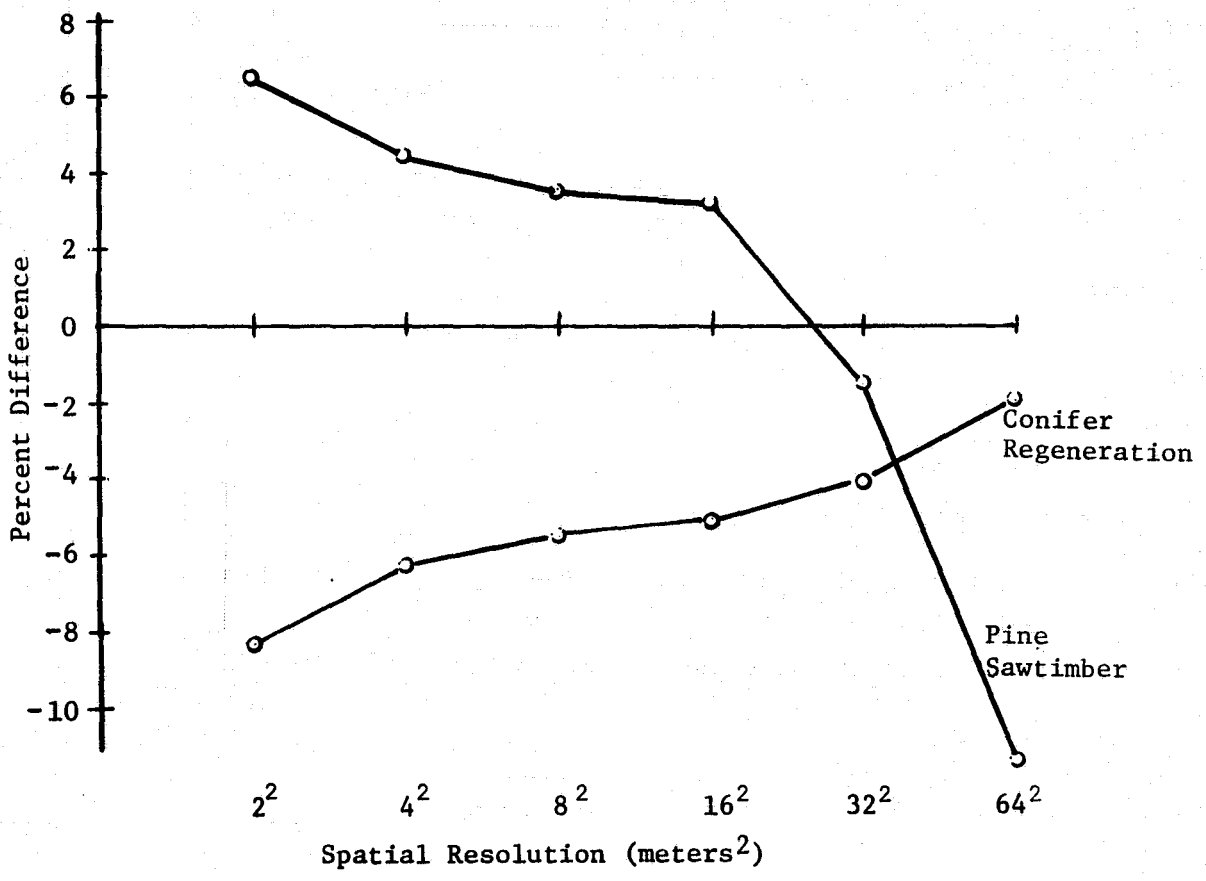


FIGURE 21. PERCENT DIFFERENCE BETWEEN TRUE GROUND PROPORTIONS AND ESTIMATED PROPORTIONS CALCULATED FOR ALL ELEMENTS OF DATA SEGMENT 1

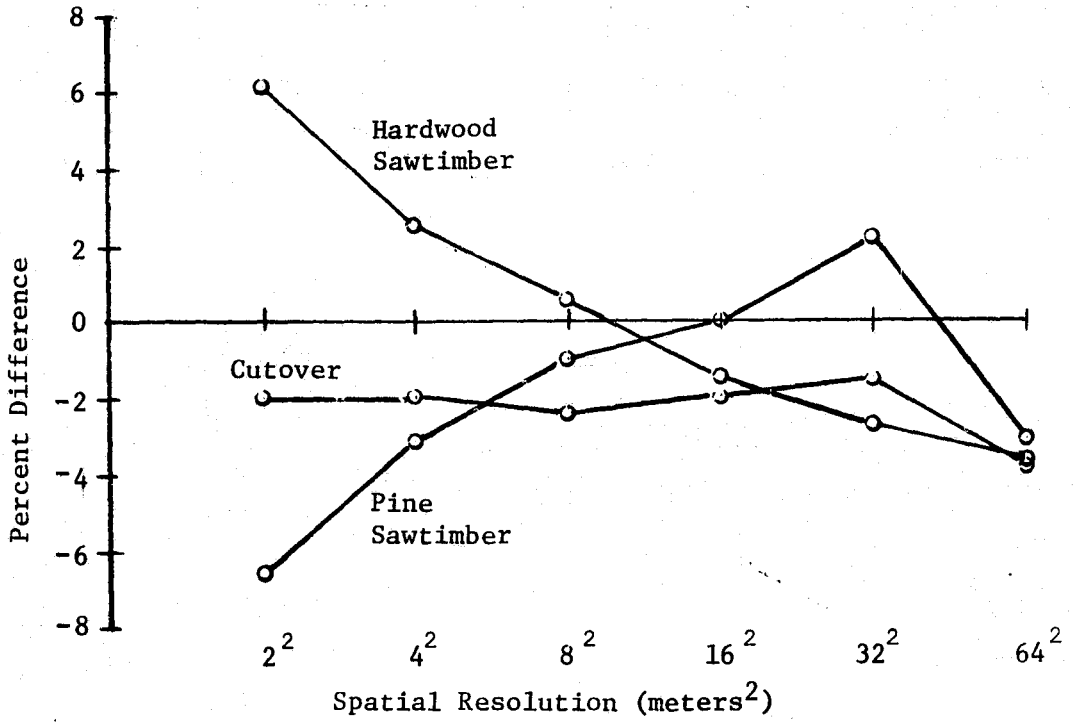


FIGURE 22. PERCENT DIFFERENCE BETWEEN TRUE GROUND PROPORTIONS AND ESTIMATED PROPORTIONS CALCULATED FOR ALL ELEMENTS OF DATA SEGMENT 2

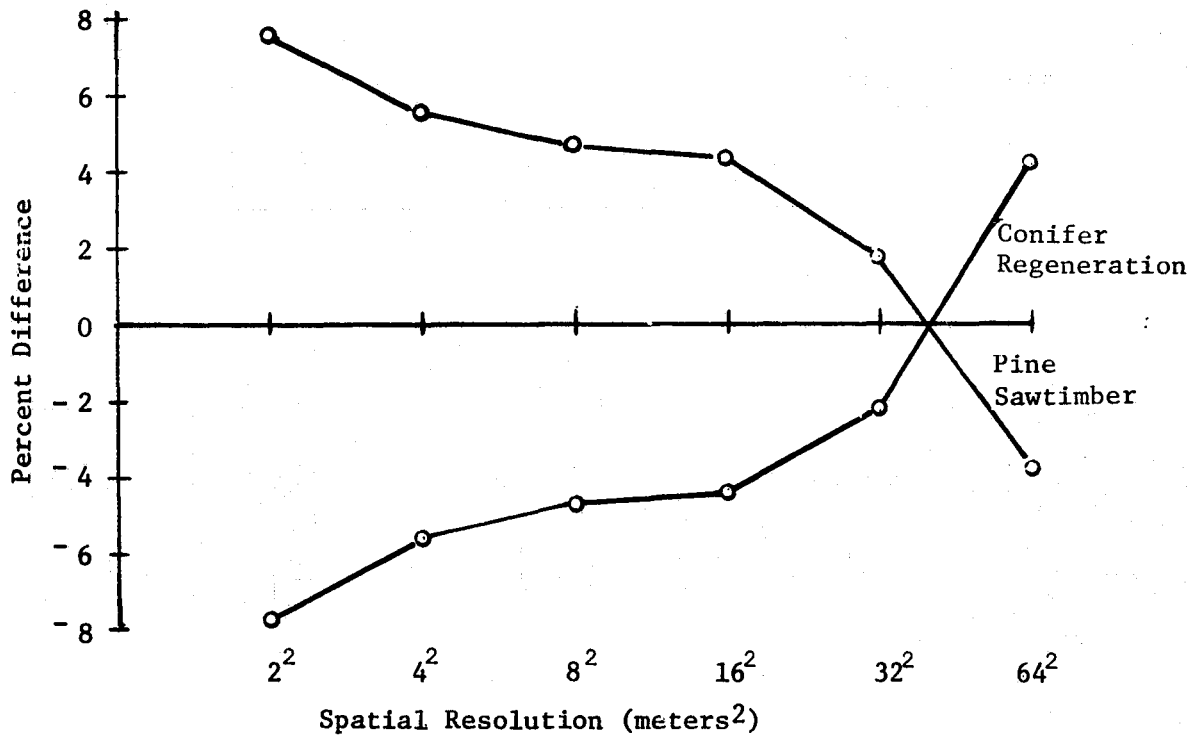


FIGURE 23. PERCENT DIFFERENCE BETWEEN TRUE GROUND PROPORTIONS AND ESTIMATED PROPORTIONS CALCULATED FOR CLASSIFIED ELEMENTS OF DATA SEGMENT 1

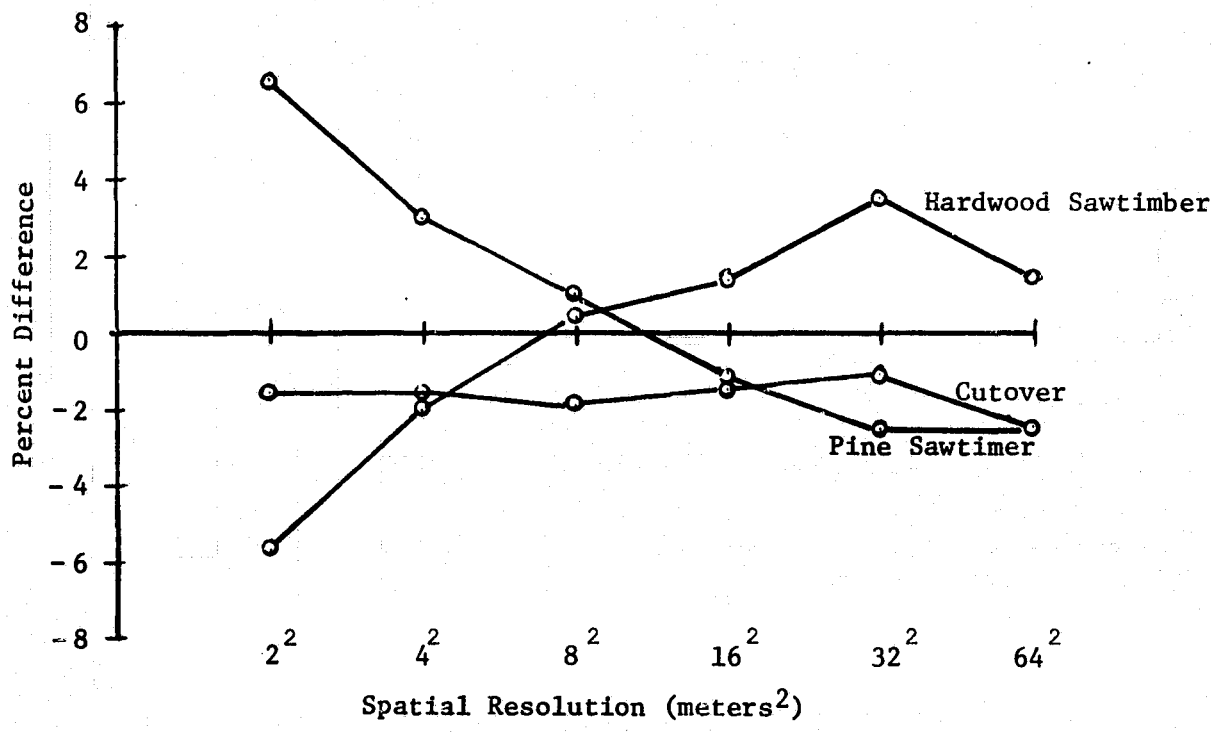


FIGURE 24. PERCENT DIFFERENCE BETWEEN TRUE GROUND PROPORTIONS AND ESTIMATED PROPORTIONS CALCULATED FOR CLASSIFIED ELEMENTS OF DATA SEGMENT 2

For both data segments, the changes in estimated proportions of physiognomic features that occur with changes in spatial resolution seem principally due to changes in the misclassification of those features having greater variability. Within such features, the averaging of extreme data values as spatial resolution degrades was seen to improve the estimate of their scene proportion. Thus, fewer misclassifications of elements within conifer regeneration (data segment 1) and hardwood sawtimber (data segment 2) were noted. The different optimum spatial resolutions noted for proportion estimation in each data segment indicates some dependency on the types of features.

# 5

# CONCLUSIONS AND RECOMMENDATIONS

## 5.1 CONCLUSIONS

A supervised multispectral data classification approach that utilized a standard single-element linear decision rule with a conventional constant decision threshold was used to classify forest features in 6 MSS data sets that ranged in spatial resolution from $(2 \text{ meters})^2$ to $(64 \text{ meters})^2$. The classification accuracies, averaged over all features for training and test sets were seen to improve from $(2 \text{ meters})^2$ to $(32 \text{ meters})^2$ cases of resolution. Improvement was attributed to a reduction in the number of misclassified resolution elements that occurred as a result of reduced competition among signature distributions. Reduced competition presumably resulted from a reduction in scene variation that is inherent in the averaging of information over larger ground areas.

When spatial resolution was degraded to the $(64 \text{ meters})^2$ case, the percentage of unclassified elements in test sets increased greatly. Because unclassified elements were considered to be errors, this caused a net decrease in classification accuracy for the test sets of hierarchies in data segment 2 and in the simulated results of test sets in data segment 1. Therefore, it appears that unclassified resolution elements can exert a strong influence on classification results; and rejection threshold levels should be selected with great care. The results of this study indicated that a resolution of $(32 \text{ meters})^2$ provided the most accurate element-by-element classification of these forest features. However, for $(64 \text{ meters})^2$ data, a selection of a different rejection threshold might have yielded different indications.

Very definite improvements in classification performance as spatial resolution was degraded were noted for hierarchies of more general (aggregated) forest features by virtue of the fact that misclassifications of resolution elements between certain specific

features canceled for their aggregated feature class. Although very similar trends were noted for all hierarchies as a function of spatial resolution, we point out the differences in performance that occur between equivalent hierarchies of the two data segments as illustrating the dependency of the performance on the characteristics of the features in the scene. These differences suggest that strategies for the automatic classification of forest features with MSS data possibly can not be generalized, but rather need to be reconsidered anew for specific areas or applications.

The application of multi-element decision rules to the classification of forest features attempts to provide the improved classification advantages of coarser spatial resolutions while maintaining the locational accuracy and area measurement capabilities inherent in fine resolutions. Results of applying four different nine-point rules to the classification of the $(32 \text{ meters})^2$ data indicate that the judicious selection of such rules can offer improved classification performance that is greater than an improvement that might be realized with standard classification techniques used on coarser resolution data. Nine-point rules appear to offer a significant advantage for improving the classification of detailed features. We postulate that multi-element approaches might provide even more benefit if applied to finer resolution data.

The Thematic Mapper simulation indicated that classification accuracy was higher for $(64 \text{ meters})^2$ data than for $(32 \text{ meters})^2$ data. The five channels selected to simulate the proposed Thematic Mapper channels compared favorably in terms of classification accuracy to the full complement of $M^2S$ channels for general hierarchies such as physiognomy but do not appear to be able to give the accuracy for condition classes that is possible with all the $M^2S$ channels.

Area proportion estimation is of great practical importance for large area surveys, especially extensive ones. In this study, forest

features at the level of physiognomies were well estimated. The best spatial resolution for such estimates varied between the two data segments which is most likely a result of the fact that there are different features present in the two segments.

## 5.2 RECOMMENDATIONS

As a result of this study, a number of issues can be stated as requiring further investigation. Some of the issues clearly could not be addressed within the scope of this study. Others are raised as a result of this study.

1. A signature analysis study should be undertaken to resolve the variations in classification performance that occur for individual features and some hierarchies as spatial resolution degrades. Obvious questions remaining unanswered by this study include:
   a. the possible biases of using several signatures for some features versus a single signature for others,
   b. changes in the location, shape, and size of feature signatures relative to the data values as resolution varies, and
   c. the effect that would have resulted from varying the decision threshold of signatures to allow a constant proportion of unclassified elements for all resolutions,
   d. additionally, the inherent (2 meters)$^2$ resolution of this data set would enable an examination of the fundamental influences affecting forest canopy signatures.

2. Investigate the merits of other training approaches for classifying forest features. In order to recognize U.S. Forest Service designated features, we utilized a supervised training approach. Other approaches worth investigating might include both supervised and unsupervised clustering.

3. The promising results of the nine-point rules for forest feature classification shown in this report suggest that additional investigation and development of multi-element processing techniques has potential for improving the classification and boundary location of forest areas.

4. The very limited ground area encompassed by this study has prevented any statistical assessment of classification performance for features and hierarchies as a function of spatial resolution. It is recommended that an approach similar to the one reported herein be applied to a more extensive forest area.

5. Area proportion estimation of forest features at the physiognomic level looks very promising. More data segments should be studied to evaluate if there is one optimum spatial resolution or to define how the optimum changes as the character of the feature within the segment changes.

# APPENDIX I
# MSS DATA QUALITY ANALYSIS

Prior to the procedural processing steps of this study, we analyzed the quality of the MSS data in order to detect potential problems that could affect the accuracy of the classification results. Such problems could be instrument-related or they could be associated with the radiation environment and the scene being scanned.

## I.1 ANALYSIS OF INSTRUMENT-RELATED DATA QUALITY

The purpose of this analysis was to assess signal-to-noise characteristics and signal instabilities in the MSS data. Signal-to-noise was assessed by determining dynamic range and high frequency noise variations for each spectral channel. Dynamic range in this case is defined as the range of signal values that are representative of total scene variability. It was quantified by using histogram limits that encompassed 96% of a one percent sample of the signal values taken in a systematic fashion from each segment of data. High frequency noise was measured by averaging rms fluctuations in signal value that had been computed for a dark level calibration source at several regions along the flightline of each segment.

Table I-1 lists dynamic range, noise quantities, and resultant signal-to-noise values for data segment 1. Signal-to-noise, obtained by dividing the dynamic range of each channel by its respective noise quantity, indicates the number of quantum contrast levels available and thus provides some relative measure for ranking channels according to the ability to distinguish between two sources of radiance. Note that Channel 1 (0.41-0.44 μm) was very noisy which resulted in a substantially lower signal-to-noise value than for other channels.

Further observations of signal values from the calibration sources indicated that a shift in mean signal level occurred in all spectral channels along the flightline of each data segment. A similar shift

TABLE I-1. DATA QUALITY FOR $M^2S$ DATA OF MISSION 290 -- DATA SEGMENT 1

| Sensor Channel | Spectral Band Limits (μm) at 50% Response Points | Dynamic Range (Signal Values) | RMS "Noise" Fluctuations (Signal Values) | Signal-to-Noise Ratio Value | Ranking |
|---|---|---|---|---|---|
| 1 | 0.41-0.44 | 114 | 33.1 | 3.4 | 11 |
| 2 | 0.45-0.49 | 52 | 3.9 | 13.3 | 10 |
| 3 | 0.49-0.54 | 33 | 2.3 | 14.3 | 9 |
| 4 | 0.53-0.57 | 31 | 1.8 | 17.2 | 8 |
| 5 | 0.57-0.61 | 27 | 1.4 | 19.3 | 7 |
| 6 | 0.61-0.65 | 31 | 1.5 | 20.7 | 6 |
| 7 | 0.65-0.69 | 31 | 1.3 | 23.8 | 5 |
| 8 | 0.69-0.73 | 48 | 1.2 | 40.0 | 3 |
| 9 | 0.76-0.86 | 123 | 4.9 | 25.1 | 4 |
| 10 | 0.95-1.03 | 104 | 1.8 | 57.8 | 1 |
| 11 | 8-12 | 105 | 2.5 | 42.0 | 2 |

in signal could be noted for the video portion of the data as a contrast variation that occurred between the groups of scan lines (see Figure I-1). This change in contrast or "banding" could be caused by some instability in the scanner electronics. The magnitude of the shift varied from channel to channel and was calculated to be as high as 30% of the dynamic range for some channels. The detrimental effect of such a low frequency signal variation on automatic classification procedures required that it be removed.

A dynamic clamp algorithm was developed and applied to each segment of data. The algorithm implemented an additive correction to the data by adjusting signal values in the video portion of each scanline according to a continuously updated correction term. The correction term was computed as an average of the dark level calibration source signals contained in a window that spanned several successive scanlines immediately preceding and following the scanline being corrected. Updating the correction term was accomplished by sliding the window along the flightline and re-computing the average for each scanline corrected.

By averaging dark level calibration source signals within a window of several scanlines, we strived to normalize the low frequency signal variation along the flightline without introducing additional high frequency noise on a scanline to scanline basis. Occasional calibration source signals of inordinately different magnitude that might wrongly influence the computed correction term were automatically excluded from the averaging process by virtue of an editing limit. Since such widely varying calibration source signals might be indicative of a bad scan line or excessive system noise, they alone were used to adjust video signal values in their respective scanlines. Thus, bad scanlines remained as bad scanlines.

Application of the dynamic clamp algorithm constituted the only preprocessing correction to the data. Figure I-2 illustrates data

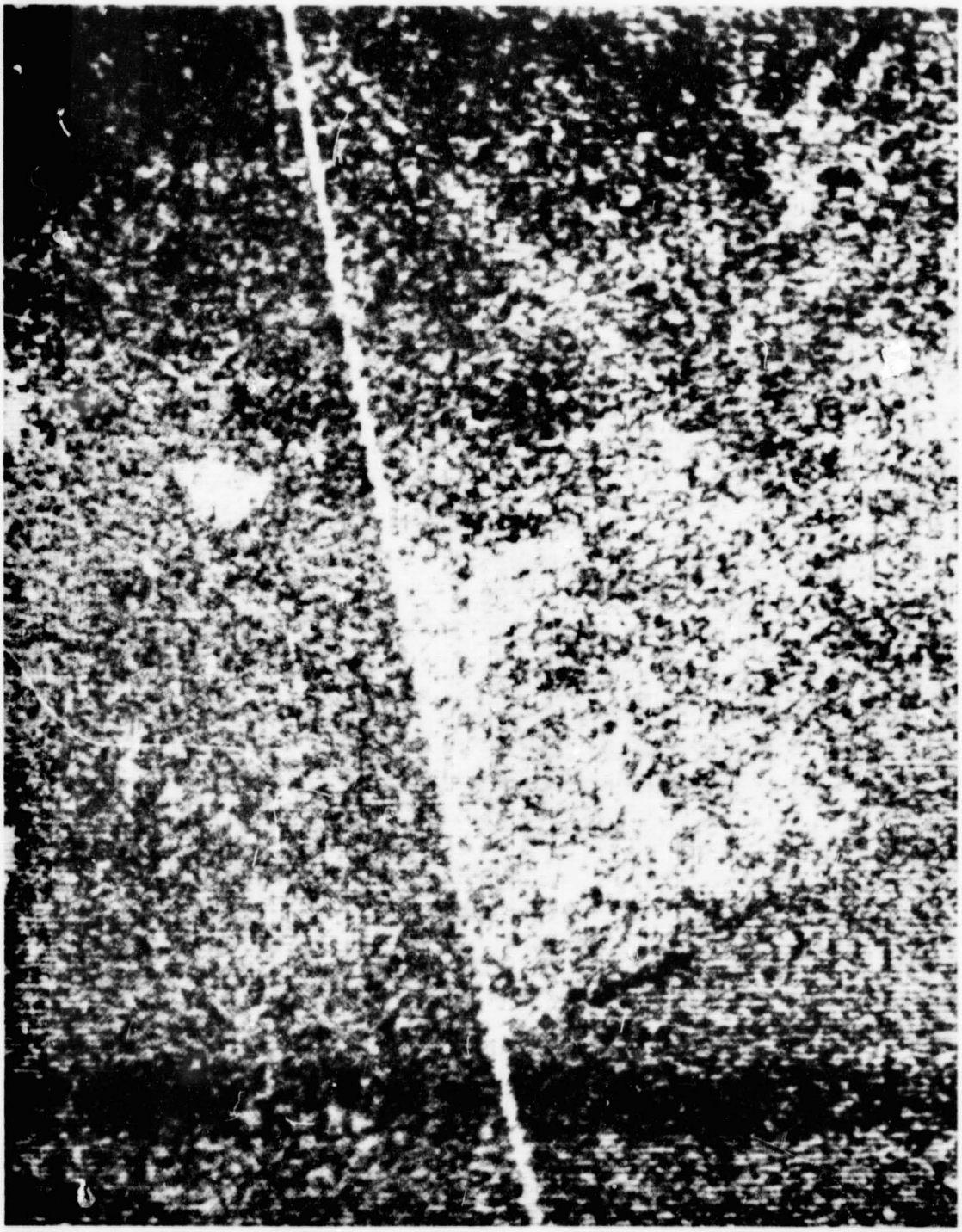

FIGURE I-1. CONTRAST VARIATION OR 'BANDING' IN DATA SEGMENT 1 RESULTING FROM A SHIFT IN SIGNAL LEVEL ALONG THE FLIGHTLINE. Image is a five interval level-slice of Channel 7 (0.65 - 0.69 $\mu$m).

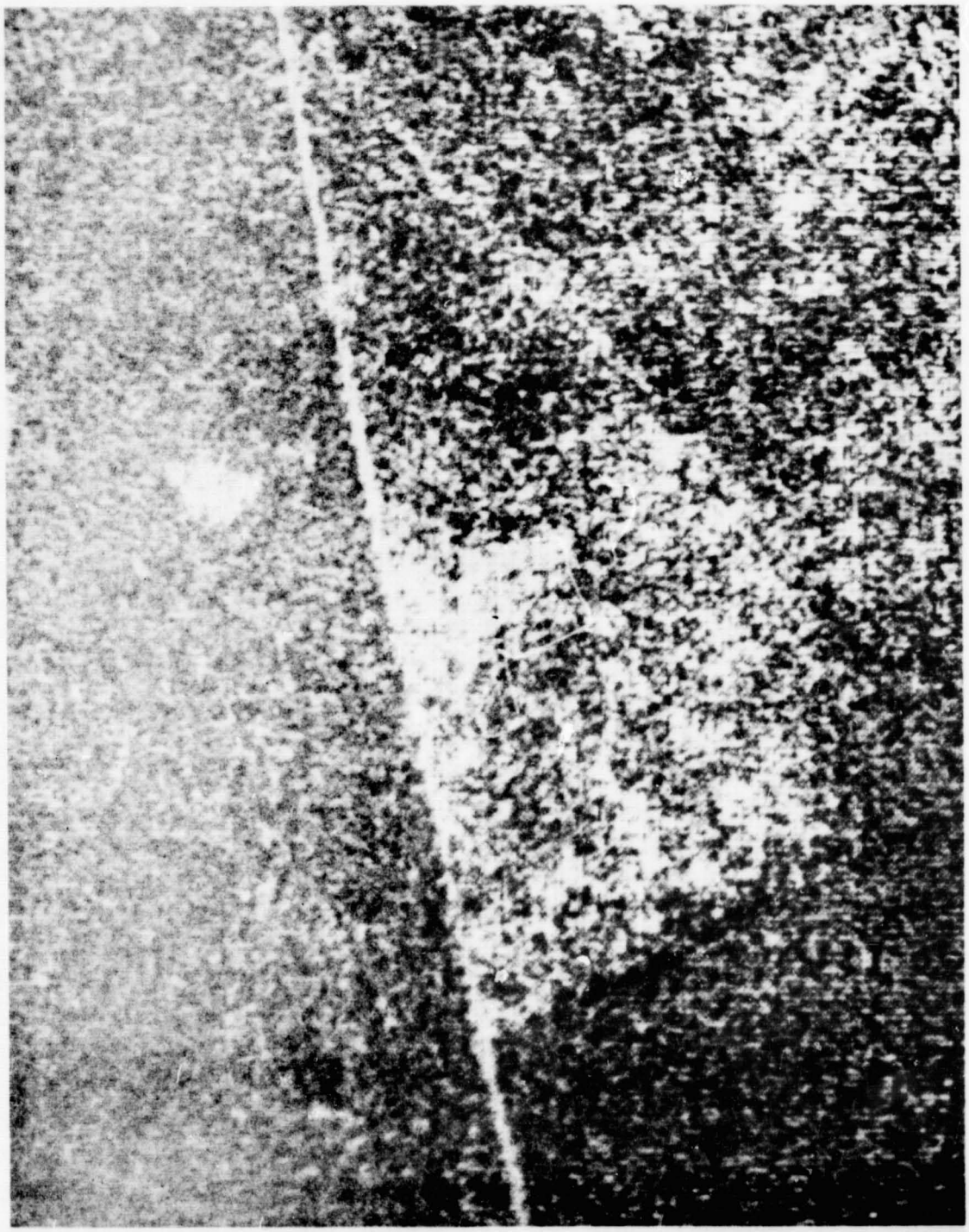

FIGURE I-2. DATA SEGMENT 1 AFTER REMOVAL OF THE 'BANDING' ARTIFACT BY THE DYNAMIC CLAMP PROCEDURE. Image is a five interval level-slice of Channel 7 (0.65 - 0.69 $\mu$m).

segment 1 after removal of the banding artifact by the clamping procedure. Table I-2 shows the resultant dynamic range and noise quantities for the segment after clamping. For most channels, dynamic range varied only slightly from original levels (see Table I-1) and noise quantities were generally reduced by about 25%. These results agreed with our expectations that the clamping procedure would not significantly alter the basic character of the data set. The large increase in dynamic range for Channel 1 occurred by virtue of the noisy calibration source signals frequently exceeding the editing limit of the window used for computing the correction term.

To be complete, the dynamic range and noise quantities for data segment 2 after clamping are presented in Table I-3. Because brighter and darker scene classes exist in this data segment, the dynamic range for each channel is greater than for data segment 1. Noise quantities are comparable between the two data segments.

## I.2 ANALYSIS OF SIGNAL VARIATIONS ASSOCIATED WITH SCAN ANGLE

Because of the large range of view angles common to aircraft multispectral scanners ($\pm$ 60$^{o}$ from nadir in the case of this data set), scene radiance values recorded by the scanner can include systematic variations that are associated with scan angle. Such variations can be caused by the scattering and attenuating influences of the atmosphere as path length from sensor to ground varies with scan angle [ 5 ]. The bidirectional reflectance properties of the scene components are another major cause [ 6 ]. The presence of such variations in the data can pose a serious problem for classifying forest features across the entire flightline.

Variations in signal associated with scan angle were assessed for the data set of inherent (2 meters)$^{2}$ spatial resolution. We computed average scan lines for three different regions of each segment of data. An average scan line contained average signal values for

TABLE I-2. DATA QUALITY FOR $M^2S$ DATA OF MISSION 290 -- DATA SEGMENT 1, AFTER CLAMPING

| Sensor Channel | Spectral Band Limits (μm) at 50% Response Points | Dynamic Range (Signal Values) | RMS "Noise" Fluctuations (Signal Values) | Signal-to-Noise Ratio Value | Ranking |
|---|---|---|---|---|---|
| 1 | 0.41-0.44 | 153 | 17.0 | 9.0 | 11 |
| 2 | 0.45-0.49 | 47 | 2.7 | 17.4 | 10 |
| 3 | 0.49-0.54 | 28 | 1.7 | 26.3 | 6 |
| 4 | 0.53-0.57 | 25 | 1.3 | 23.7 | 8 |
| 5 | 0.57-0.61 | 23 | 1.0 | 23.0 | 9 |
| 6 | 0.61-0.65 | 25 | 1.0 | 25.0 | 7 |
| 7 | 0.65-0.69 | 28 | 1.0 | 28.0 | 5 |
| 8 | 0.69-0.73 | 47 | 1.0 | 47.0 | 3 |
| 9 | 0.76-0.86 | 122 | 3.2 | 38.1 | 4 |
| 10 | 0.95-1.03 | 106 | 1.6 | 66.2 | 1 |
| 11 | 8-12 | 106 | 1.7 | 62.4 | 2 |

TABLE I-3. DATA QUALITY FOR $M^2S$ DATA OF MISSION 290 -- DATA SEGMENT 2, AFTER CLAMPING

| Sensor Channel | Spectral Band Limits (μm) at 50% Response Points | Dynamic Range (Signal Values) | RMS "Noise" Fluctuations (Signal Values) | Signal-to-Noise Ratio Value | Ranking |
|---|---|---|---|---|---|
| 1 | 0.41-0.44 | 203 | 17.9 | 11.3 | 11 |
| 2 | 0.45-0.49 | 80 | 2.5 | 32.0 | 9 |
| 3 | 0.49-0.54 | 44 | 1.4 | 31.4 | 10 |
| 4 | 0.53-0.57 | 38 | 1.1 | 34.5 | 8 |
| 5 | 0.57-0.61 | 34 | 0.9 | 37.8 | 7 |
| 6 | 0.61-0.65 | 36 | 0.8 | 45.0 | 6 |
| 7 | 0.65-0.69 | 43 | 0.9 | 47.8 | 5 |
| 8 | 0.69-0.73 | 56 | 1.0 | 56.0 | 3 |
| 9 | 0.76-0.86 | 149 | 3.1 | 48.1 | 4 |
| 10 | 0.95-1.03 | 148 | 1.6 | 92.5 | 2 |
| 11 | 8-12 | 134 | 1.4 | 95.7 | 1 |

80 divisions, each of which had been computed by averaging 10 adjacent resolution elements over 100 successive scan lines in the original data. The gross averaging of 1000 resolution elements into each of the divisions in the average scan line thus enable smoothing over high frequency variations in radiance within scene features in order that radiance variations associated with scan angle could be observed more clearly.

Figure I-3 illustrates several average scan lines computed over a region at the southern end of data segment 1. Except for pine regeneration at the extreme right side, most of the region covers a fairly homogeneous scene of pine sawtimber features. Obvious differences in average signal value between features exist only where the average scan lines cross a pipeline right-of-way (exposed bare soil at division no. 46) and the pine regeneration (division no. 79). In the figure, plots for four of the 11 MSS channels illustrate representative scan angle variations in radiance for the blue, green, red, and near-infrared spectral regions. Because the direction of the flightline was toward the sun, the direction of scan was perpendicular to the direction of illumination. Thus, any variations in scene radiance caused by sun position will be symmetrical either side of nadir.

With the exception of the short wavelength regions, computed average scan lines displayed a lack of obvious signal variations associated with scan angle. In other words, the circumstances of data collection seemed to minimize effects of the atmosphere and the bi-directional reflectance properties of forest features in modifying scene radiance across the flightline.

To make a case for the observed average scan lines from the standpoint of the atmosphere, we exercised the Turner Atmospheric Model [ 5 ] to illustrate trends in scene radiance caused by increasing path length from sensor to ground. The components of radiance are given by the relationship

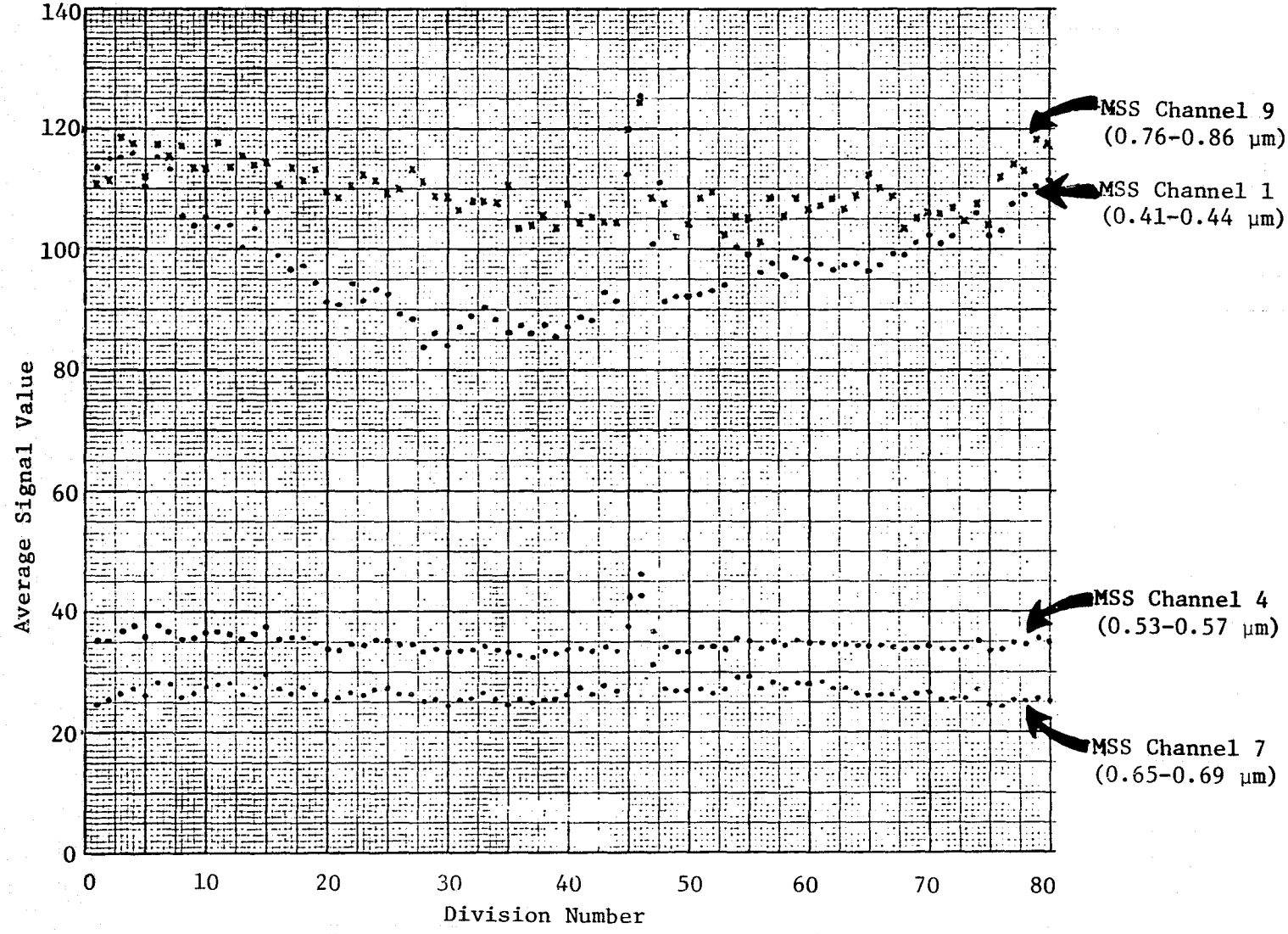


FIGURE I-3. REPRESENTATIVE AVERAGE SCAN LINES FOR FOUR SPECTRAL CHANNELS COMPUTED FROM DATA SEGMENT 1

$$L_{T_\lambda} = \frac{\rho_\lambda E_\lambda \tau_\lambda}{\pi} + L_{p_\lambda}$$

where

$L_{T_\lambda}$ is the total spectral radiance received from the target at the sensor,

$\rho_\lambda$ is spectral reflectance of the target,

$E_\lambda$ is spectral irradiance on the target,

$\tau_\lambda$ is spectral transmittance of the atmosphere between sensor and target,

and $L_{p_\lambda}$ is path radiance introduced by the atmosphere between sensor and target.

The effect of increasing path length on total radiance will be manifested by virtue of changes in atmospheric transmittance and path radiance.

For the model calculations, illumination and viewing geometries specified were those that existed at the time of data collection. Target and surrounding background reflectance parameters were set equal and were based on typical vegetation canopy reflectance values for wavelengths of 400, 550, 650, and 800 nm. Atmospheric parameters were specified for two assumed cases of atmosphere condition as stated by horizontal visibilities of 23 km (clear) and 8 km (hazy).

Results of the model calculations are presented in Table I-4. Scan angles of $0^\circ$ and $60^\circ$ provide results for atmospheric path lengths to the nadir and edge of the flightline respectively. For the clear atmosphere case, as scan angle varies from $0^\circ$ to $60^\circ$, changes in total radiance (column 8) are relatively small for the green, red, and near-infrared wavelength regions while the change for the shorter wavelength

TABLE I-4. TURNER ATMOSPHERIC MODEL RESULTS FOR ATMOSPHERIC PATH LENGTHS APPROPRIATE TO MSS SCAN ANGLES OF 0° AND 60°; TWO CASES OF ATMOSPHERE CONDITION ARE ASSUMED.

**VISIBILITY = 23 km**

| | 0° Scan Angle | | | 60° Scan Angle | | | |
|---|---|---|---|---|---|---|---|
| Wavelength (nm) (1) | Total Radiance ($mw\ cm^{-2}sr^{-1}\mu m^{-1}$) (2) | Percent Total Radiance Represented by Path Radiance (3) | Transmittance (4) | Total Radiance ($mw\ cm^{-2}sr^{-1}\mu m^{-1}$) (5) | Percent Total Radiance Represented by Path Radiance (6) | Transmittance (7) | Percent Change in Total Radiance 0° → 60° (8) |
| 400 | 1.0888 | 67.1 | 0.8825 | 1.4364 | 78.0 | 0.7788 | +24.2 |
| 550 | 2.1241 | 22.5 | 0.9204 | 2.3143 | 34.5 | 0.8470 | + 8.2 |
| 650 | 1.0518 | 27.2 | 0.9287 | 1.2010 | 40.8 | 0.8624 | +12.4 |
| 800 | 8.8386 | 4.6 | 0.9399 | 8.6898 | 8.8 | 0.8834 | - 1.7 |
| **VISIBILITY = 8 km** | | | | | | | |
| 400 | 1.5599 | 81.5 | 0.7269 | 2.0247 | 89.6 | 0.5283 | +23.0 |
| 550 | 2.4662 | 45.6 | 0.7626 | 2.7896 | 63.3 | 0.5816 | +11.6 |
| 650 | 1.2661 | 47.7 | 0.8138 | 1.5372 | 65.0 | 0.6623 | +17.6 |
| 800 | 8.6187 | 8.6 | 0.8834 | 8.3335 | 16.5 | 0.7804 | - 3.3 |

blue region is much greater. As the condition of the atmosphere degrades to the 8 km visibility case, changes in total radiance with scan angle increase for the longer wavelength regions. Thus, on the basis of model calculations, a "clear" atmosphere at the time of data collection would tend to minimize signal variations associated with scan angle for wavelength regions longer than the blue region.

A combination of circumstances attributable to sun elevation and azimuth angles may have combined to reduce any appreciable variations in radiance as a function of scan angle that would be caused by the bidirectional reflectance properties of the forest canopy. Because of the low sun elevation angle of $40^{\circ}$, large shadows cast by the trees within each forest stand resulted in little illuminated background being visible between trees for the nadir scan angle. Thus, the loss of observed illuminated background as scan angle changed from nadir would not have been a factor to influence scan angle variations in radiance. In addition, because the direction of scan was perpendicular to the direction of illumination, sun azimuth angle relative to scan angle remained constant. This insured that radiance variations with scan angle were symmetrical either side of nadir and of lower magnitude than for situations where the direction of scan is alternately toward and away from the direction of illumination.

The lack of strong signal variations associated with scan angle for most spectral channels in this data set was significant for the objectives of this study. Because of the low altitude from which the data were collected, any severe or non-symmetrical scan angle variations might have seriously reduced the amount of already limited ground coverage. On the basis of this analysis, we concluded that signature extraction and classification performance procedures could be conducted within $30^{\circ}$ either side of the flightline nadir with a reasonable degree of independence from scan angle variations. This region would provide coverage for several forest features and yet maintain a view angle



C-2

geometry between sensor and ground that would exclude large variations in atmospheric path length or bidirectional reflectance phenomena.

# APPENDIX II

# A SPATIAL FILTERING TECHNIQUE FOR SIMULATING DEGRADED RESOLUTION OF DIGITIZED DATA

## II.1 INTRODUCTION

The spatial frequency response of a multispectral scanner (MSS) is usually specified by a modulation transfer function (MTF) which designates the MSS system throughput (amplitude, and sometimes phase as well) as a function of spatial frequency. The equivalent, in the spatial domain, to this MTF is a spatial weighting function which can be visualized in either of two ways: (1) as a specification of the relative weighting of each point in the scene within an effective instantaneous field of view (IFOV), or (2) as the effective analog spatial response of the MSS to a spatial impulse (point source) input. MTF's and their equivalent spatial weighting functions are fundamental to the understanding of spatial resolution and to the following discussion.

Degradation of MSS spatial resolution has often been simulated in the past by simply averaging together digitized signals within blocks of pixels and replacing each block with its average signal, representing the simulated signal for each new pixel in the degraded data set. The dimensions of these blocks of pixels can be determined by registering a grid with the original data, with the spacing of the grid representing the approximate size and spacing desired for the degraded pixels. The average signals are then calculated and recorded for each square (or rectangle) of the grid. This technique simulates enlarging the MSS aperture, reducing the sampling rate, and increasing the ground speed of the sensor. It also simulates a fundamental change in the overall scanner system MTF. This changed MTF is somewhat unrealistic for studies of MSS data utility as a function of scanner resolution, particularly with regard to simulating the performance of a satellite system, using aircraft MSS data.

A more valid basis for studies of changing scanner resolution can be achieved by spatially filtering and resampling MSS data in a manner which simulates a realistic system MTF at the degraded resolution. In this case we choose to keep the effective system MTF unchanged, as if only the altitude of the sensor, its ground speed, and the time interval between instantaneous samples of the analog signal were changed. Such a simulation requires that one first specify the nature of the overall MSS system MTF.

## II.2 SIMULATION OF THE OVERALL SCANNER SYSTEM RESPONSE

For a simulation, an overall scanner system MTF is most easily specified by components, corresponding to the various factors which together comprise the total system response. For this study three components were chosen which are typical for most modern scanner instruments.

The first scanner system response component chosen was one corresponding to the instantaneous field of view associated with the scanner aperture. The spatial weighting function for this IFOV is plotted in Figure II-1 for a two meter square IFOV. The points plotted (connected by straight line segments) correspond to digitization of the curve at the rate of 8 samples for every meter. This high sampling rate was chosen to illustrate (approximately) the analog form of the weighting function, meant to correspond to a scanner system with a sampling interval (i.e., pixel spacing) of two meters.

Since the geometry of scanner optics, their imperfections, and atmospheric effects all contribute to blur of the instantaneous field of view of the instrument, the second response component chosen was one corresponding to gaussian blur with a standard deviation of 1/3 meter. The spatial weighting function corresponding to this blur is plotted in Figure II-2. When the effects of this blur are combined with the IFOV represented by the first response component, above,

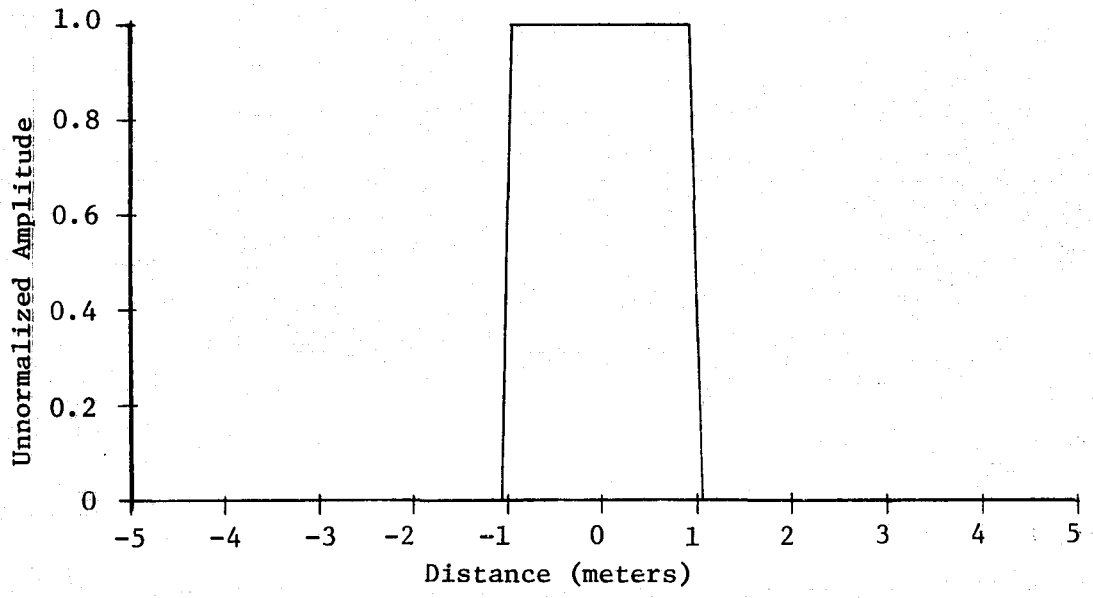


FIGURE II-1. SIMULATED SPATIAL WEIGHTING COMPONENT ASSOCIATED WITH SCANNER APERTURE (2 meter resolution)

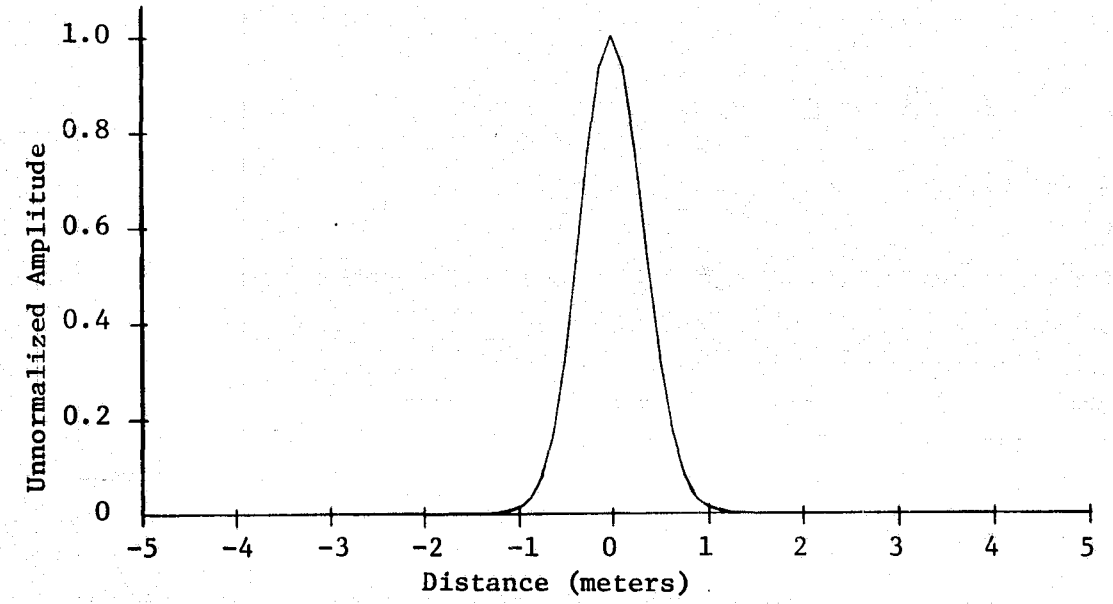


FIGURE II-2. SIMULATED SPATIAL WEIGHTING COMPONENT ASSOCIATED WITH SCANNER GAUSSIAN BLUR ($\sigma$ = 1/3 meter, 2 meter resolution)

(by convolution in the spatial domain), one obtains the spatial weighting function representing the total combined optical and atmospheric effects simulated for this study. This combined weighting function is plotted in Figure II-3. Again, the curves are plotted using 8 sample points per meter. The MTF corresponding to the combination of these is plotted in Figure II-4. Note that the assumed spatial sampling frequency for the simulated scanner system is one sample for every two meters, while the MTF curve has been plotted for spatial frequencies as high as one sample per meter. The significance of spatial frequencies in excess of one half the simulated sample rate (greater than one sample per four meters) will be discussed below.

While the first two scanner response components simulated above are two-dimensional effects, the third component chosen is strictly a one-dimensional effect, applying only to the shape of the spatial weighting function in the scanning direction. This third component simulates electronic filtering used within the scanner to remove high frequency information which is of little use due to the limitations imposed by the choice of a finite sampling rate, and to trim the shape of the within-scan spatial weighting function and the corresponding MTF curve to produce the desired resolution size for the effective (overall for the system) instantaneous field of view. For this purpose a two pole Butterworth filter was simulated, whose spatial weighting function is plotted in Figure II-5. The impulse response of the two pole Butterworth filter is an exponentially damped sinusoid, represented by

$$H(x)_3 = 2\sqrt{2}\pi k_c \, e^{-\sqrt{2}\pi k_c x} \sin \sqrt{2}\pi k_c x \qquad \text{(II-1)}$$

with x representing distance in meters, $k_c$ = 0.364 cycles per meter representing the cutoff frequency (half power point) for the filter, and the subscript 3 designating that this response pertains to the

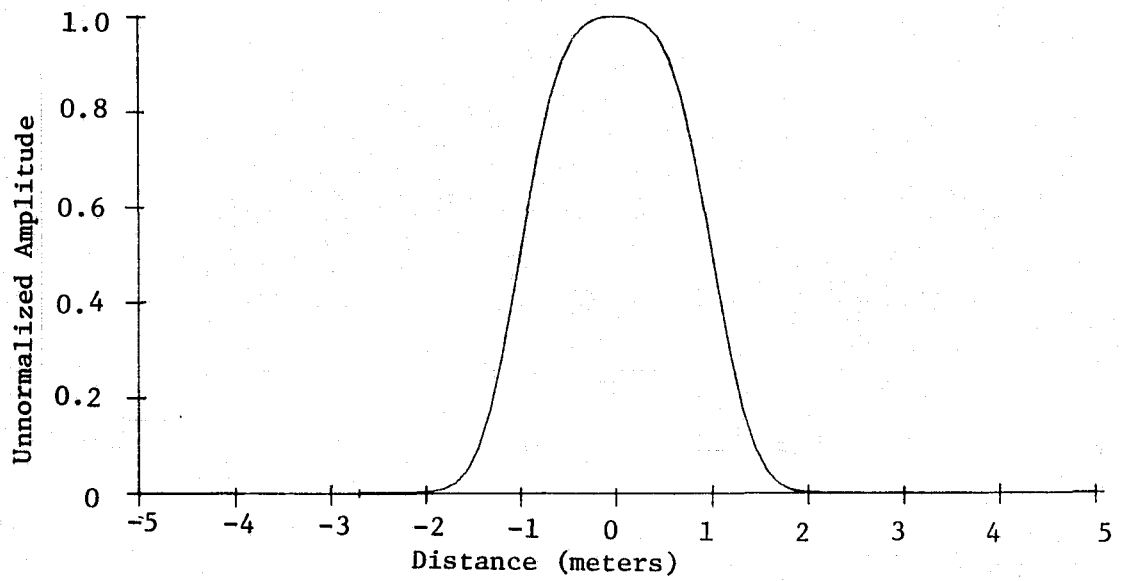


FIGURE II-3. SIMULATED COMPOSITE ALONG-TRACK SPATIAL WEIGHTING FUNCTION ASSOCIATED WITH SCANNER SYSTEM (2 meter resolution)

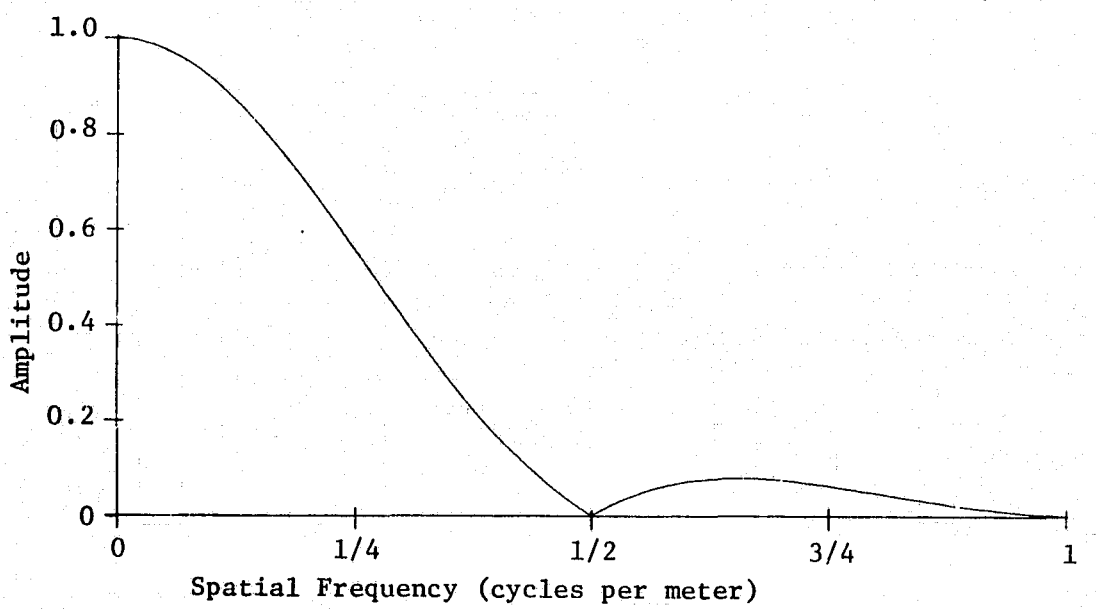


FIGURE II-4. SIMULATED COMPOSITE ALONG-TRACK MODULATION TRANSFER FUNCTION ASSOCIATED WITH SCANNER SYSTEM (2 meter resolution)

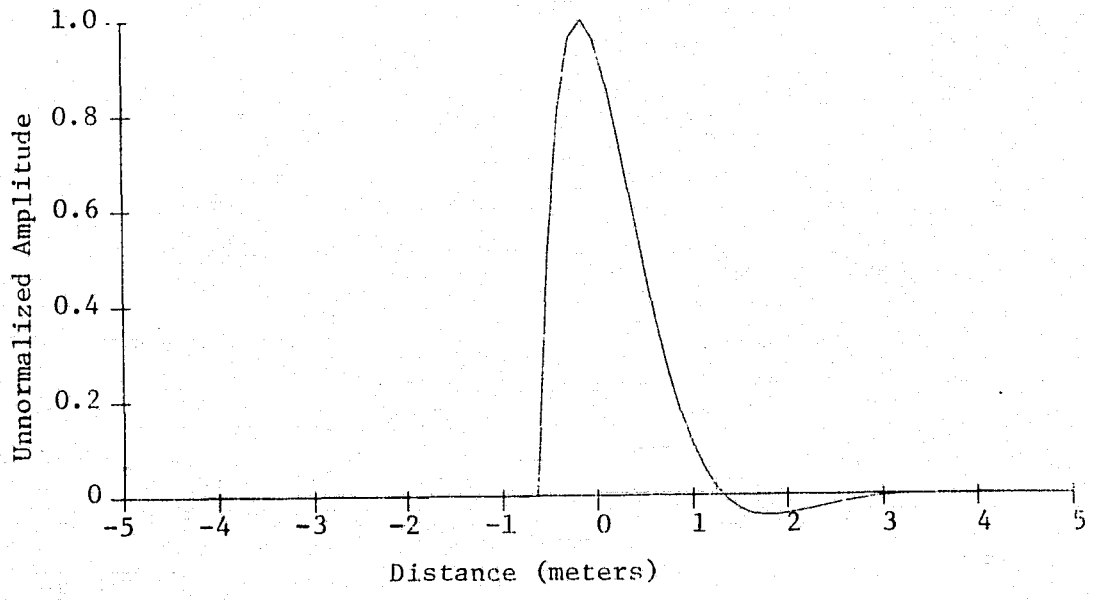


FIGURE II-5. SIMULATED SPATIAL WEIGHTING COMPONENT ASSOCIATED WITH TWO POLE BUTTERWORTH FILTER ($k_c$ = 0.364 cycles per meter, scanner with 2 meter resolution)

third scanner response component simulated. The combined spatial weighting function within-scan, which includes all three response components, is plotted in Figure II-6. The MTF corresponding to this combination is plotted in Figure II-7. Note in this figure that the spatial frequency at which the combined MTF amplitude equals 0.5 is one cycle per four meters. By convention this is interpreted to correspond to a two meter resolution system. The along-track overall MTF for this simulation (plotted in Figure II-4) is specified by

$$|A(k)|_{1\ 2} = \left|\frac{\sin(k \times 2\pi M)}{k \times 2\pi M}\right| e^{-\frac{1}{2}(k \times \frac{2}{3}\pi M)^2} \qquad \text{(II-2)}$$

while the within-scan overall MTF (plotted in Figure II-7) is specified by

(II-3)

$$|A(k)|_{1\ 2\ 3} = \left|\frac{\sin(k \times 2\pi M)}{k \times 2\pi M}\right| e^{-\frac{1}{2}(k \times \frac{2}{3}\pi M)^2} [1 + (k \times 3.25M)^4]^{-1/2}$$

with k representing spatial frequency in cycles per meter, and with the subscripts 1, 2, and 3 specifying the response components comprising each MTF. The response of this simulated system to an edge in a scene is plotted for the along-track direction in Figure II-8, and for the within-scan direction in Figure II-9. This latter response is quite similar to the published edge response for the $M^2S$ scanner whose data was used for this study, and is also reasonable for a modern satellite scanner system.

## II-3 DERIVATION OF THE REQUIRED SPATIAL FILTERS IN ANALOG FORM

Having specified the simulated scanner system MTF's both along-track and within-scan, one may next address the problem of spatially filtering the two meter resolution MSS data to simulate four meter data. Since the order in which the separate components of the simulated scanner response are combined makes no difference mathematically, one can determine three separate spatial filtering components, each

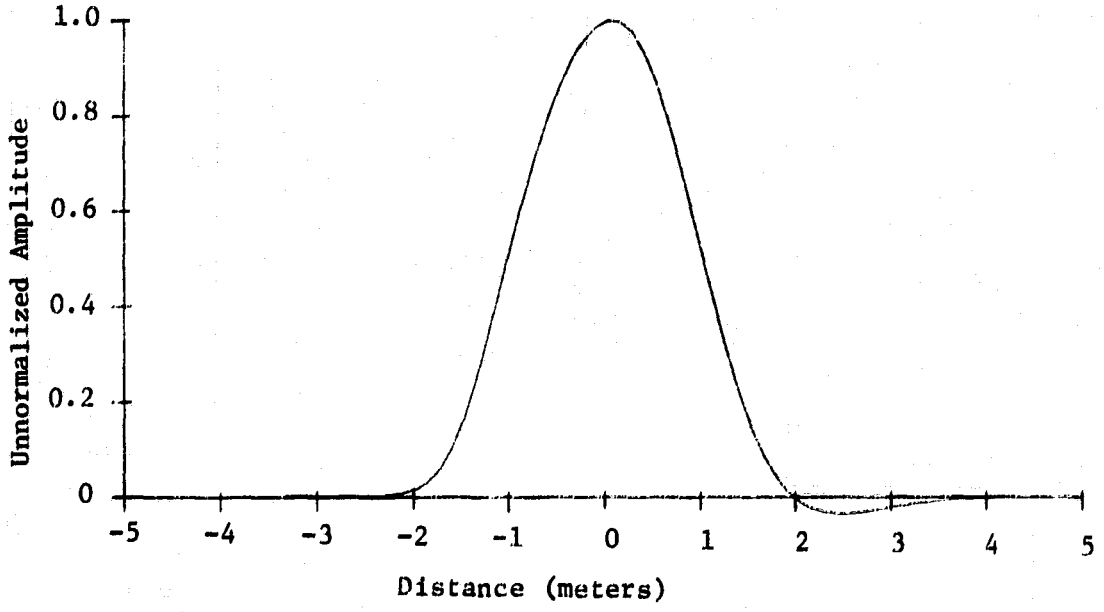


FIGURE II-6. SIMULATED COMPOSITE WITHIN-SCAN SPATIAL WEIGHTING FUNCTION ASSOCIATED WITH SCANNER SYSTEM (2 meter resolution)

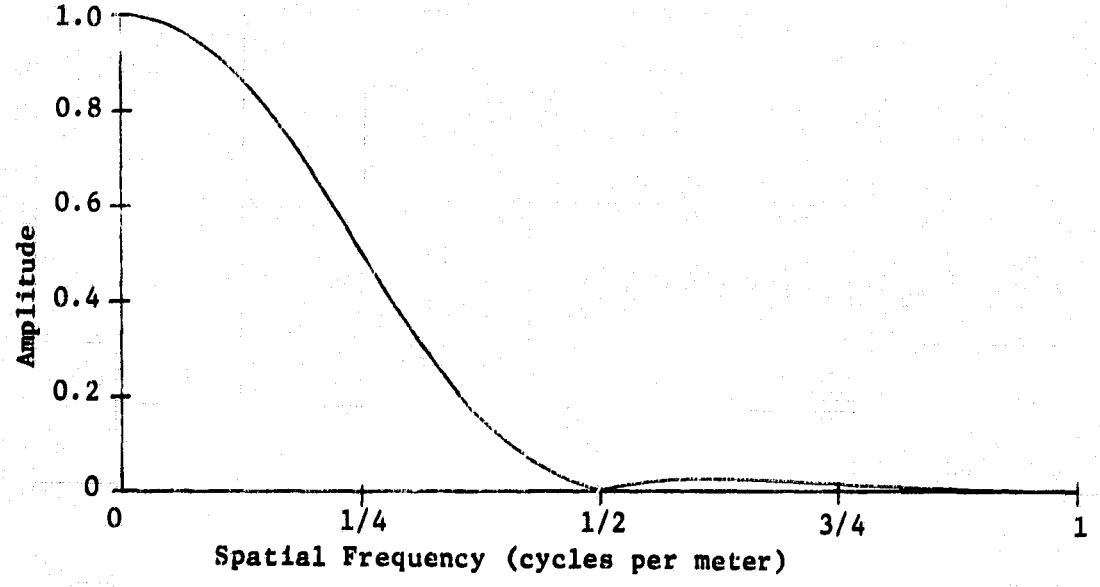


FIGURE II-7. SIMULATED COMPOSITE WITHIN-SCAN MODULATION TRANSFER FUNCTION ASSOCIATED WITH SCANNER SYSTEM (2 meter resolution)

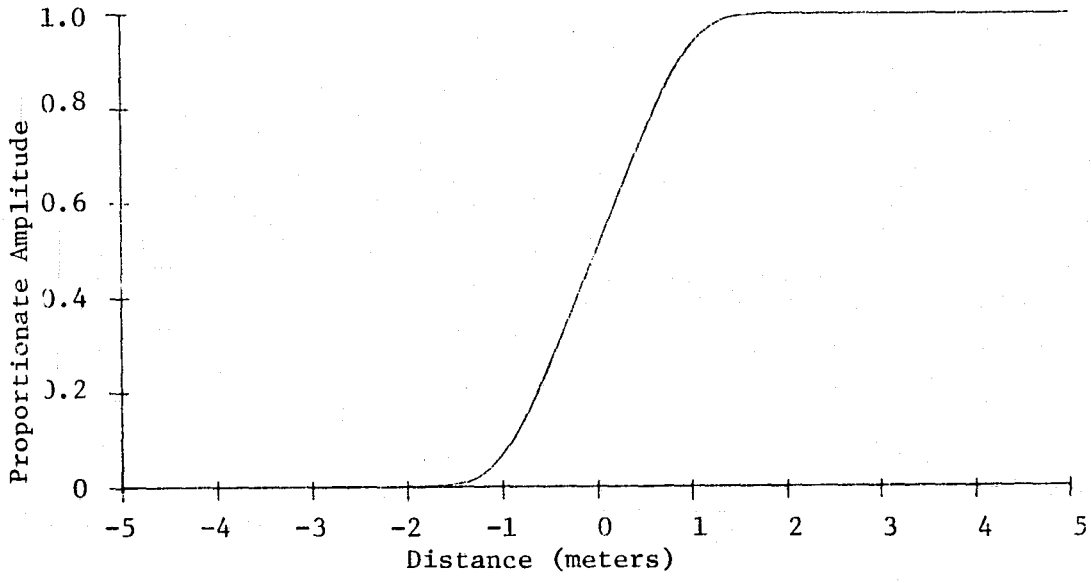


FIGURE II-8. SIMULATED ALONG-TRACK EDGE RESPONSE ASSOCIATED WITH SCANNER SYSTEM (2 meter resolution)

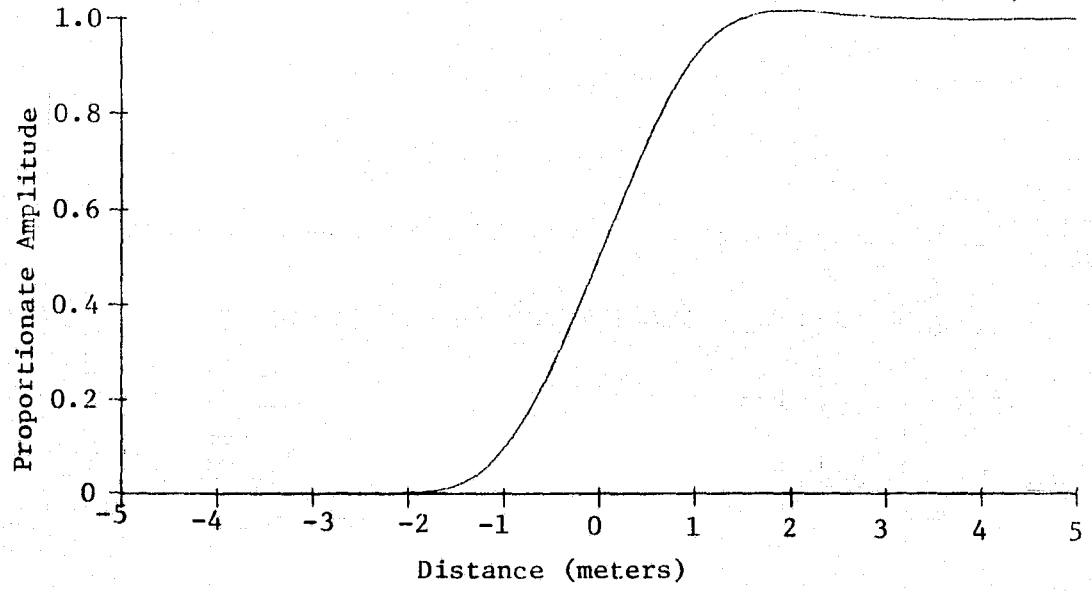


FIGURE II-9. SIMULATED WITHIN-SCAN EDGE RESPONSE ASSOCIATED WITH SCANNER SYSTEM (2 meter resolution)

associated with a separate member among the original three spatial weighting components, which perform the appropriate separate conversions. These three spatial filtering components, when suitably combined, will then represent the total spatial filtering function that is required (in analog form).

The first spatial filtering function required is a pair of unit impulses spaced two meters apart, as shown in Figure II-10. In two dimensions this first spatial filtering function can be visualized as four unit impulses located at the corners of a two meter square. This is equivalent to applying the one-dimensional filtering function shown in Figure II-10 first in the within-scan direction, and then in the along-track direction (or vice versa). This relation between one-dimensional and two-dimensional representations of the aperture and blur weighting and filtering functions holds in all cases simulated for this study, hence the along-track and within-scan filtering and weighting procedures are treated independently as one-dimensional problems. When combined with the first spatial weighting component (Figure II-1), this first filtering function produces a function representing a four meter square IFOV associated with the scanner aperture, simulating a doubling of the sensor altitude (with blur yet to be considered). This aperture function is plotted in Figure II-11. Note that sample points for the graph are still plotted at a spacing of 8 samples per meter.

The second spatial filtering function required is a gaussian function with a standard deviation of $1/3 \times \sqrt{3}$ meters, which is plotted in Figure II-12. This is another two-dimensional filtering function which may be considered as two separate one-dimensional functions, as shown in the figure, applied in the within-scan and along-track directions, respectively. The combination of this second filtering function with the second weighting function component is plotted in Figure II-13, with the horizontal axis compressed to facilitate

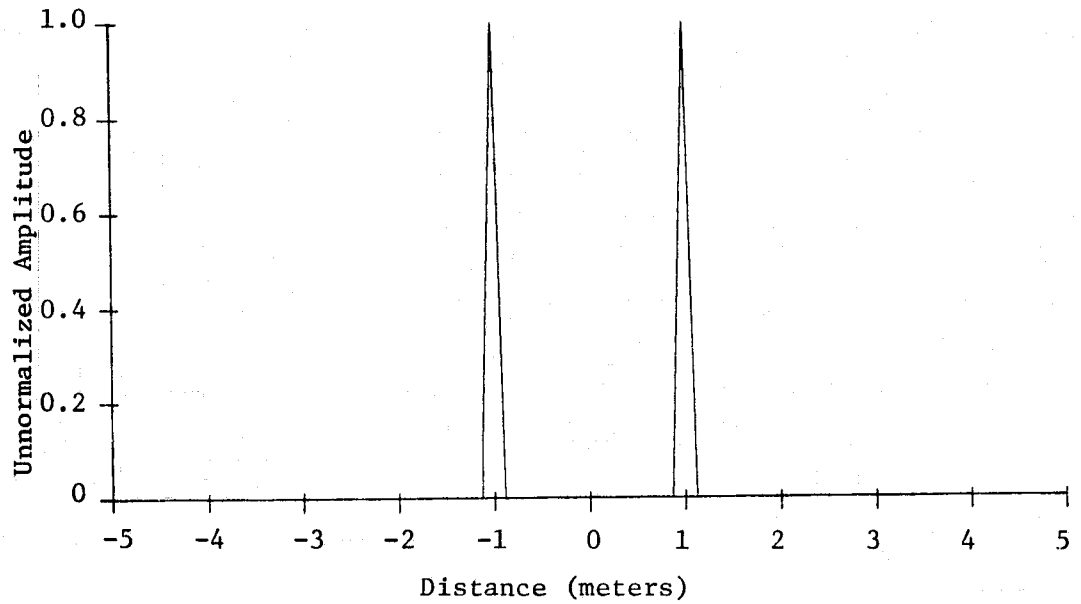


FIGURE II-10. ANALOG SPATIAL FILTERING COMPONENT FOR INCREASING SIMULATED SCANNER APERTURE (to 4 meter resolution)

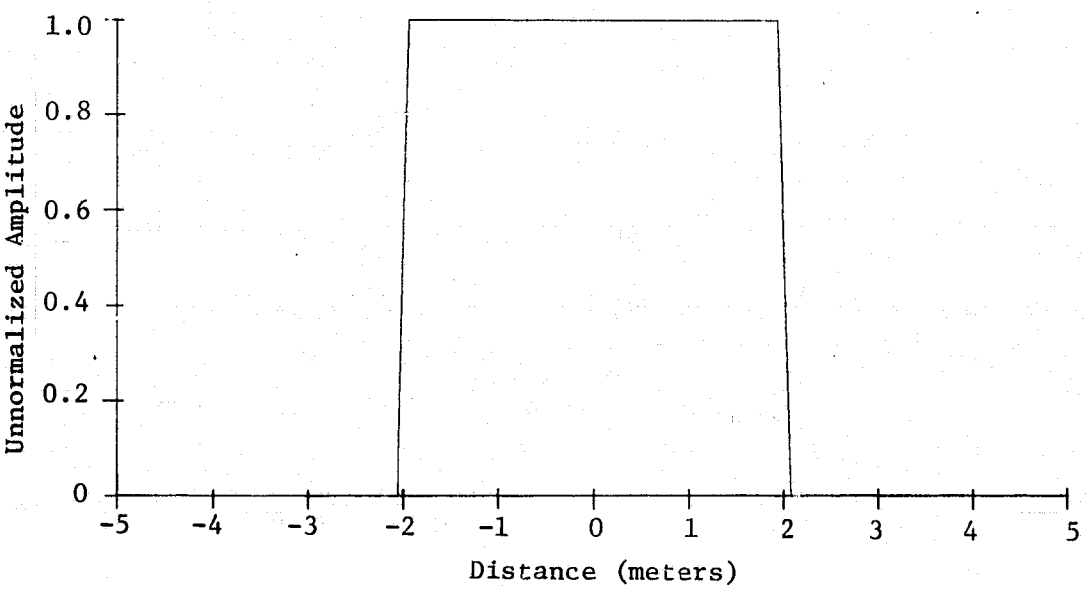


FIGURE II-11. SIMULATED SPATIAL WEIGHTING COMPONENT ASSOCIATED WITH SCANNER APERTURE AFTER FILTERING TO SIMULATE CHANGE TO 4 METER RESOLUTION

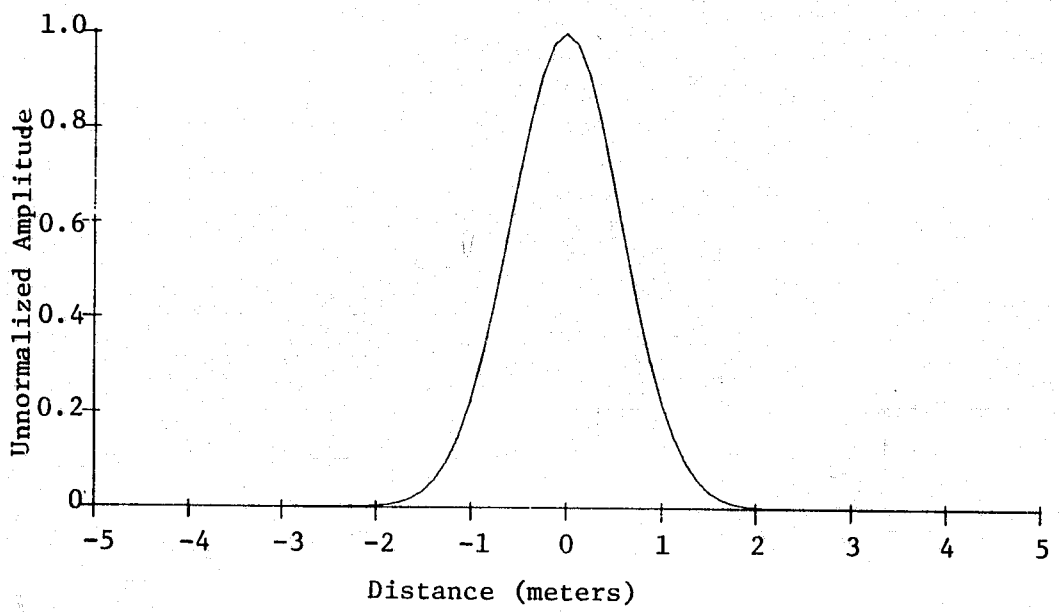


FIGURE II-12. ANALOG SPATIAL FILTERING COMPONENT FOR INCREASING SIMULATED SCANNER GAUSSIAN BLUR (to 4 meter resolution)

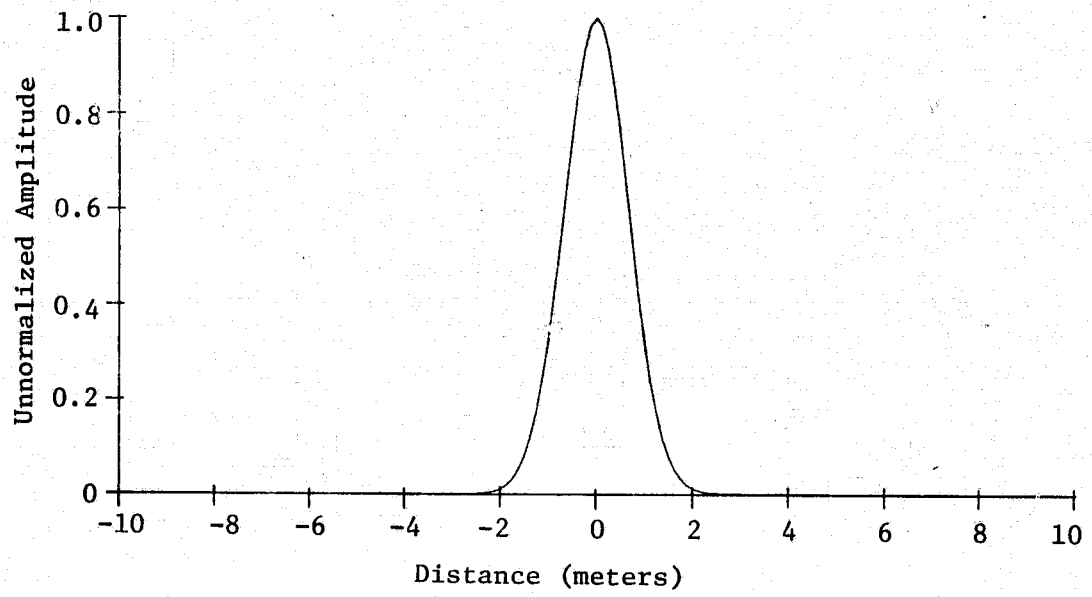


FIGURE II-13. SIMULATED SPATIAL WEIGHTING COMPONENT ASSOCIATED WITH SCANNER GAUSSIAN BLUR AFTER FILTERING TO SIMULATE CHANGE TO 4 METER RESOLUTION ($\sigma$ = 2/3 meter)

comparison with the original second weighting component plotted in Figure II-2. As can be seen, the filtering function succeeds in doubling the spatial width of the blur function, as desired. The apparent added smoothness of the curve in Figure II-13 is due to the preservation of sampling for the plot at 8 samples per meter. When the second spatial filtering function is combined with the first, one obtains the results shown in Figure II-14. This is the analog form of the required composite spatial filter for the along-track direction. The MTF for this composite filter is plotted in Figure II-15.

The third spatial filtering component required is one which would appropriately transform the response of the two pole Butterworth filter. The details of the mathematical derivation for this third filtering function will not be presented, however, the result is given by

(II-4)

$$H(x)_{F\ 3} = \frac{1}{4}\,\delta(x) + \frac{1}{4}\,2\sqrt{2}\pi k_c'\, e^{-\sqrt{2}\pi k_c' x}\,[2 \sin \sqrt{2}\pi k_c' x + \cos \sqrt{2}\pi k_c' x]$$

with x representing distance in meters, $\delta(x)$ representing a unit impulse, $k_c' = 0.182$ cycles per meter representing the cutoff frequency (half power point) for the new two pole Butterworth filter component to be simulated through the spatial filtering operation, and the subscripts F and 3 designating that this response pertains to the third filter component. This third spatial filtering component is plotted in Figure II-16. The result of applying this filter to the original third weighting function component, simulating the original two pole Butterworth filter response (Figure II-5), is shown in Figure II-17, with the horizontal axis compressed to facilitate comparison with Figure II-5. From these figures the filtering operation can be seen to succeed, with the apparent added smoothness of the curve plotted for the result (in Figure II-17) caused by retaining the sampling rate for plotting at 8 samples per meter. The combined spatial filtering function within-scan, which includes all three filter components, is

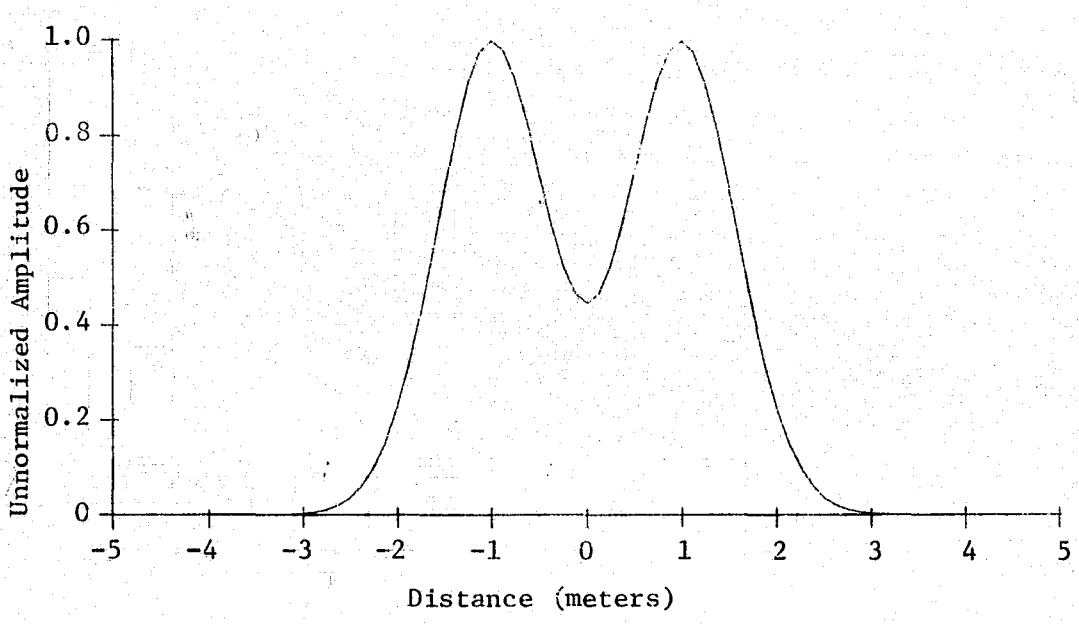


FIGURE II-14. COMPOSITE ANALOG SPATIAL FILTER FOR ALTERING SIMULATED ALONG-TRACK SCANNER RESPONSE (to 4 meter resolution)

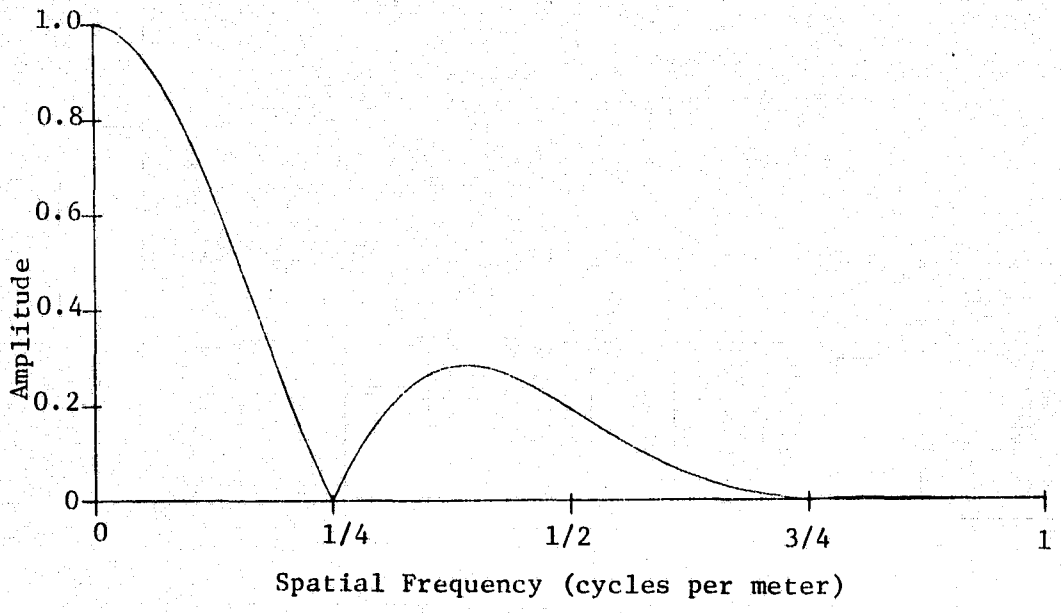


FIGURE II-15. COMPOSITE ANALOG FILTER MODULATION TRANSFER FUNCTION FOR ALTERING SIMULATED ALONG-TRACK SCANNER RESPONSE (to 4 meter resolution)

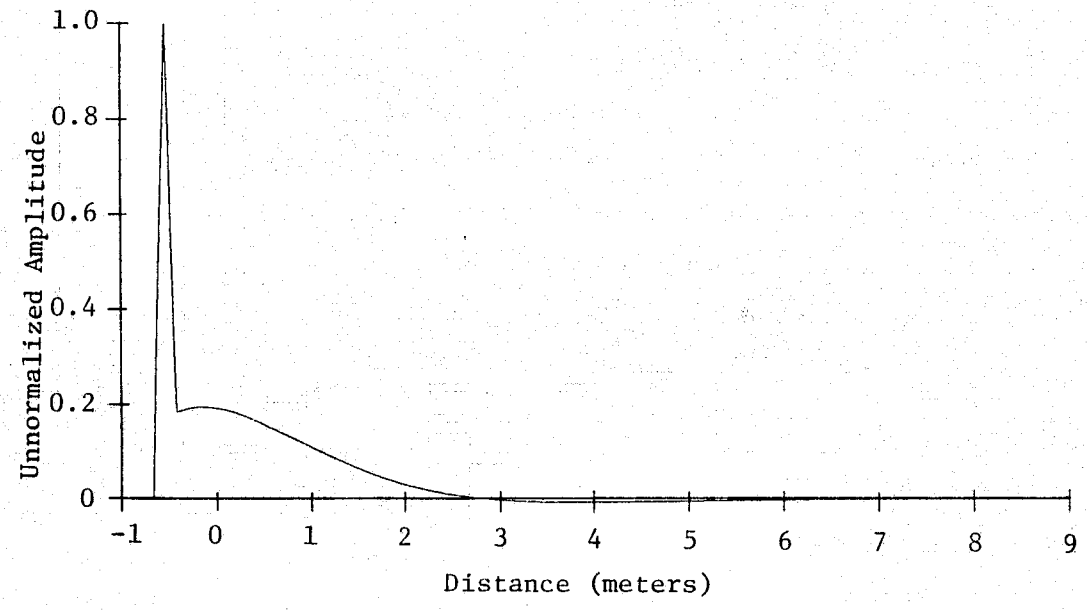


FIGURE II-16. ANALOG SPATIAL FILTERING COMPONENT TO ALTER TWO POLE BUTTERWORTH FILTER (to simulate 4 meter resolution)

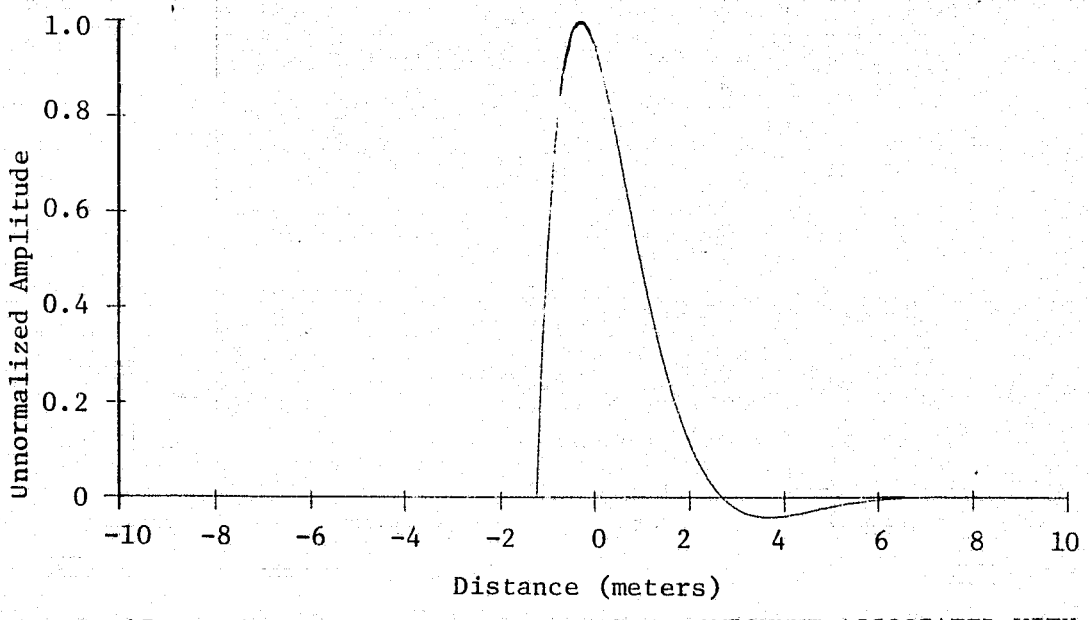


FIGURE II-17. SIMULATED SPATIAL WEIGHTING COMPONENT ASSOCIATED WITH TWO POLE BUTTERWORTH FILTER AFTER FILTERING TO SIMULATE CHANGE TO 4 METER RESOLUTION ($k_c'$ = 0.182 cycles per meter)

plotted in analog form in Figure II-18 (with compressed horizontal axis). The MTF corresponding to this combination is plotted in Figure II-19. The composite MTF for the along-track spatial filtering function (Figure II-15) is specified in analog form by

$$|A(k)_F|_{1\ 2} = |\cos(k \times 4\pi M)|\ e^{-\frac{3}{2}(k \times \frac{2}{3}\pi M)^2} \qquad \text{(II-5)}$$

while the analog form for the composite MTF of the within-scan spatial function (Figure II-19) is specified by

$$|A(k)_F|_{1\ 2\ 3} = |\cos(k \times 4\pi M)|\ e^{-\frac{1}{2}(k \times \frac{2}{3}\pi M)^2} \left\{\frac{1 + (k \times 6.50M)^4}{1 + (k \times 3.25M)^4}\right\}^{-1/2} \qquad \text{(II-6)}$$

with k representing spatial frequency in cycles per meter, and with the subscripts 1, 2, and 3 specifying the filter components comprising each MTF.

## II.4 DIGITIZATION OF THE ANALOG SPATIAL FILTERS

The next task is to determine appropriate digital filter equivalents to the analog along-track and within-scan spatial filtering functions. Since the original two meter resolution data is sampled only once for every two meters, the same sample spacing must be used for the digital filters which are derived. Clearly such a sample spacing would skip most of the detail of the analog filter representations shown in Figures II-14 and II-18. This finer detail in the curves is caused by the presence of high frequency information in the filters For data sampled at two meter intervals, only spatial frequencies up to one cycle per four meters (half the sample rate) can be perceived unambiguously. The higher frequencies masquerade as frequencies at or below the one cycle per four meters limit, as if the portions of the MTF curves which are above this limit were accordion folded back and forth between this one cycle per four meters limit and the origin. This masquerading effect on the high frequencies of an analog scene

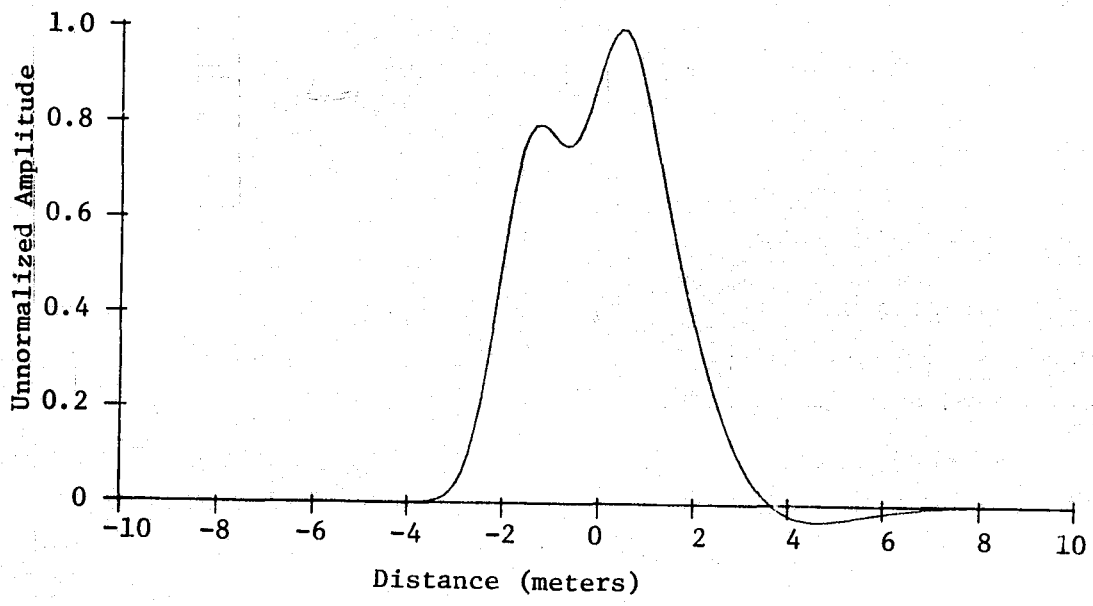


FIGURE II-18. COMPOSITE ANALOG SPATIAL FILTER FOR ALTERING SIMULATED WITHIN-SCAN SCANNER RESPONSE (to 4 meter resolution)

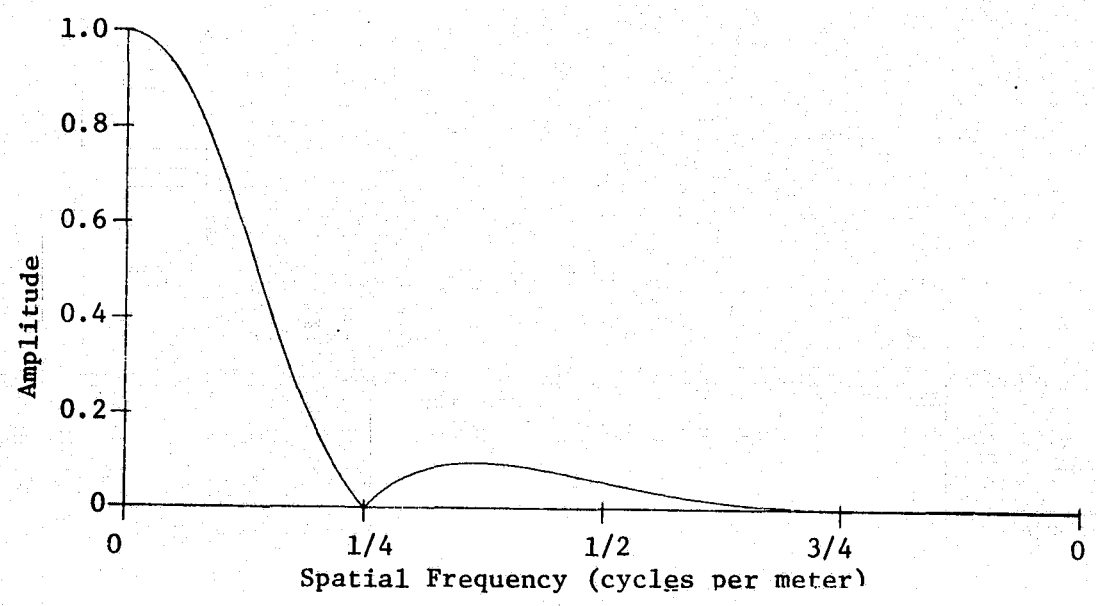


FIGURE II-19. COMPOSITE ANALOG FILTER MODULATION TRANSFER FUNCTION FOR ALTERING SIMULATED WITHIN-SCAN SCANNER RESPONSE (to 4 meter resolution)

or function, when it is sampled at equal intervals, is called aliasing. The analog scanner response at the two meter resolution (Figures II-4 and II-7) has already caused some aliasing. This must be accepted as a limit (although not a severe one) to the accuracy of any proposed simulation of altered scanner resolution through digital filtering of digitized data. Fortunately, the analog filters which have been derived do not contain substantial amounts of high frequency information (frequencies above one cycle per four meters), hence simulating degradation of spatial resolution by a linear factor as small as two, using the procedure to be derived below, is not an unreasonable task.

The first step taken toward generating a digital form for the filters was to truncate the spatial frequency response of the filters at the one cycle per four meters limit. This was accomplished by defining and applying a fourth analog spatial filter component given by

$$H(x)_{F\ 4} = \frac{1}{2} \frac{\sin(\pi x/2M)}{\pi x/2} \qquad \text{(II-7)}$$

with x representing distance in meters, and with the subscripts F and 4 designating that this is a fourth filter component. A computer program limitation on the number of weighting factors that could be used for nonrecursive filters restricted the spatial extent of this fourth filter component to $\pm$20 meters, half of which is shown in Figure II-20. This truncated representation of the fourth filter produced a least squares approximation, based on the number of weighting factors retained, to the abrupt low pass spatial frequency response that was intended for the filter component. The effects of this least squares approximation are noncritical, as will be evident in the final results to be presented below. The results of applying this fourth filter component to the along-track and within-scan analog spatial filtering functions are shown in Figures II-21 and II-23, respectively. By comparing these figures to Figures II-14 and II-18, it is clear that much of the finer

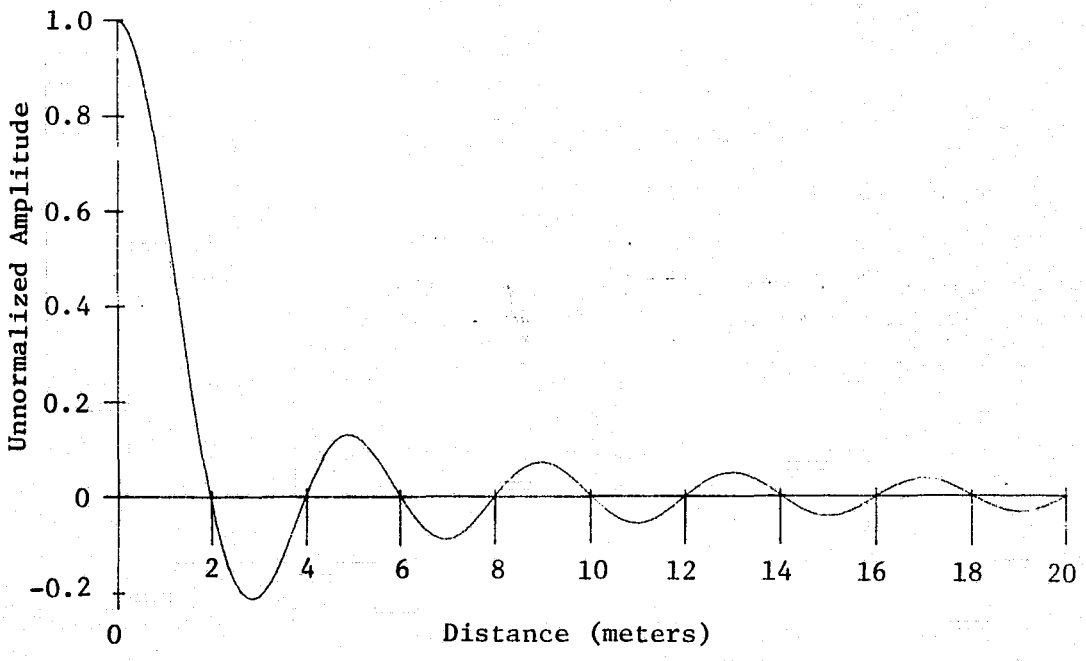


FIGURE II-20. LOW PASS FILTER USED TO TRUNCATE ANALOG FILTER MTF's AT 1/4 CYCLE PER METER

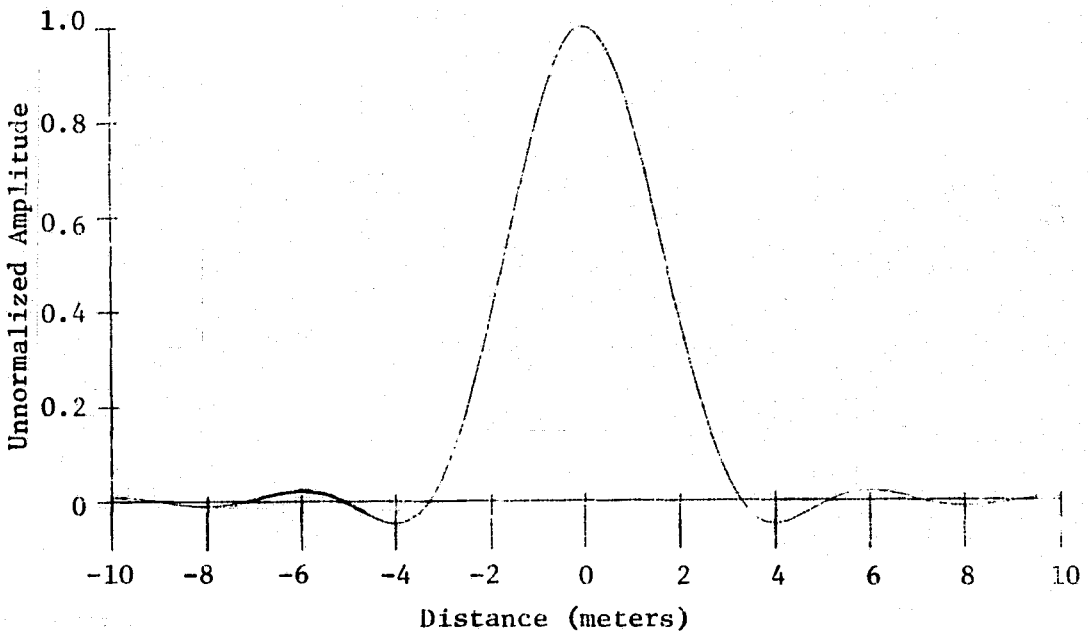


FIGURE II-21. COMPOSITE ANALOG SPATIAL FILTER FOR ALTERING SIMULATED ALONG-TRACK SCANNER RESPONSE (to 4 meter resolution) AFTER LOW PASS FILTERING

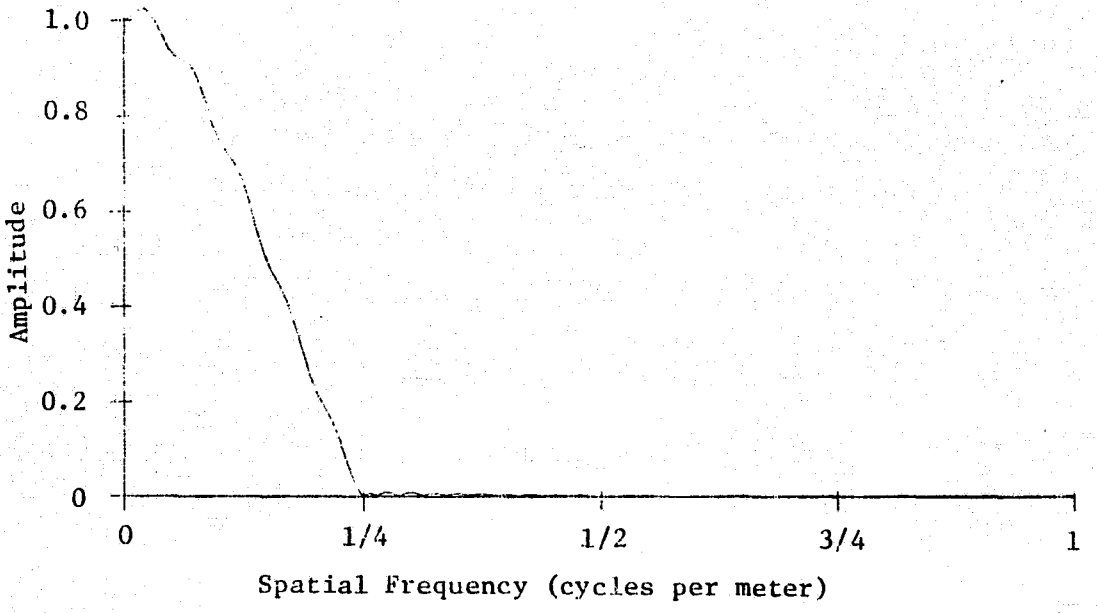


FIGURE II-22. COMPOSITE ANALOG FILTER MODULATION TRANSFER FUNCTION FOR ALTERING SIMULATED ALONG-TRACK SCANNER RESPONSE (to 4 meter resolution) AFTER LOW PASS FILTERING

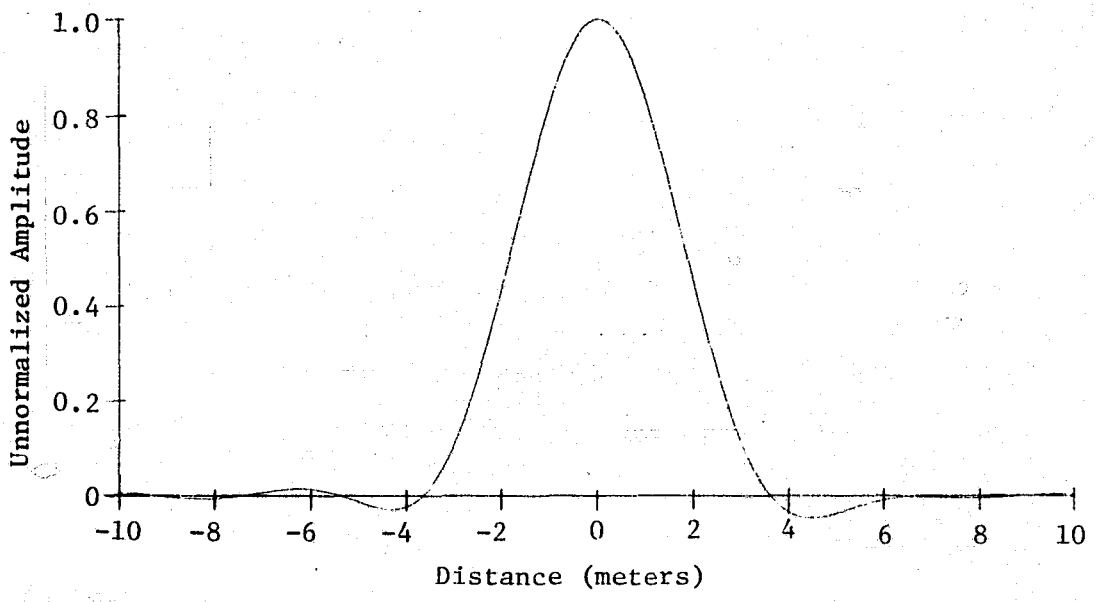


FIGURE II-23. COMPOSITE ANALOG SPATIAL FILTER FOR ALTERING SIMULATED WITHIN-SCAN SCANNER RESPONSE (to 4 meter resolution) AFTER LOW PASS FILTERING

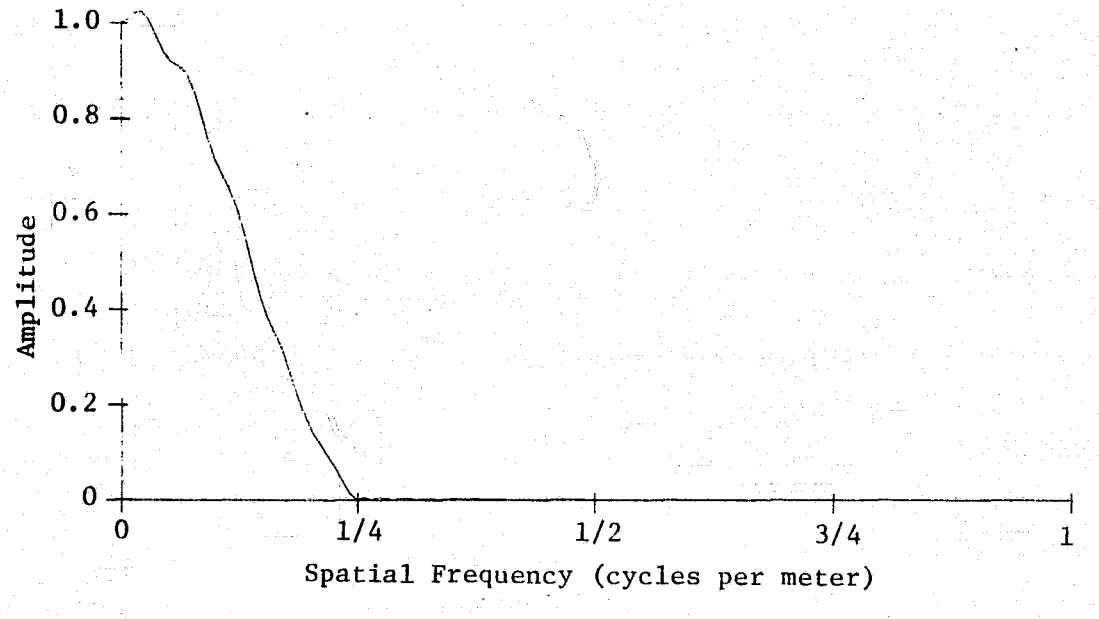


FIGURE II-24. COMPOSITE ANALOG FILTER MODULATION TRANSFER FUNCTION FOR ALTERING SIMULATED WITHIN-SCAN SCANNER RESPONSE (to 4 meter resolution) AFTER LOW PASS FILTERING

detail (high frequency content) of these filtering functions has been removed, as intended. The along-track and within-scan MTF's for the low pass filtered spatial filtering functions are plotted in Figures II-22 and II-24. Here the ripple that is apparent in the MTF curves is due to the truncation of the low pass filter weighting function, discussed above. These MTF curves have been normalized for plotting so that the steady state response equals unity, and hence, are not normalized to correspond to the least squares approximation of the respective MTF curves, shown in Figures II-15 and II-19, which are not low pass filtered.

The next step in generating the required digital form for the along-track and within-scan filtering functions was to sample the low pass filtered analog spatial filtering functions at two meter intervals. The resulting series of weights were then truncated, retaining different odd numbers of weighting factors, and MTF's were calculated to determine the number of weighting factors that were reasonable to use. The choice of an odd number of weighting factors and the registration of the sampling with the analog curves (Figures II-21 and II-23) were dictated by the requirement to retain unaltered line and point numbering in the filtered result. The number of weighting factors was also important, since the greater the number of weighting factors retained, the greater would be the processing cost for the spatial filtering, while the fewer the number of weighting factors, the less accurate the simulation would be. Retaining 5 weighting factors for each digitized spatial filtering function appeared to be a reasonable compromise.

For the along-track digitized filtering function, the error in matching the desired MTF curve was around $\pm 3\%$ with 5 weighting factors, while 3 and 7 weighting factors produced errors in the MTF of about $\pm 7\%$ and $\pm 1.5\%$, respectively. The digitized along-track spatial filtering

function, with 5 weighting factors, is plotted in Figure II-25 (which may be compared to the analog function shown in Figure II-21). The 5 along-track weighting factors, normalized to sum to unity (corresponding to a steady state response of unity), are

$$\begin{aligned} w_{a\text{-}t\ 1} &= -0.028771 \\ w_{a\text{-}t\ 2} &= 0.228514 \\ w_{a\text{-}t\ 3} &= 0.600513 \\ w_{a\text{-}t\ 4} &= 0.228514 \\ w_{a\text{-}t\ 5} &= -0.028771 \end{aligned} \qquad \text{(II-8)}$$

The MTF corresponding to the 5 weighting factor along-track digitized spatial filter is plotted in Figure II-26 (with expanded horizontal axis). Figure II-15 is reproduced with this same scaling of the horizontal axis in Figure II-27. Comparison of these two figures indicates the close approximation to the analog along-track filter MTF that has been attained. The spatial frequency response for this digitized and truncated filter (Figure II-26) is only plotted for frequencies below one cycle per four meters, however, remembering that aliasing accordion folds the higher spatial frequencies back and forth between the limits of the frequency range shown, one may visualize the form of the MTF for higher spatial frequencies as an unfolded graph of successive mirror images of the segment shown, like a chain of "paper dolls". The resulting large amplitudes of the MTF at high frequencies are not critical, since the two meter resolution data is already partly low pass filtered by the along-track scanner MTF (Figure II-4 -- note the scale of the horizontal axis before comparing with Figure II-26).

For the within-scan digitized filtering function, the error in matching the desired MTF curve was around $\pm 1.3\%$ with 5 weighting factors, while 3 and 7 weighting factors produced errors in the MTF of

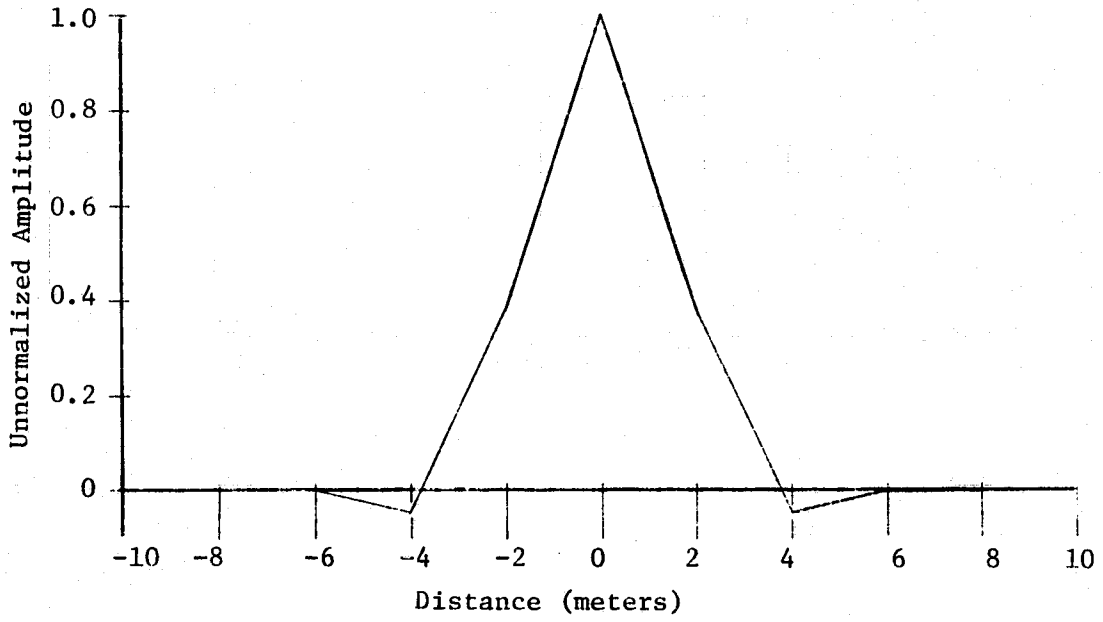


FIGURE II-25. DIGITIZED COMPOSITE SPATIAL FILTER FOR ALTERING SIMULATED ALONG-TRACK SCANNER RESPONSE (to 4 meter resolution)

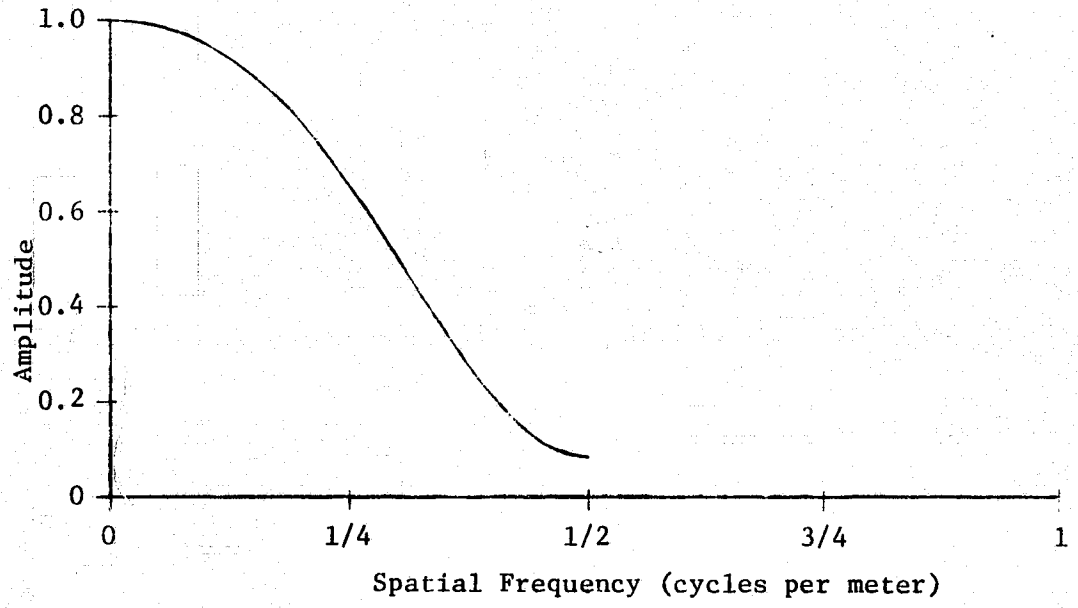


FIGURE II-26. DIGITIZED COMPOSITE FILTER MODULATION TRANSFER FUNCTION FOR ALTERING SIMULATED ALONG-TRACK SCANNER RESPONSE (to 4 meter resolution)

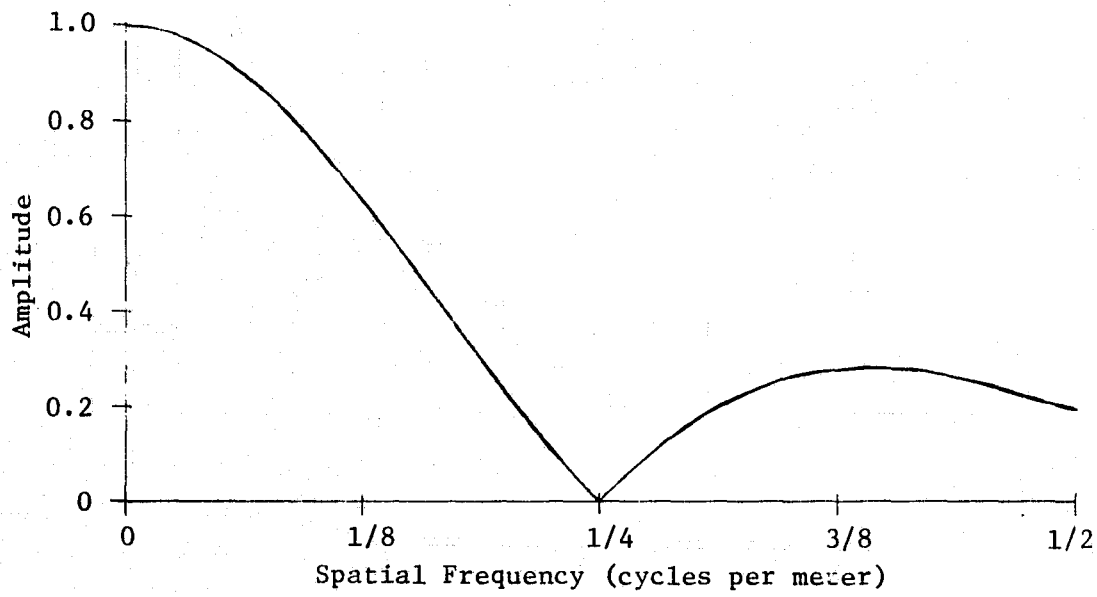


FIGURE II-27. COMPOSITE ANALOG FILTER MODULATION TRANSFER FUNCTION FOR ALTERING SIMULATED ALONG-TRACK SCANNER RESPONSE (to 4 meter resolution)

about ±5% and ±1%, respectively. The digitized within-scan spatial filtering function, with 5 weighting factors, is plotted in Figure II-28 (which may be compared to the analog function shown in Figure II-23). The 5 within-scan weighting factors, normalized to sum to unity), are

$$\begin{aligned} w_{w\text{-}s\ 1} &= -0.013533 \\ w_{w\text{-}s\ 2} &= 0.235758 \\ w_{w\text{-}s\ 3} &= 0.548425 \\ w_{w\text{-}s\ 4} &= 0.248356 \\ w_{w\text{-}s\ 5} &= -0.019006 \end{aligned} \qquad \text{(II-9)}$$

The MTF corresponding to the 5 weighting factor within-scan digitized spatial filter is plotted in Figure II-29 (with expanded horizontal axis). Figure II-19 is reproduced with this same scaling of the horizontal axis in Figure II-30. Comparison of these two figures again indicates that a close approximation to the analog within-scan filter MTF has been attained. Again the spatial frequency response for this digitized and truncated filter (Figure II-29) is only plotted for frequencies below one cycle per four meters. The form of the MTF for higher spatial frequencies can be visualized by the unfolding ("paper doll") technique mentioned above. The large amplitudes of the within-scan filter MTF at high spatial frequencies again are not critical, due to the low pass filtering effect of the within-scan scanner MTF at the two meter resolution, shown in Figure II-7 (note the scale of the horizontal axis before comparing with Figure II-29).

## II-5 APPLICATION OF THE DIGITIZED FILTERS TO THE DATA

The 5 weighting factors for the along-track and within-scan digital filters that have been derived may be combined into a 5x5 matrix of weighting factors, with rows of the matrix representing within-scan filtering and columns of the matrix representing along-track filtering

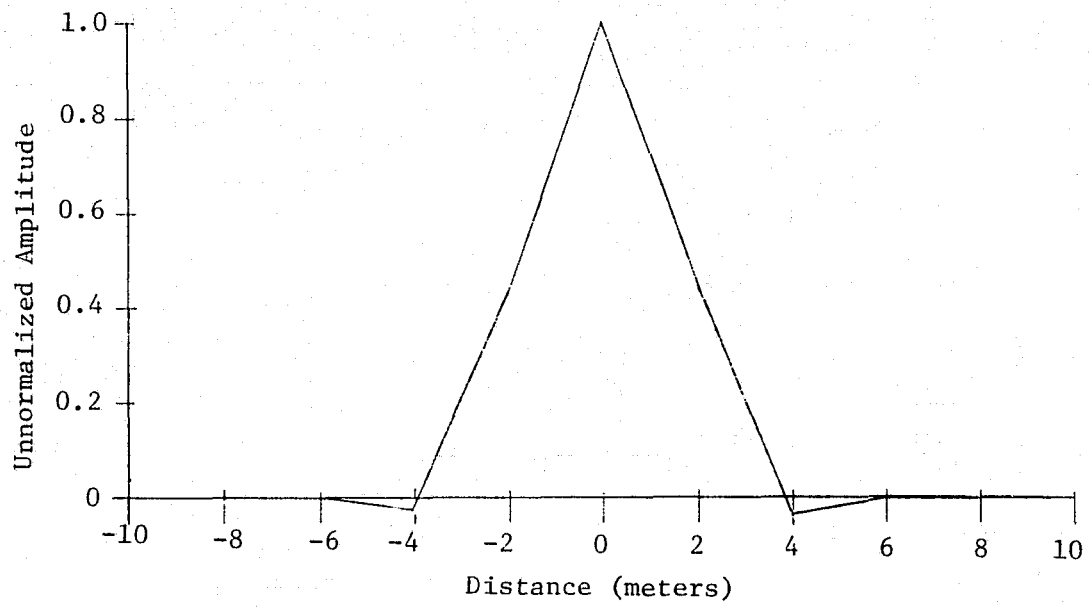


FIGURE II-28. DIGITIZED COMPOSITE SPATIAL FILTER FOR ALTERING SIMULATED WITHIN-SCAN SCANNER RESPONSE (to 4 meter resolution)

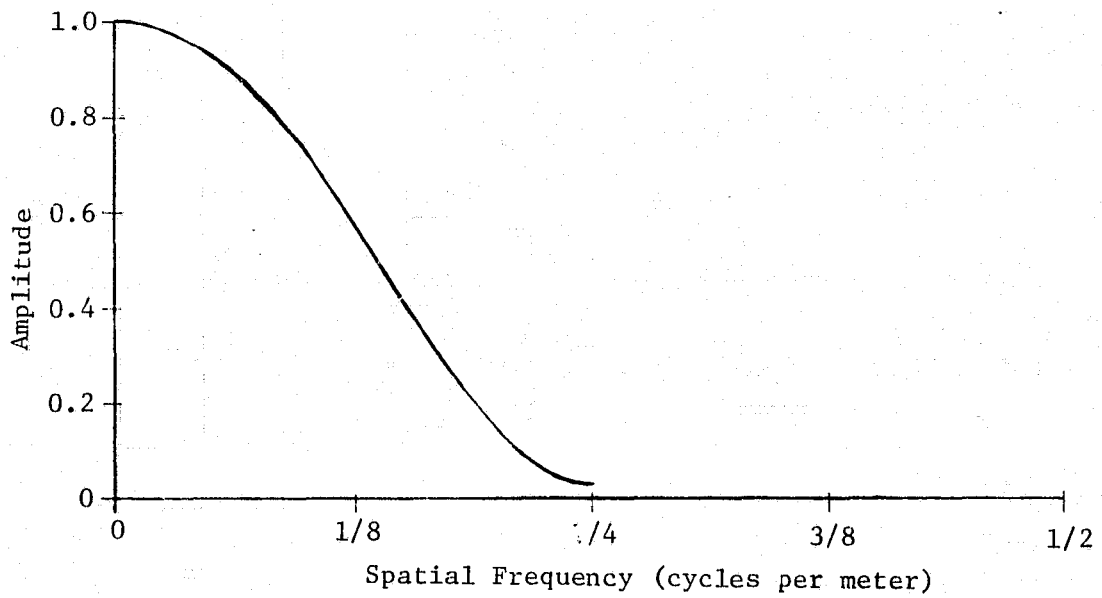


FIGURE II-29. DIGITIZED COMPOSITE FILTER MODULATION TRANSFER FUNCTION FOR ALTERING SIMULATED WITHIN-SCAN SCANNER RESPONSE (to 4 meter resolution)

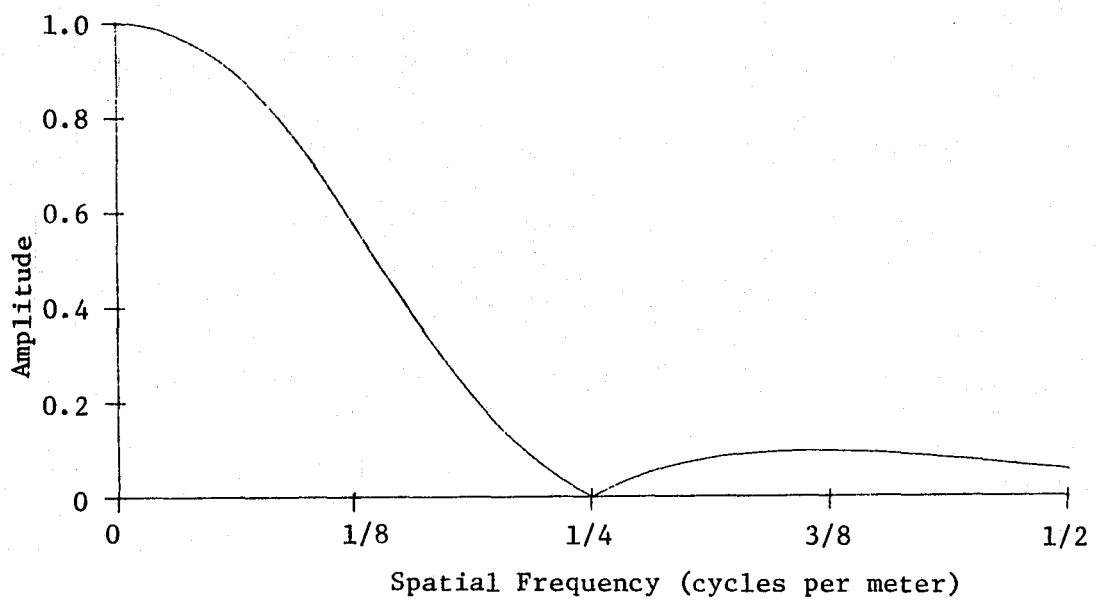


FIGURE II-30. COMPOSITE ANALOG FILTER MODULATION TRANSFER FUNCTION FOR ALTERING SIMULATED WITHIN-SCAN SCANNER RESPONSE (to 4 meter resolution)

$$W = \begin{bmatrix} 0.000389 & -0.006783 & -0.015779 & -0.007145 & 0.000547 \\ -0.003092 & 0.053874 & 0.125323 & 0.056753 & -0.004343 \\ -0.008127 & 0.141576 & 0.329336 & 0.149141 & -0.011413 \\ -0.003092 & 0.053874 & 0.125323 & 0.056753 & -0.004343 \\ 0.000389 & -0.006783 & -0.015779 & -0.007145 & 0.000547 \end{bmatrix} \quad \text{(II-10)}$$

which then may be applied to the 5x5 pixel vicinity surrounding each point to be sampled in the two meter resolution scene. (Note that in applying the spatial filter matrix to the data -- essentially a convolution procedure -- the left to right sequence of the rows and the top to bottom sequence of the columns should be reversed relative to the ascending sequence of point and line numbers, respectively. However, since the columns of the matrix are symmetric, one only needs to be careful about the sequencing within the rows of the matrix relative to the point numbering.) Since alternate points in alternate scan lines are to be sampled (to simulate the reduced spatial sampling rate at the four meter resolution), the mechanics of the filtering and sampling procedure are slightly complex, as indicated in Figure 3 (in the text).

## II-6 RESTORATION OF THE GAUSSIAN NOISE LEVEL

The weighted sum over the 5x5 blocks of pixels, used to apply the filters to the scene, has a smoothing effect on the data, low pass filtering not only the scenic content, but the noise content as well. The amount of change in the gaussian noise amplitude after the filtering is proportional to the RMS value of the filter MTF. Appropriate RMS calculations indicate that the gaussian noise level in the two meter resolution scene is reduced in amplitude (through filtering) by a factor of 0.680, due to the along-track filtering, and by a factor of 0.648, due to the within-scan filtering. Hence, overall there is a reduction in the noise amplitude by a factor of 0.439. This is equivalent to a reduction in the variance of the noise by a factor of $0.439^2$, or 0.193.

To restore the noise level of the data at the four meter resolution to the level that was present at the two meter resolution, one must add gaussian noise to the filtered result, with variance equal to 0.807 times the original variance. This variance corresponds to 0.899 times the original gaussian noise amplitude.

## II-7 GENERAL NATURE OF THE FILTERING TECHNIQUE

Since the above discussion all hinges on sampling rates and sampling intervals, which are only related to spatial frequencies and distances by changes in the sensor altitude, the procedure presented actually is suitable for any simulation of linear doubling of spatial resolution, using digitized data from a scanner system with along-track and within-scan spatial response similar to that shown in Figures II-3 and II-6. Hence, repeated applications of the same filtering and sampling technique can be used to simulate 8 meter resolution, using the 4 meter results, then 16 meter resolution, etc. Of course propagation of sampling errors could be minimized in such cases by deriving new filters specifically for each simulation, however, the repeated doubling technique presented should be accurate enough for any but the most exacting simulations.

# APPENDIX III
# DECISION RULES

The computer-implemented spectral classification techniques discussed in this study made use of 6 decision rules. The quadratic decision rule is the standard Bayes formulated maximum-likelihood ratio. The linear decision rule is based on the quadratic rule and involves a linear approximation of the decision boundaries. Both rules [7] are based on information from one resolution element at a time.

The remaining four decision rules were the so-called "nine-point" or multi-element rules [3] whose objective is to increase the accuracy of multispectral classification by using information from groups of resolution elements. These rules determine the classification of a resolution element on the basis of information from that element and its 8 immediate neighbors. Such rules are applicable whenever a resolution element is likely to represent the same material as its neighbors. A brief definition of each rule follows. The interested reader can find complete details in reference 3.

BAYES9 is based on the assumption that a pixel probably represents the same material as its neighbor. The degree of dependence can be specified.

PRIOR9 makes a Bayesian decision on the center pixel based on prior probabilities estimated from neighborhood data values. The estimated prior probability of a material is the average, over 9 pixels, of the posterior probability of that material at each pixel.

PREF9 uses as its decision criterion the estimated prior probability just defined for PRIOR9. It is conceptually an improved voting rule that takes account of all the information at each pixel rather than just a vote for the winning material.

VOTE9, applied after QRULE decisions have been made on the 9 pixels, assigns to the center pixel the material most frequently recognized among the 9 pixels.

## REFERENCES

1. E. Kan and D. L. Ball, Data Resolution Versus Forestry Classification, Document No. JSC-09478, NASA Johnson Spacecraft Center, Houston, Texas, December 1974.

2. F. J. Thomson, J. D. Erickson, R. F. Nalepka, J. D. Weber, and J. Braithwaite, Multispectral Scanner Data Applications Evaluation: Volume 1 -- User Applications Study, Report No. 102800-40-F, Environmental Research Institute of Michigan, Ann Arbor, Michigan, December 1974.

3. W. Richardson and J. M. Gleason, Multispectral Processing Based on Groups of Resolution Elements, Report No. 109600-18-F, Environmental Research Institute of Michigan, Ann Arbor, Michigan, May 1975, 120 pp.

4. R. M. Bizzell, A. H. Feiveson, F. G. Hall, M. E. Bauer, B. J. Davis, W. A. Malila, and D. P. Rice, Crop Identification Technology Assessment for Remote Sensing (CITARS), Interpretation of Results, Vol. 10, Report No. JSC-09393, NASA Johnson Space Center, Houston, Texas, December 1975.

5. R. E. Turner, Radiative Transfer in Real Atmospheres, Report No. 190100-24-T, Environmental Research Institute of Michigan, Ann Arbor, Michigan, July 1974.

6. G. H. Suits, The Calculation of the Directional Reflectance of a Vegetative Canopy, Remote Sensing of Environment, Vol. 2, 1972, pp. 117-125.

7. R. B. Crane and W. Richardson, Performance Evaluation of Multispectral Scanner Classification Methods, Proceedings of the Eighth International Symposium on Remote Sensing of Environment, Vol. II, Report No. 195600-1-X, Environmental Research Institute of Michigan, Ann Arbor, Michigan, 1972, pp. 815-31.